Max-Planck-Institut
für Herz- und Lungenforschung
W.G. Kerckhoff-Institut

JUSTUS-LIEBIG-
UNIVERSITÄT
GIESSEN

The long non-coding RNA *AS-Trdn* controls the balance of triadin isoform expression and cardiac excitation-contraction coupling

Inaugural-Dissertation

For the award of the degree of doctor of natural sciences

- Doctor rerum naturalium -

(Dr. rer. nat.)

Presented to the faculty of biology and chemistry (FB 08)

Justus-Liebig-Universität, Gießen

Submitted by

M. Sc. Theresa Kathalyn Hofmann

Bad Nauheim, February 2024

1. Referee: Prof. Dr. Thomas Böttger

2. Referee: Prof. Dr. Albrecht Bindereif

I declare that I have completed this dissertation single-handedly without the unauthorized help of a second party and only with the assistance acknowledged therein. I have appropriately acknowledged and referenced all text passages that are derived literally from or are based on the content of published or unpublished work of others, and all information that relates to verbal communications. I have abided by the principles of good scientific conduct laid down in the charter of the Justus Liebig University of Giessen in carrying out the investigations described in the dissertation.

Theresa Kathalyn Hofmann (geb. Gerhardt)

Department of Cardiac Development and Remodelling (Prof. Dr. Dr. Thomas Braun)
AG Böttger (Prof. Dr. Thomas Böttger)
Max Planck Institute for Heart and Lung Research,
Bad Nauheim

Publications:

Klockner, I., Schutt, C., **Gerhardt, T**., Boettger, T. and Braun, T., 2022. Control of CRK-RAC1 activity by the miR-1/206/133 miRNA family is essential for neuromuscular junction function. *Nature Communications*, *13*(1), p.3180

Weiss, Maria; Hettrich, Sara; **Hofmann, Theresa**; Hachim, Salma; Günther, Stefan; Braun, Thomas; Boettger, Thomas. “Mitolnc controls cardiac BCAA metabolism and heart hypertrophy by allosteric activation of BCKDH.” *Nucleic Acids Research* – under revision.

Abstract

The molecular function of long non-coding RNAs (lncRNAs) has become an emerging scientific field focusing on various molecular pathways across species. One specific subclass known as antisense lncRNAs, was defined by its genomic localization antisense to one or more protein-coding genes. In numerous instances, these lncRNAs play a crucial role in cis-regulation by modulating the expression and splicing of the associated sense protein-coding gene. In the present study, the functional significance and the physiological implications of the cardiomyocyte-specific antisense lncRNA *AS-Trdn* were investigated in *mus musculus* as well as human cells. The expression of *AS-Trdn* in cardiac tissue leads to a shift in triadin isoform expression, replacing the long skeletal muscle triadin with the short cardiac specific isoform. Employing various NGS approaches and CRIPR/Cas9 based genomic interventions to elucidate the molecular mechanism, this study demonstrates that *AS-Trdn* regulates triadin splicing and alternative polyA usage *in-cis* through a RNA Polymerase II transcriptional interference. Investigations involving the loss of single exons and the overexpression of the spliced transcript indicate no alterations in triadin isoform abundance. However, endogenous overexpression in differentiated satellite cells results in a preference for the skeletal muscle isoform. The conserved underlying molecular mechanism is shown to rely on the *AS-Trdn* transcription, inducing sequence-dependent transcriptional pausing, wherein the antisense polymerase acts as a Roadblock for the opposing polymerase. Although an R-loop dependent transcription termination is postulated due to high GC-content and m6a deposition within a specific region, confirmation of the occurrence of an RNA:DNA hybrid is pending. Physiologically, AS-Trdn and the consequent expression of cardiac triadin is essential for a regular calcium cycling, normal heart rate and a accurate response to β-adrenergic signalling. Through isoform specific interaction studies, it is revealed that skeletal muscle triadin extensively binds to the microtubule and actinin cytoskeleton resulting in significant deformation of the cardiac dyad structure compared to the healthy situation. The subsequent increase in calcium handling and heart rate leads to a commencing dilated cardiomyopathy in ageing mice, characterized by decreased cardiac function, reduced cardiomyocyte cross-sectional area and an overall increase in heart size. Consequently, *AS-Trdn* and triadin emerge as pivotal regulators of cardiac contraction and cardiac dyad structure, influencing both health and disease.

Zusammenfassung

Die molekulare Funktion langer nicht-kodierender RNAs (lncRNAs) ist zu einem zunehmend bedeutsamen wissenschaftlichen Gebiet geworden, das sich auf diverse molekulare Prozesse in verschiedensten Spezies konzentriert. Eine Unterklasse dieser lncRNAs stellen die so genannten antisense-lncRNAs dar, welche durch ihre antisense Lokalisation zu einem oder mehreren protein-kodierenden Genen definiert sind. In den meisten Fällen weisen diese lncRNAs wichtige regulatorische Funktionen in Bezug auf die Expression und das Spleißen des zugehörigen Protein-kodierenden Gens *in-cis* auf. In der zugrundeliegenden Studie werden die molekularen und physiologischen Funktionen der Kardiomyozyten-spezifischen antisense lncRNA *AS-Trdn* sowohl in *mus musculus* als auch im Menschen untersucht. Dafür wurde ein Herz-spezifischer Verlust der lncRNA Transkription induziert und die Folgen experimentell untersucht. Der Verlust von *AS-Trdn* im Herzgewebe führt primär zu einer Alternation in der Expression des Proteins triadin, wobei die kurze herzspezifische Isoform durch die lange Skelettmuskel-Isoform ersetzt wird. Zur Aufklärung des molekularen Mechanismus wurden verschiedene NGS Datensätze sowie CRIPR/Cas9-basierte genomische Veränderungen analysiert. Dabei zeigt sich, dass *AS-Trdn* die triadin Isoform Abundanz *in-cis* durch eine RNA-Polymerase II Transkriptionsinterferenz reguliert. Der Verlust einzelner Exone als auch die Überexpression des gespleißten Transkripts zeigen keine Veränderungen in der Expression der triadin-Isoform, wohingegen die endogene Überexpression in differenzierten Satellitenzellen zu einer Präferenz für die Skelettmuskulatur-Isoform führt. Der konservierte molekulare Mechanismus basiert ausschließlich auf der Transkription von *AS-Trdn*, die eine sequenzabhängige transkriptionelle Interferenz auslöst, bei der die antisense-Polymerase als Roadblock für die konvergierende Polymerase fungiert. Aufgrund des hohen GC-Gehalts und der Anreicherung von m6a in einer bestimmten genomischen Region wurde eine R-Loop abhängige Transkriptionstermination postuliert, die Bestätigung des Auftretens eines RNA:DNA-Hydrids steht jedoch noch aus. Physiologisch gesehen ist die Expression von AS-Trdn und die daraus resultierende herzspezifische triadin Isoform notwendig, um einen normalen Kalziumzyklus, sowie eine stetige Herzfrequenz zu gewährleisten und um eine angemessene Reaktion auf β-adrenerge Stimulation zu ermöglichen. Durch Isoform-spezifische Interaktionsstudien wird aufgedeckt, dass Skelettmuskel-triadin im Gegenteil zur

Herzspezifischen Isoform extensiv an das Mikrotubuli- und Aktinin-Zytoskelett bindet, was zu einer erheblichen Deformation der kardialen Dyadenstruktur führt. Der anschließende Anstieg des Kalziumhaushalts und der Herzfrequenz führt bei alternden Mäusen zu einer beginnenden dilatativen Kardiomyopathie, die durch eine verminderte Herzfunktion, eine verringerte Querschnittsfläche der Kardiomyozyten und eine allgemeine Zunahme der Herzgröße gekennzeichnet ist. Folglich erweisen sich *AS-Trdn* und triadin als zentrale Regulatoren der Herzkontraktion und der Struktur der Herzdyaden, die sowohl Gesundheit als auch Krankheit beeinflussen.

Contents

Abstract III

Zusammenfassung IV

List of abbreviations IX

List of figures XIV

List of tables XVI

1. Introduction 1

1.1. The cardiovascular system 1

1.1.1. Heart anatomy, function and electrophysiology 2

1.1.2. Heart physiology: Regulatory networks at the basis of heart contraction 5

1.2. Electrophysiology of the heart: excitation-contraction coupling 7

1.2.1. The calcium-release complex: the role of triadin in regulating SR structure and calcium cycling 8

1.3. Long non-coding RNAs: Multi-talents of gene regulation 14

1.3.1. Mechanism and functions of *trans*- and *cis*-acting lncRNAs 16

1.3.2. Long non-coding RNAs in cardiac function and disease 21

1.3.3. The lncRNA *AS-Trdn* regulates the isoform balance of the protein coding gene triadin in the heart 23

1.4. Aim 26

2. Material and Methods 27

2.1. Materials 27

2.1.1. Public available NGS Data sets 29

2.2. Methods 30

2.2.1. Animal husbandry 30

2.2.1.1. Animal experiments, sacrifice procedure and organ harvest 30

2.2.2. Mouse-line generation and cloning 30

2.2.2.1. Generation of AS-Trdn polyA mouse-lines using CRISPR/Cas9 30

2.2.2.2. Generation of AS-Trdn Downstream deletion mutants 34
2.2.3. Molecular methods 35
2.2.3.1. Isolation of genomic DNA and genotyping 35
2.2.3.2. RNA isolation and fractionation for RT-qPCR and RNAseq 36
2.2.3.3. Quantitative reverse transcription PCR (RT-qPCR) 37
2.2.3.4. Isolation of proteins, membrane isolation and western blotting 38
2.2.3.5. Immunoprecipitation 40
2.2.3.6. Cleavage under targets and release using nuclease (Cut&Run) 40
2.2.3.7. Identification of native R-loops using MapR 42
2.2.4. Histological methods 44
2.2.4.1. Cryo- and paraffin sectioning 44
2.2.4.2. Haematoxylin/Eosin staining according to Gill 44
2.2.4.3. Immunohisto- and Immunocytochemistry 45
2.2.4.4. Single-molecule Fluorescence in-Situ Hybridization (smFiSH) 45
2.2.4.5. Transmission electron microscopy (TEM) 46
2.2.5. Physiological methods 47
2.2.5.1. Magnetic resonance imaging (MRI) 47
2.2.5.2. Telemetric measurements using ECG-transmitter 48
2.2.5.3. Calcium imaging using the IonOptix system 49
2.2.6. Cell culture 50
2.2.6.1. Culture, transfection and harvest of immortalized cell lines 50
2.2.6.2. Culture and transfection of mESC and cardiac body differentiation 50
2.2.6.3. Isolation, culture and transfection of neonatal and adult cardiomyocytes 54
2.2.6.4. Isolation and culture of mouse primary satellite cells 55
2.2.6.5. Endogenous overexpression of AS-Trdn using dCas9-SPH in satellite and C2C12 cells 56
2.2.7 Statistical analysis 57
3. Results 58
3.1. Molecular analysis of *AS-Trdn* lncRNA mechanism & function 58
3.1.1. Genomic locus and sequence analysis of a heart specific antisense lncRNA in human and mice 58

3.1.2. Loss of *AS-Trdn* induces long *Trdn* isoform expression 61
3.1.3. *AS-Trdn* transcription is driven by GATA4 and expands the annotated 3'-termination site..... 66
3.1.4. *AS-Trdn* expression leads to transcriptional interference via roadblock formation.... 70
3.2. Phenotypical characterization of the *AS-Trdn* KO mouse model..... 76
3.2.1. Loss of *AS-Trdn* and consequent expression of trisk95 leads to elevated calcium cycling, increased heart rate and blunted isoproterenol response..... 76
3.2.2. Trisk95 reshapes dyad structure in the heart by binding to the cytoskeleton..... 82
3.2.3. Loss of *AS-Trdn* and consequent expression of trisk95 induces dilated cardiomyopathy in ageing mice..... 87
4. Discussion..... 90
4.1. *AS-Trdn* is a conserved nuclear lncRNA, expressed upon CM transition 90
4.2. *AS-Trdn* regulates triadin isoform balance in the heart on a transcriptional level 92
4.3. GATA4 is the main driver of *AS-Trdn*, inducing bi-directional expression of the lncRNA..... 93
4.4. *AS-Trdn* regulates triadin isoform balance by transcriptional interference 95
4.5. The *AS-Trdn* regulatory stalling site is stabilized by widespread m^6A deposition 98
4.6. Conclusion and outlook of the molecular mechanism of *AS-Trdn* 100
4.7. The long skeletal muscle isoform of triadin is able to increase CRC activity resulting in a "fight or flight" response failure 102
4.8. Triadin is an important regulator of CRC structure and integrity – and beyond?..... 103
4.9. Trisk95 dependent elevated calcium cycling and dyad reshaping induces DCM in ageing mice..... 106
4.10. Conclusion and outlook on the physiological mechanism and function of triadin in the heart..... 107
Literature..... 111
Appendix..... 119
Acknowledgment..... 122

List of abbreviations

°C	Grad Celsius
µg	microgram
µl	microliter
µM	micro molar
µm	micrometre
AC	Adenylate cyclase
aCM	adult cardiomyocyte
Actn	*Actinin*
Adipor1	*Adiponectin receptor 1*
Airn	*antisense to insulin-like growth factor 2 receptor*
ANRASSF1	*antisense long non-coding RNA RASSF1*
ANRIL	*CDKN2B-AS*
APOLO	*AUXIN-REGULATED PROMOTER LOOP*
as	antisense
ATP2a	*Sarcolemmal Na+/K+-ATPase*
BIRDHs	break-induced RNA:DNA hybrids
bp	basepair
Brd1as	*bromodomain containing 1 antisense RNA*
BVHT	*lncRNA Braveheart*
Ca^{2+}	calcium
Calu	*Calumenin*
CAMKII	*Ca^{2+}/calmodulin-dependent protein kinase II*
cAMP	cyclic adenosine monophosphate
Casq2	*Calsequestrin 2*
CaV1.2	*Calcium channel, voltage-dependent, L type, alpha 1C subunit*
CB	cardiac body
cDNA	complementary DNA
CICR	calcium-induced calcium release
circRNA	circular RNA
Ckap4/5	*cytoskeleton-associated protein 4/5*
cMyBP-C	*Cardiac myosin-binding protein C*
CnR; C&R	Cleavage under targets and release using nuclease (Cut&Run)
CO	cardiac output
COOLAIR	*cold-induced FLOWERING LOCUS C antisense lncRNA transcript*
CPVT	catecholaminergic polymorphic ventricular tachycardia

CRC	calcium-release complex
CRISPR	Clustered regularly interspaced palindromic repeats
CRU	calcium-release unit
ctr.	control
CVD	cardiovascular disease
Cxcr4	*chemokine receptor 4*
DAD	delayed after depolarization
Dapi	4′,6-diamidino-2-phenylindole
dCAS9	Endonuclease Dead CRISPR associated protein 9
DCM	dilated cardiomyopathy
ddH2O	distilled water
del	deletion
DMEM	Dulbecco's Modified Eagle Medium
DNA	Desoxyribonucleic acid
e.g.	exempli gratia
ECC	Excitation-contraction coupling
ECG	electrocardiogram
EDTA	Ethylendiamintetraessigsäure
EDV	end-diastolic volume
EF	ejection fraction
eRNAs; elncRNAs	enhancer RNA
ESV	end-systolic volume
FC	fold change
FCS	fetal calve serum
Fendrr	*Fetal-lethal noncoding developmental regulatory RNA*
FIRRE	*Firre Intergenic Repeating RNA Element*
FS	fractional shortening
g	gram
Gapdh	*Glyceraldehyde 3-phosphate dehydrogenase*
Gata4	*GATA Binding Protein 4*
GRK	*G protein-coupled receptor kinase*
Gs	GαS proteins
H&E	hematoxylin and eosin
H2O	water
HCN	Hyperpolarization-activated cyclic nucleotide-gated ion channels
hIPSC-CMs	human induced Pluripotent Stem Cells derived cardiomyocytes

HOTAIR	*HOX antisense intergenic RNA*
HRAT13	*heart related antisense transcript 13*
Hrc	*histidine-rich calcium binding protein*
HRP	horseradish peroxidase
Hz	Herz
I.p.	Intraperitoneal
Igf2r	*insulin-like growth factor 2 receptor*
IgG	immunoglobulin G
IGV	integrative genomics viewer
IP	immunoprecipitation
Ip3r	*inositol 1, 4, 5 - trisphosphate receptor*
Iso	Isoproterenol
Jnt; Jun; Asph	*Junctin*
Jph2	*Junctophilin 2*
j-SR	junctional sarcoplasmic reticulum
kb	kilobases
KCNQ1OT1	*potassium voltage-gated channel subfamily KQT member 1 opposite strand 1*
KD	knock down
kDa	kilo Dalton
KO	knock out
lincRNA	long intergenic non coding RNA
lncMyh	*myosin heavy chain gene cluster associated lncRNA*
lncRNAs	long non-coding RNA
LOF	loss of function
LQTS	long QT syndrome
l-SR	longitudinal sarcoplasmic reticulum
LTCC	L-type calcium channels
MALAT1	*metastasis-associated lung adenocarcinoma transcript 1*
MapR	Mapping Native R-Loops
mESC	mouse embryonic stem cells
Mettl3	*methyl transferase 3*
MI	myocardial infarct
min	minute
miRNA	micro RNA
mM	mill molar
MRI	Magnetic resonance imaging

mRNA	messenger ribonucleic acid
msec	milliseconds
nCM	non-cardiomyocytes
ncRNA	non-coding RNA
NCX	*Sodium-calcium exchanger*
Neat1	nuclear paraspeckle assembly transcript 1
neoCM	neonatal cardiomyocyte
NGS	Next-generation-sequencing
ON	overnight
PCR	polymerase chain reaction
PFA	paraformaldehyde
piRNA	piwi interacting RNA
PKA	*protein kinase A*
Plb	*Phospholamban*
Plm	*Phospholemman*
PNCTR	*pyrimidine-rich non-coding transcript*
polyA	polyadenylation signal
Prc2	*polycomb repressive complex 2*
pval	*p-value*
PVCs	premature ventricular contractions
qRT-PCR	quantitative reverse transcription PCR
rel.	relative
RME2	*non-coding antisense transcript regulator of meiosis 2*
RNA	ribonucleic acid
RNA Pol II	RNA polymerase II
rpm	rounds per minute
RT	reverse transcriptase
RT	room temperature
RyR1/2	Ryanodine receptor
SCs	satellite cells
seq	sequence or sequencing
Serca2a	*SR Ca^{2+}-ATPase; ATP2a2*
Serpine1	*plasminogen activator inhibitor 1*
siRNA	small interfering RNA
smFiSH	single molecule fluorescent in-situ hybridization
snoRNA	small nucleolar RNA
snRNA	small nuclear RNA

SR	sarcoplasmic reticulum
Sri	*Sorcin*
Srl	*Sarcalumenin*
Srsf	*SR splicing factors*
SV	stroke volume
TA	*tibialis anterior*
TAD	topologically associated domain
TARID	*TCF21 Antisense RNA Inducing Promoter Demethylation*
TBS	Tris Buffered Saline
TBS-T	Tris Buffered Saline – Tween20
TE	Trypsin/EDTA
Tead1	*TEA domain transcription factor 1*
TKOS	Triadin knockout syndrome
Tmem258	*Transmembrane protein 258*
Tnl	*Troponin-I*
Trdn	*Triadin*
trisk35	cardiac specific Triadin isoform
trisk51	skeletal muscle short Triadin isoform
trisk95	skeletal muscle specific Triadin isoform
Tub	*Tubulin*
untr.	untransfected
Uph	*Upperhand lncRNA*
UTR	untranslated region
Vamp3	*vesicle associated membrane protein 3*
WT	wildtype
Xist	*X-Chromosom inaktivierendes Transkript*
Zeb2	*zinc finger E-box-binding homeobox 2*
ZEB2-AS1	*ZEB2 antisense RNA 1*
Zmynd8as	*zinc finger, MYND-type containing 8 antisense RNA*
ZNF593-AS	*Zinc Finger Protein 593 antisense transcript*
β-AR	β-adrenergic receptors

List of figures

Number	Title	Page
Figure 1	Comparison of the human and mouse heart anatomy	2
Figure 2	Excitation propagation and action potential of the working myocardium	4
Figure 3	Adrenergic and cholinergic signalling pathways and PKA response in cardiomyocytes	6
Figure 4	Schematic representation of the cardiac dyad and the calcium-release complex	9
Figure 5	Structural characteristics of striated muscle cells, the sarcoplasmic reticulum and triadin localisation	11
Figure 6	The molecular basis of the triadin knockout syndrome	13
Figure 7	The non-coding genome and its classification	15
Figure 8	The molecular mechanisms of lncRNA functions	17
Figure 9	Co-transcriptional effects of non-coding antisense transcripts	20
Figure 10	Regulatory pathways of lncRNAs in different cardiac cell-types	22
Figure 11	*AS-Trdn* is a cardiac specific lncRNA responsible for triadin isoform abundance in the heart	24
Figure 12	*AS-Trdn* transcript regulates trisk32 isoform splicing but has no effect on trisk95	25
Figure 13	Modified MapR workflow	42
Figure 14	Schematic drawing of the IonOptix measurement system for sarcomere contraction and intracellular calcium cycling	49
Figure 15	Genomic localization and sequence analysis of the long non-coding RNA *AS-Trdn*	59
Figure 16	*AS-Trdn* is a heart exclusive and nuclear enriched lncRNA	60
Figure 17	*AS-Trdn* KO strategy and evaluation	62
Figure 18	Loss of *AS-Trdn* transcription leads to expression of the long skeletal muscle isoform of triadin in the heart	64
Figure 19	Loss of *AS-TRDN* transcription induces skeletal muscle triadin isoform expression in hIPSC cardiomyocytes	65
Figure 20	Long-range sequencing reveals new *AS-Trdn* termination site and potential bidirectionality of its promoter	67
Figure 21	*AS-Trdn* promoter exhibits bi-directionality and is driven by GATA4	69
Figure 22	Transcriptional activation of *AS-Trdn* leads to cardiac triadin isoform generation in satellite cells	71
Figure 23	RNA Polymerase II transcription analysis of *AS-Trdn* locus revealed stalling before exon 9 of Trdn	73
Figure 24	miCLIP2 analysis of WT hearts reveals accumulation of m6A deposition on the antisense-transcript	75
Figure 25	*AS-Trdn* KO mice exhibit no obvious phenotypical alterations until 16 weeks of age but reveal changes in calcium handling	77
Figure 26	Elevated calcium cycling and aberrant calcium release after KO of *AS-Trdn* in adult CMs	80

Figure 27	Telemetric measurements reveal an increased heart rate and blunted β-adrenergic response in *AS-Trdn* KO mice	81
Figure 28	Expression of trisk95 leads to cardiac dyad deformation and changes in CRC related proteins abundance	83
Figure 29	Triadin immunoprecipitation in WT and KO hearts reveals strong binding of trisk95 to the microtubule cytoskeleton over CKAP4/5	85
Figure 30	The induced expression of trisk95 in KO hearts leads to an increased actinin and tubulin binding accompanied by interactions with related proteins	86
Figure 31	MRI measurements reveal depressed cardiac contraction in *AS-Trdn* KO mice and commencing DCM	88
Figure 32	*AS-Trdn* KO mice exhibit a progressive dilative cardiomyopathy after 40 weeks of age	89
Figure 33	*AS-Trdn* regulates triadin isoform balance via an R-loop dependent transcriptional interference	101
Figure 34	*AS-Trdn* KO leads to a change in triadin isoform abundance resulting in a change in cardiac dyad structure and excitation contraction coupling	109
Figure 35	Deletion of intronic polyA sites between exon 8 & 9 of triadin has contradictory effects on triadin isoform abundance	119
Figure 36	Insertion of additional polyA sites downstream of *AS-Trdn* exhibit no effect on antisense transcription	120
Figure 37	Putative CTCF binding site has no functional role in triadin termination	120
Figure 38	HiCseq analysis of publicly available heart data reveals no TAD boundaries at the triadin locus	121

List of tables

Number	Title	Page
Table 1	Generated mouse lines	27
Table 2	Cell lines & primary cells	27
Table 3	Common buffers	28
Table 4	Software	28
Table 5	T4-ligase reaction set-up	32
Table 6	CRISPR/Cas9 sgRNAs, repair Oligos and corresponding plasmids	33
Table 7	PCR Mastermix	35
Table 8	PCR standardized program	35
Table 9	Mouse-line specific genotypings	36
Table 10	Sequences of primers used for genotyping	37
Table 11	Sequences of RT-qPCR primer	38
Table 12	antibodies used for Cut&Run	41
Table 13	mESC media composition	52
Table 14	generated mESC stable lines	53
Table 15	*AS-Trdn* promoter sgRNA sequences	57
Table 16	Cas9-SPH containing plasmids	57
Table 17	Gorilla Gene Ontology top 20 processes of WT and *AS-Trdn* KO RNAseq	78

1. Introduction

1.1. The cardiovascular system

The cardiovascular system, also called the circulatory system, orchestrates various physiological processes to sustain life. It is comprised of the heart, blood vessels called arteries, veins and capillaries, and blood itself. As the name already implicates, the major function carried out by the cardiovascular system is to retain the blood flow within the closed circle of vessels to ensure the transportation of vital nutrients, hormones, oxygen and immune cells to every corner of the body and at the same time to remove waste products. Since this function of maintaining the homeostasis is the basis of every living system, the cardiovascular system is one of the first to arise during embryogenesis. As of this, in human embryos the first heartbeat can already be observed 4 weeks after fertilization, much earlier than all other developing organ systems (NIH; National Institutes of Health; Chaudhry, Miao & Rehman, 2022).

The tight coordination of the hearts rhythmic beating, the vascular tone and the blood flow ensures a continuous and steady supply throughout the whole body. In this regard, the autonomic nervous system plays a pivotal role in regulating the cardiovascular system. The sympathetic and parasympathetic nervous system modulate heart rate, contractility and blood vessel diameter constantly on varying physiological demands, mainly through the release of neurotransmitters (e.g. adrenaline to increase heart rate or acetylcholine to reduce heart rate; section 1.1.2; Gründer & Schlüter, 2023; Deetjen, Speckmann et al., 2005). In the centre of the cardiovascular system lays the heart, which is the only self-innervating organ throughout the whole body and thereby ensures the coordinated pumping of the blood by electrical signals throughout the four chambers. As a result, these electrical signals induce the so-called excitation-contraction coupling, which is the basis for a regular and steady heart contraction and therefore for heart function (Sandow, 1952). Multiple regulatory proteins and transmitters are involved in maintaining the precise regulation of excitation and heart contraction. An imbalance or dysregulation of any of these regulators can lead to severe diseases and even sudden cardiac arrest in humans, making a well-functioning excitation-contraction coupling indispensable for overall health and vitality (Tiso et al., 2001; Pogwizd et al., 2001). The next sections will explore the physiology, function and regulation of the human and mouse cardiovascular system with particular focus on the molecular mechanisms behind heart contraction.

1.1.1. Heart anatomy, function and electrophysiology

At the centre of the cardiovascular system lies the heart, a muscular pump that provides the force to push the blood throughout the whole body and thereby supplying oxygenated blood through arteries and returning deoxygenated blood back via veins. The vertebrate heart, a hollow muscle, is divided into two halves, each containing two chambers: left and right atrium, as well as a left and right ventricle (Figure 1). The right atrium receives oxygen-poor blood from the *Vena cava superior* or *inferior*, pumping it to the lungs through the right ventricle over the *Truncus pulmonaris*. Simultaneously, the left atrium receives the returning oxygen-enriched blood from the *Vena pulmonaris*, while the left ventricle ejects it back into the circulatory system through the aorta and arteries. Throughout this cycle, four heart valves ensure one-way blood flow and prevent backflow. The cardiac cycle encompasses two phases: contraction (systole) and relaxation (diastole) (Rosenthal & Harvey, 2010).

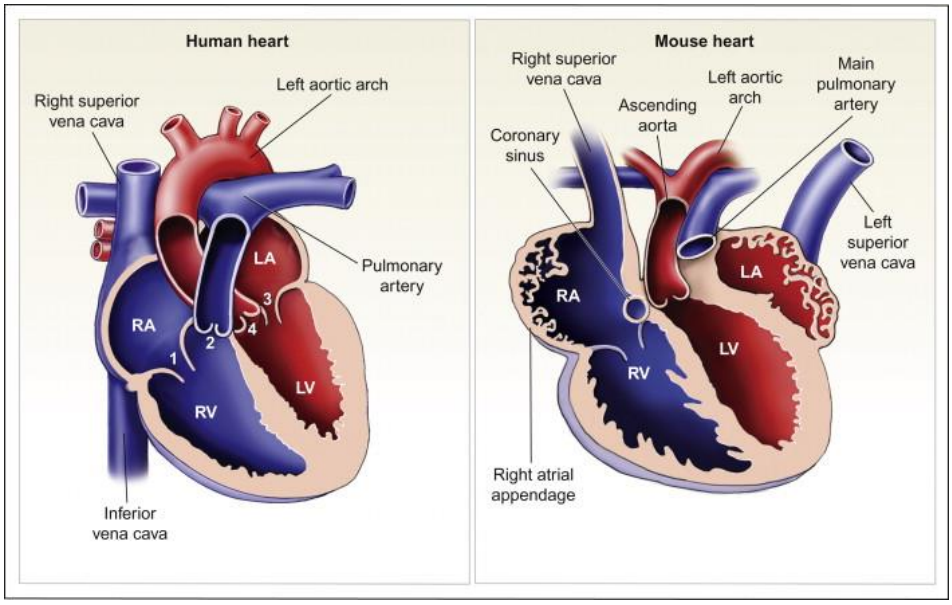

Figure 1 | Comparison of the human and mouse heart anatomy. The human as well as the mouse heart display a similar four-chambered heart anatomy, compromising the left and right atria, left and right ventricles as well as four heart valves: (1) the tricuspid valve, (2) the pulmonary valve, (3) the mitral valve and the aortic valve (4). This structure is needed in order to sufficiently pump the deoxygenated (blue) blood into the lungs over the pulmonary artery and oxygenated (red) blood into the whole body via the aorta. There are two major differences between human and mouse heart: the additional left superior vena cava in mouse heart, which empties into the coronary sinus and the bigger and more unstructured atrial appendages, which do not show distinct right versus left trabeculations. (Taken from Rosenthal & Harvey, 2010)

The heart itself is made up of the contractile myocardium, a striated musculature composed of individual myofibers. These myofibers originate from connections between specialized, rod-shaped cells known as cardiomyocytes (CMs). These cellular

bonds are established through intercalated discs that harbour gap-junctions, serving as intercellular channels formed by connexins. The transmission of excitation over gap-junctions from depolarized cells forms the foundation of heart contraction, rendering the heart a functional syncytium. Cardiomyocytes are primarily categorized into two classes: excitation-generating and conducting cells (pacemaker cells) and working myocardial cells. The excitation generation and conduction system cells, including the sinus node, atrioventricular node (AV node), His bundle, Purkinje fibres and Tawara bundle (ventricular bundle), can autonomously excite without external nervous innervation, exhibiting autorhythmicity. The sinus node, typically determining the heart rate, is considered the primary pacemaker (Gründer & Schlüter, 2023; Figure 2A).

Cardiomyocytes belonging to the working myocardium are mainly responding to and transmitting the signal received by the conducting cells over the intercalated discs towards the next CMs, which leads to the actual and full heart contraction. This means that an incoming action potential (AP) of the conducting cells is transferred throughout the whole heart in a short period of time (milliseconds depending on the body size) in an all-or-nothing manner. The action potential of a myocardial cell can be divided into 5 different phases (phase 0 – 5; Figure 2B):

Phase 0: The initial depolarization of the cell is mostly triggered by an incoming AP of an adjacent cell. Once the membrane potential reaches values over – 70 mV, voltage dependent Na^+ channels (NaV) open, leading to a rapid influx of positive sodium ions and thereby to a fast depolarization of the cell to approx. 20 - 30 mV (overshoot).

Phase 1: The rapid depolarization of the cell leads to the opening of voltage-gated K+ channels (KV4.x = *Kcndx; potassium voltage-gated channel*), which initiate the efflux of positive ions and thereby repolarisation to around 0 mV.

Phase 2: The second phase resembles the so-called plateau phase. After the short initial repolarisation by efflux of K^+ ions, an equilibrium is set up by a slow calcium influx through voltage-gated L-type calcium channels (CaV = *Cacna1*). These channels are activated during phase 0 at currents of around – 55 mV and a slow calcium influx persists for a long time, which is important for the duration of the AP and to restore the calcium storage of the myocardial cell.

Phase 3: The terminal repolarization phase is accomplished by steady increase in K^+ efflux due to the opening of further potassium channels and closing of the voltage-gated calcium channels (Figure 2C).

Phase 4: To restore normal levels within the myocytes, calcium ions are recycled into the sarcoplasmic reticulum (SR) by the ATP dependent calcium pump SERCA2 (*Atp2a2*) or into the extracellular space by NCX-1 (*Slc8a1*) until a normal electrochemical state is re-established. The resting state potential of – 85 mV is maintained by inwardly rectifying potassium channels (IK1) and the cells are ready for the next depolarization.

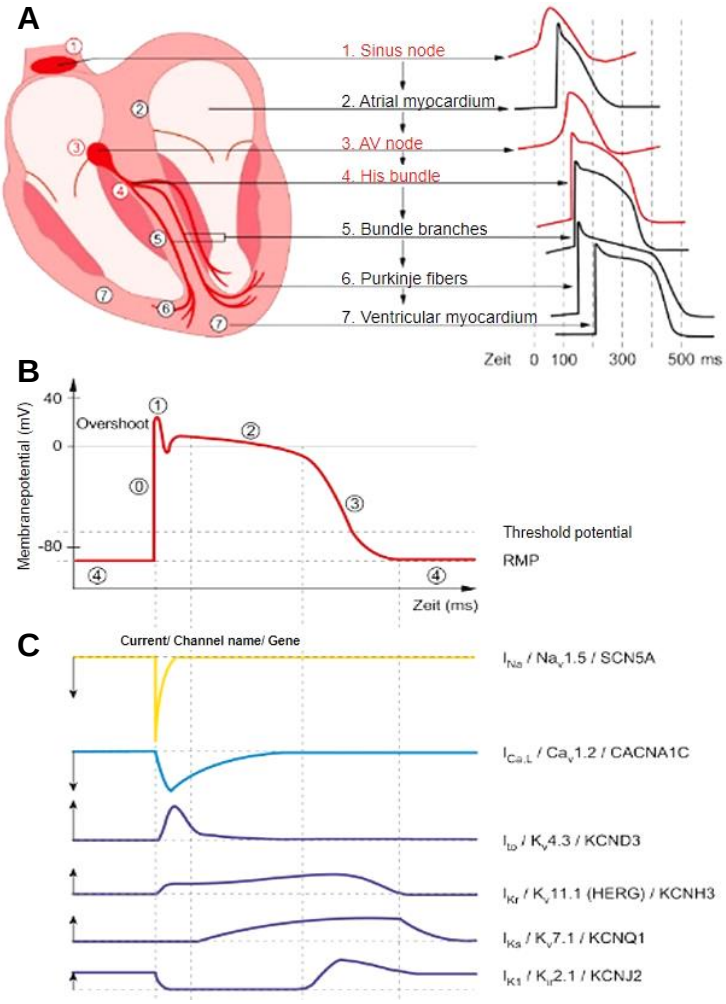

Figure 2 | Excitation propagation and action potential of the working myocardium. A scheme of the membrane potential changes of individual functional structures of the heart belonging to the working myocardium. In red are the parts with pacemaker function (1. sinus node, 3. atrioventricular node (AV node) and 4. His bundle) while parts without spontaneous excitation (2. atrial myocardium, 5. Bundle branches, 6. Purkinje fibers, 7. Ventricular myocardium) are marked in black. **B** phases of the action potential of the working myocard cells until resting membrane potential (RMP) is re-established. ms = milliseconds. **C** relative currents of the most important ion channels with corresponding gene names. Arrows indicate the direction of the currents with downward arrows = inward currents and upward arrows = outward currents. (Modified after Gründer & Schlüter, 2023)

Upon depolarization, the action potential travels along the T-tubules to activate voltage dependent calcium channels, thereby initiating the release of calcium into the cell and consequently from the SR into the cytosol. The increased concentration leads to the competitive binding of calcium to troponin C and in doing so, to the release of the whole troponin complex from the actin-binding site. The Myosin head is now able to attach to the actin filaments and thereby contract the muscle fibre. Afterwards the troponin complex reattaches to the actin-binding site due to the decrease in calcium ions and the muscle fibre relaxes, ending the heart contraction cycle (Gründer & Schlüter, 2023).

1.1.2. Heart physiology: Regulatory networks at the basis of heart contraction

The tight control of these ion channels and thereby of the heart rhythm, vascular tone and blood flow ensures a continuous and steady supply of blood throughout the whole body and underlays a series of regulatory networks. In this regard, the autonomic nervous system (ANS) plays an important role in balancing the signalling between adrenergic and cholinergic signalling pathways and is composed of two primary divisions: the sympathetic and parasympathetic nervous system. While the sympathetic system originates from the thoracolumbar region of the spinal cord and has an enhancing effect via adrenergic signalling pathways, the parasympathetic nervous system, originating from the craniosacral region, has a calming effect by using cholinergic signalling pathways. The most important functions influenced by the ANS are cardiac output (inotropy), myocardial relaxation (lusitropy), heart rate (chronotropy) and conduction (dromotropy) (Gründer & Schlüter, 2023).

The **parasympathetic nervous system (PNS)** is often associated with the “rest and digest” response. The synapses of parasympathetic fibres, originating from the *nervus vagus*, sit on muscarinic receptors in the heart and can induce a reduction in heart rate and contractility by releasing acetylcholine in the AV and sinus node as well as the ventricles. This parasympathetic release of acetylcholine inhibits the adenylate cyclase and activates membrane bound potassium channels by binding to M2-cholinoceptors, leading to a hyperpolarisation of the heart and thereby to a negative effect.

In contrast, the **sympathetic nervous system (SNS)** stimulates the so-called “fight or flight” response via adrenergic signalling pathways over the *nervi cardiac* and thereby increases heart activity. Sympathetic nerve fibres travel along the epicardial vascular structures of the heart and reach into the myo- as well as endocardium as nerve terminals, effecting the whole heart. Upon stimulation, these fibres release the transmitter norepinephrine or the hormone epinephrine, which both primarily bind to β1/2-adrenergic receptors on cardiac myocytes. The coupled GαS protein activates the production of cyclic AMP (cAMP) by the adenylate cyclase, leading to an increased activity of protein kinase A (PKA), which in return phosphorylates L-type calcium channels (LTCC; *CaV1.2*) and other calcium related proteins of the so-called excitation-contraction-coupling (Figure 3; ECC, section 1.2) machinery. The enhanced phosphorylation ultimately increases calcium influx, promoting greater myocardial contractility, impulse conduction via the AV node and increasing heart rate through the

modulation of pacemaker cells in the sinoatrial node (Deetjen, Speckmann et al., 2005; Florea and Cohn, 2014; Gründer & Schlüter, 2023).

Simultaneously, the heart is able to adapt its ventricular ejection to the blood inflow via modulation of the contraction force. This autoregulation of the heart is called the "**Frank-Sterling mechanism**" and is achieved in a nerves and hormones independent manner. The mechanism works via a strain-dependent change in calcium sensitivity of the contractile myocardium, leading to an increased sarcomere length and thereby to an increased elastically force through titin. With this increase in radial forces, the contractile filaments come into closer proximity, making it easier for cross-bridge binding. The Frank-Sterling mechanism enables the adaption of the ejection capacities of the left and right ventricle accordingly and to react to pressure differences in an autonomous manner (Gründer & Schlüter, 2023; Speckmann, 2019).

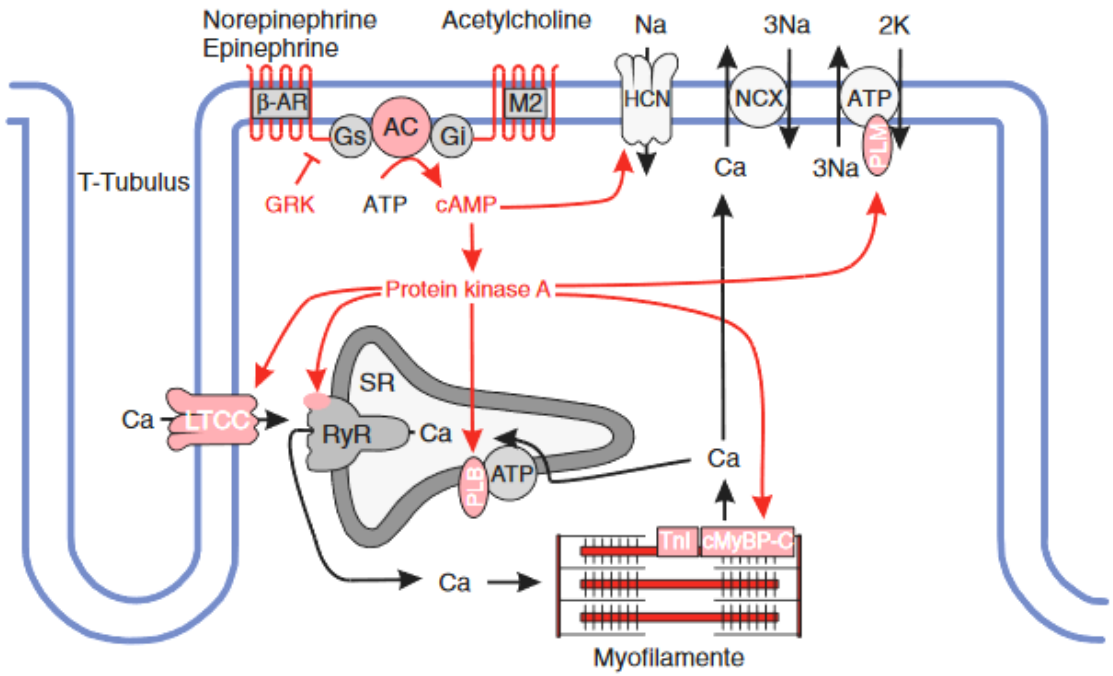

Figure 3 | Adrenergic and cholinergic signalling pathways and PKA response in cardiomyocytes. While acetylcholine inhibits cAMP production by binding to M2-cholinoceptors (M2), the binding of norepinephrine/epinephrine to β-adrenergic receptors (β-AR) enhances the production of cAMP, thereby leading to an activation of protein kinase A (PKA). In response, active PKA phosphorylates key regulatory proteins controlling excitation-contraction coupling. LTCC, L-type calcium channels; Gs, GαS proteins; AC, adenylate cyclase; HCN, hyperpolarization-activated cyclic nucleotide-gated ion channels; NCX, sodium-calcium exchanger; ATP, sarcolemmal Na+/K+-ATPase; PLM, phospholemman; RyR, ryanodine receptor; PLB, phospholamban; GRK, G protein–coupled receptor kinase; TnI, troponin-I; cMyBP-C, cardiac myosin-binding protein C. (Taken from El-Armouche & Eschenhagen, 2009)

1.2. Electrophysiology of the heart: excitation-contraction coupling

Excitation-contraction coupling (ECC) is a fundamental process for cardiac and skeletal muscle contraction, which involves the conversion of electrical excitation of the cell membrane (action potential) into mechanical contraction (Sandow, 1952; Bers, 2002). In the heart, an ECC initiates when an action potential travels along the sarcolemma into the T-tubules, leading to a depolarization and thus to an opening of L-type calcium channels (LTCC; *CaV1.2*) within the membrane. A small amount of calcium is released into the cytoplasm, which in return leads to a large increase in [Ca^{2+}] in the dyadic space. The calcium sensitive Ryanodine receptor (RyR2; *Ryr2*) opens and releases a ten-time higher amount of calcium from the SR, a mechanism termed calcium-induced calcium release (CICR; Fabiato, 1983). The high amount of calcium released induces the troponin C dependent sliding of the filaments and thereby the actual contraction. Shortly after every contraction, relaxation has to be re-established, meaning the closing of the RyR channels and proper re-uptake of calcium into the SR by the ATPase SERCA2a (SR Ca^{2+}-ATPase*; ATP2a2*) as well as removal of excess calcium out of the cytoplasm mainly through NCX (sodium-calcium exchanger). As soon as [Ca^{2+}] declines to a certain level, troponin C is re-attached to the myosin binding sites on actin filaments and the myocyte can undergo the next round of excitation (Cheng, Lederer & Cannell, 1993; Bers, 2002; Eisner et al., 2017).

The whole process of ECC shows that an essential driver for contraction as well as relaxation is the ubiquitous second messenger calcium and its amount within certain cell compartments. The proper opening/closing of channels and the function of transporters is fundamental for proper heart function and is, as already mentioned, tightly coordinated by regulatory proteins, which are either phosphorylated by PKA and/or the *Ca^{2+}/calmodulin-dependent protein kinase II* (CAMKII) or dephosphorylated due to hydrolyzation of cAMP (Peterson et al., 1999; Wehrens et al., 2006; Anderson, Brown & Bers, 2011).

In addition, the whole EC-coupling is highly dependent on the precise localisation and spatial arrangement of all of the involved channels, transporters and interacting proteins. Dysregulation as well as mislocalisation of e.g. the LTCC, SERCA2a or components of the calcium-release complex have been linked to cardiac diseases in both mice and humans (Marks, 2013; Zhihao et al., 2020; section 1.2.1).

1.2.1. The calcium-release complex: the role of triadin in regulating SR structure and calcium cycling

The process of excitation-contraction coupling is highly dependent on the structural characteristics of the myocytes and the spatial arrangement of certain cell compartments. The most important structure in this regard is the earlier mentioned dyad (triad in skeletal muscle). Deep invaginations of the sarcolemma, which occur at the Z-line of each sarcomere, form transverse tubules (T-tubules) and make close contact to the junctional sarcoplasmic reticulum (j-SR). The adjacent association of these structures enables the close contact of L-type calcium channels on the t-tubules to the calcium-release complex on the SR membrane, thus forming a functional unit, which is essential for the initiation of CICR (Figure 4; Eisner et al., 2017).

The **calcium-release complex (CRC)** is a quaternary complex composed of the ryanodine receptor 2 (*RyR2*), triadin (*Trdn*; trisk), junctin (*Jnt*; *Jun*; *Asph*) and calsequestrin 2 (*Casq2*), presenting one of the most important complexes regarding signal transduction in the heart. The major component is the RyR2, which belongs to a class of intracellular calcium channels responsible for the release of Ca^{2+} from the sarcoplasmic reticulum. Comprising a homotetramer of RyR2 isoforms, each monomer exceeding 500 kDa, it forms a mushroom like shape consisting of a large cytoplasmic head and a transmembrane stalk. The N-terminal domain, located in the cytoplasm, engages in multiple interactions with regulatory proteins, contributing to the receptor's sensitivity to various modulators like phosphorylation, redox modifications and small ions like Mg^{2+} and Ca^{2+}(Petegem, 2012; Lanner et al., 2010). Various studies demonstrated that misregulated RyR2 can induce fatal cardiac ventricular arrhythmias, which have been linked to a disease called catecholaminergic polymorphic ventricular tachycardia (CPVT). These "triggered arrhythmias" are a consequence of an aberrant calcium release from the SR via RyR2, initiating delayed afterdepolarizations (DADs; Wehrens et al., 2003; Vest et al., 2005; Yuan et al., 2014).

Triadin is a major component of the CRC and plays a pivotal role in ryanodine receptor regulation and calcium-release. This transmembrane protein exhibits a high degree of conservation across species and was initially identified in the triads of skeletal muscle tissue in the 1990s as a sizable 95 kDa protein, termed trisk95. Subsequent studies revealed its association with excitation-contraction coupling and identified an alternative splice variant in skeletal muscle, referred to as trisk51 due to its molecular

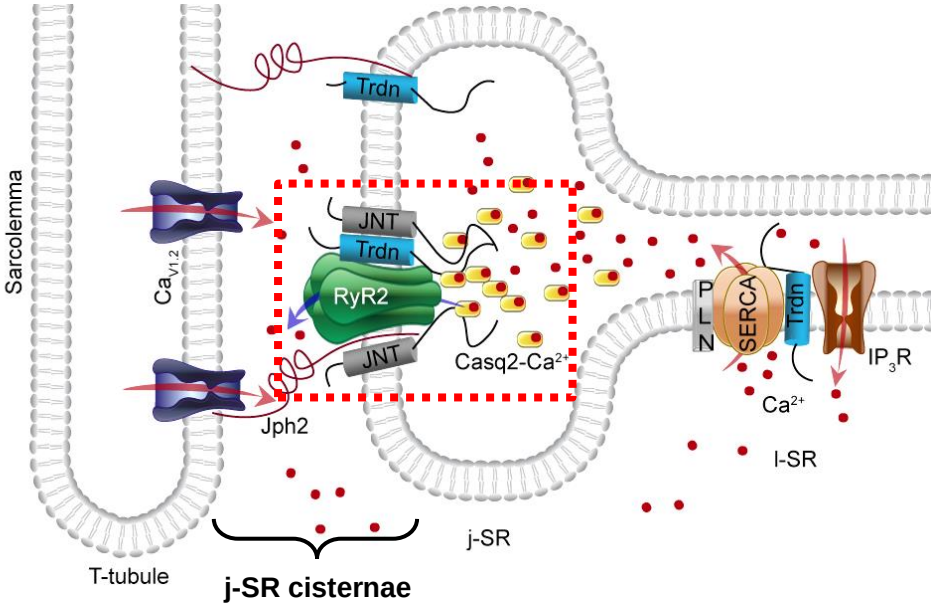

Figure 4 | Schematic representation of the cardiac dyad and the calcium-release complex. In the heart, the calcium-release complex (red dashed box) localizes to the junctional Sarcoplasmic reticulum membrane (j-SR) at the dyad. The main protein components of the CRC are the ryanodine receptor 2 (RyR2), junctin (JNT), triadin (TRDN) and the calcium carrier calsequestrin 2 (CASQ2). Within the longitudinal SR (l-SR) cardiac TRDN, the inositol 1, 4, 5 - trisphosphate receptor (IP_3R), the calcium ATPase SERCA2a and phospholamban (PLN) are localized. Junctophilin 2 (JPH2) determines the luminal width between j-SR and the t-tubule by anchoring these two membrane compartments. Blue arrows indicate calcium release from the SR while red arrows indicate release into the cytoplasm or reuptake from the cytoplasm into the SR lumen.

size of 51 kDa. Further studied across different species unveiled an additional 32 kDa cardiac specific isoform, raising inquiries about the homologous as well as tissue specific functions of distinct triadin isoforms (Figure 5A, B; Brandt et al., 1990; Kim et al., 1990; Brandt et al., 1993; Peng et al., 1994; Guo et al., 1996; Kobayashi YM, Jones LR, 1999). All these isoforms are truncated versions of the long 95 kDa isoform with C-terminal domains of variable length (Figure 5C). While trisk95 and trisk51 are specific to skeletal muscle, the smallest trisk32 constitutes less than 10% of the total TRDN protein in skeletal muscle, but is the only expressed isoform in cardiomyocytes. The subcellular localisation of triadin proteins varies based on their isoform and tissue. In skeletal muscle, studies consistently indicate that trisk95 and trisk51 are confined to the junctional SR within the triad, whereas trisk32 is observed in the longitudinal SR. Within the longitudinal SR (l-SR), trisk32 is closely associated with IP_3-receptors as well as the ATPase SERCA2a, hinting at potential roles in calcium handling as well as protein localisation throughout the entire sarcoplasmic reticulum (Vassilopoulos et al., 2005). In adult cardiomyocytes, trisk32 was initially presumed to be restricted to the j-

SR at the cardiac dyad, but there is additional evidence for its presence in the l-SR (Oddoux 2009; Marty et al., 2015).

In accordance to the expression as well as localisation of the different triadin isoforms, the interaction partners also differ between tissues and subcellular localisation. The ryanodine receptor, junctin as well as calsequestrin could be identified as direct interaction partners of trisk95, trisk51 and trisk32 in both tissues (Kobayashi YM, Jones LR, 1999; Kirchhefer, et al., 2001/2004; Vassilopoulos et al., 2005; Marty et al., 2015). In the heart as well as in skeletal muscle, triadin functions together with the transmembrane protein junctin in anchoring the ryanodine receptor to the j-SR as well as facilitating the binding of CASQ2 in close proximity to the ryanodine receptor for proper calcium release. Calsequestrin is the major calcium-binding protein within the junctional sarcoplasmic reticulum and is responsible for Ca^{2+} storage as well as buffering. It undergoes polymerization upon increasing calcium concentrations while depletion of calcium from the SR leads to depolymerisation and thereby less binding. Calsequestrin mono- and polymers also show differential binding affinities to triadin and junctin (Wang & Michalak, 2020).

This interplay was further elucidated by studies with Calsequestrin 2 KO and mutation mouse models, demonstrating that deletion and loss of function in the heart results in an increase in SR volume, spontaneous calcium release as well as developing CPVT due to ventricular arrhythmias. As a side effect, the expression of triadin as well as junctin is nearly abolished in KO mice further increasing the risk of spontaneous calcium release trigged ventricular arrhythmias (Knollmann et al., 2006; Song et al., 2007; Terentyev et al., 2008).

Various mouse models with isoform-specific, tissue-specific or full deletions have been established to elucidate triadin function and interactions. In skeletal muscle, the full deletion of triadin has been shown to impact triad morphology and reduce calcium cycling. The KO mice exhibited abnormal orientation of triads and a decrease in SR terminal cisternae volume, as well as a decline in the total amount of calcium stored within the SR lumen. The most significant changes included reduced calsequestrin as well as a substantial increase in LTCC. Physiologically, these mice suffered a reduction in muscle strength and developed muscle myopathy (Oddoux et al., 2009).

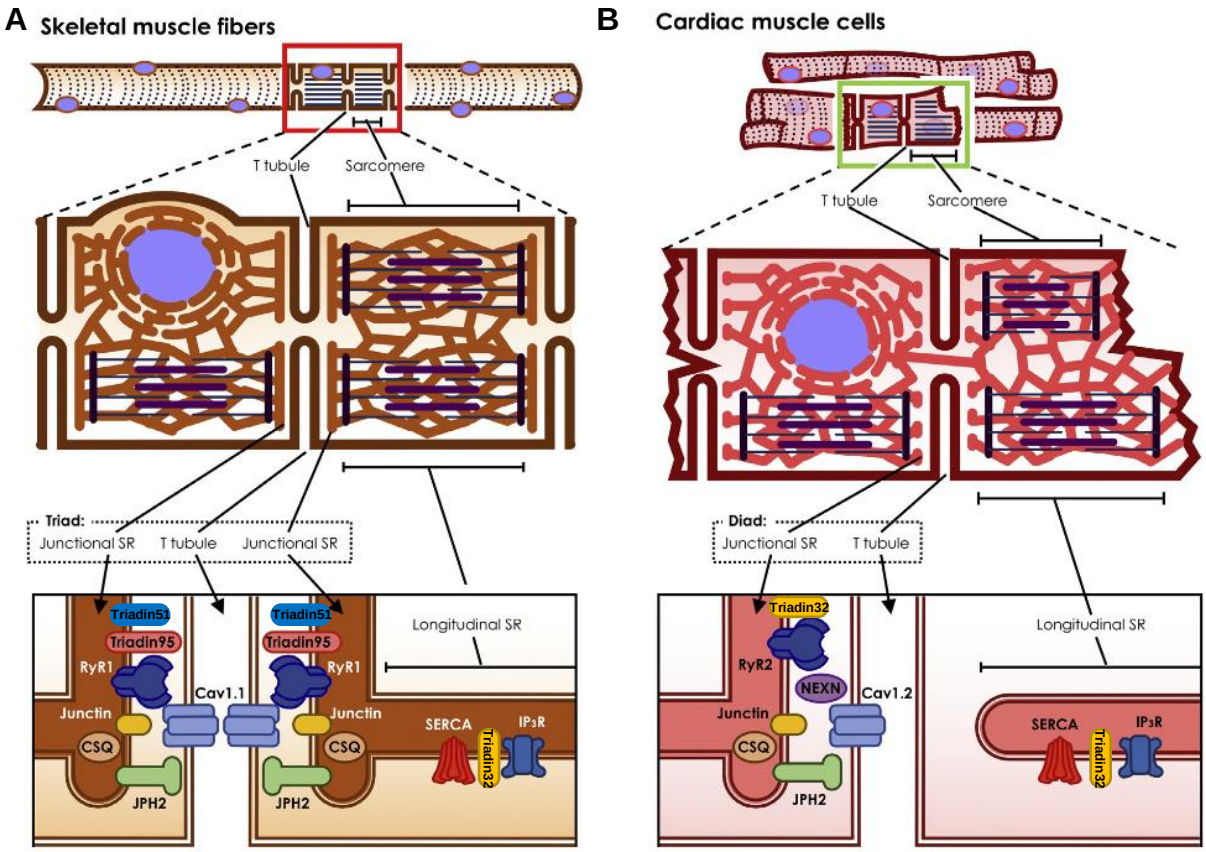

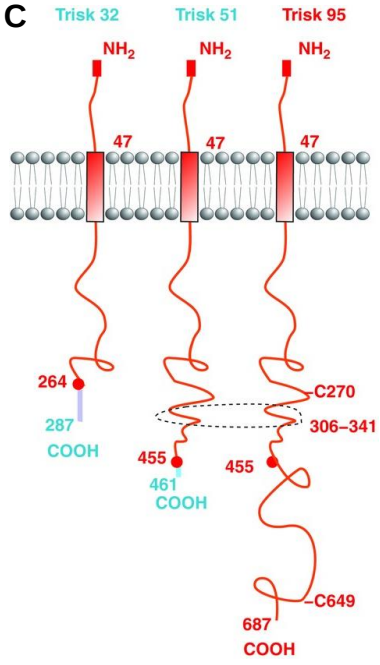

Figure 5 | Structural characteristics of striated muscle cells, the sarcoplasmic reticulum and triadin localisation. A In skeletal muscle t-tubule are aligned by j-SR on each side forming a triad structure. These triads harbour the calcium release unit (CRU), comprising the ryanodine receptor 1 (RyR1), which is in direct contact to the L-type calcium channels (Cav1.1), junctin, calsequestrin (Casq1; CSQ) and trisk95 as well as trisk51. **B** In cardiac muscle cells, the t-tubule forms a complex with only one j-SR cisternae, termed dyad. The CRU built is very similar, with the exception of trisk32 being the only triadin isoform and no direct interaction of RyR2 and CaV1.2 channels due to cardiac specific structural proteins like nexilin. **A, B** Within the l-SR, trisk32 co-localizes to the SERCA and the Inositol 1,4,5-trisphosphate receptor (IP_3R) channels in both tissues (Changed after Bravo-Sagua, 2020). **C** The three main TRDN isoforms in rat and mice share the same N-terminal domain and transmembrane helix, but have unique C-terminal ends. The two cysteins C270 and C649 as well as the coiled-coil segment 306-341 of Trisk51 and Trisk95 are involved in membrane deformations as well as indirect microtubule interaction. (Modified after Marty, 2015)

In contrast, the consequences in the heart appeared more severe, as at least three known triadin mutations result in protein degradation, leading to the development of CPVT in both mice and humans (Roux-Buisson et al., 2012). In 2015, a study by Altmann et al. linked symptoms in multiple patients with long QT syndrome (LQTS) and sudden cardiac arrest to two homozygous and compound heterozygous mutations within the *Trdn* gene. These mutations, resulting in an immediate stop codon before the KEKE motif (RyR2 and CASQ2 interaction side; p.K147fs*0) or a frameshift mutation in Exon 1 (p.N9fs*5), caused a loss in triadin protein. This led to extensive T-wave inversions and exertion or stress-induced syncope, resulting in sudden cardiac arrest or death in young patients, termed Triadin KnockOut Syndrome (TKOS; Figure 6; Altmann et al., 2015).

A similar phenotype is observed in KO mouse models, where triadin ablation leads to a nearly complete loss of associated proteins CASQ2 and JUN, and to a major decrease in RyR2 as well as JPH2 within the j-SR, whereas Cav1.2 and SERCA remained unchanged. These changes only occurred on protein level whilst mRNA levels remained largely unchanged, suggesting a potential role for triadin in stability, targeting or retention of its direct binding partners. Electron microscopy revealed a 50% reduction in j-SR and T-tubule contact sides, along with a reduced co-localisation of RyR2 and L-type calcium channels, indicating an overall loss of dyadic structure and CRC integrity, potentially due to a loss of the membrane-spanning protein JPH2 (Figure 6A). As a result, triadin KO mice exhibit reduced SR calcium release causing an increased SR Ca^{2+} load. This overload was exacerbated by the loss of negative feedback on the current inactivation of L-type Ca^{2+} channels by SR calcium channels, resulting in an increased calcium release into the cytoplasm (Figure 6B). Although *Trdn* KO mice are viable, echocardiography measurements revealed increased heart contractility leading to sinus bradycardia and increased p-wave amplitude on ECG measurements. Upon β-adrenergic stimulation with Isoproterenol (Iso), *Trdn* KO mice displayed spontaneous calcium release, causing DADs and symptomatic ventricular arrhythmias associated with CPVT (Chopra et al., 2009).

Interestingly, the overexpression of trisk32 in murine hearts resulted in a higher SR Ca^{2+} load and an increased diastolic SR calcium leak. These alterations were accompanied by a 50-70% decrease in protein levels of RyR2 and JNT, while CASQ2, SERCA2a and PLB stayed unchanged. Upon β-adrenergic stimulation, the transgenic mice exhibited a blunted response with a decrease in PLB phosphorylation as well as

LTTC peak current. In summary, overexpression of trisk32 in the heart alters SR calcium handling, resulting in depressed contractility and cardiac hypertrophy (Kirchhefer et al., 2001/2004/2007).

While the abundance and function of triadin isoforms have undergone intensive studies within skeletal muscle, our understanding of the distribution and interaction of triadin in cardiac cells remains limited. This gap is noteworthy, given the fact that dysregulation of triadin has severe consequences on calcium cycling and consequently on cardiac function both in mice and humans. In future investigations, elucidating triadin localisation and interaction in the heart could be fundamental to understand the underlying mechanisms of excitation-contraction coupling, shedding light on the pathogenesis of human CPVT diseases.

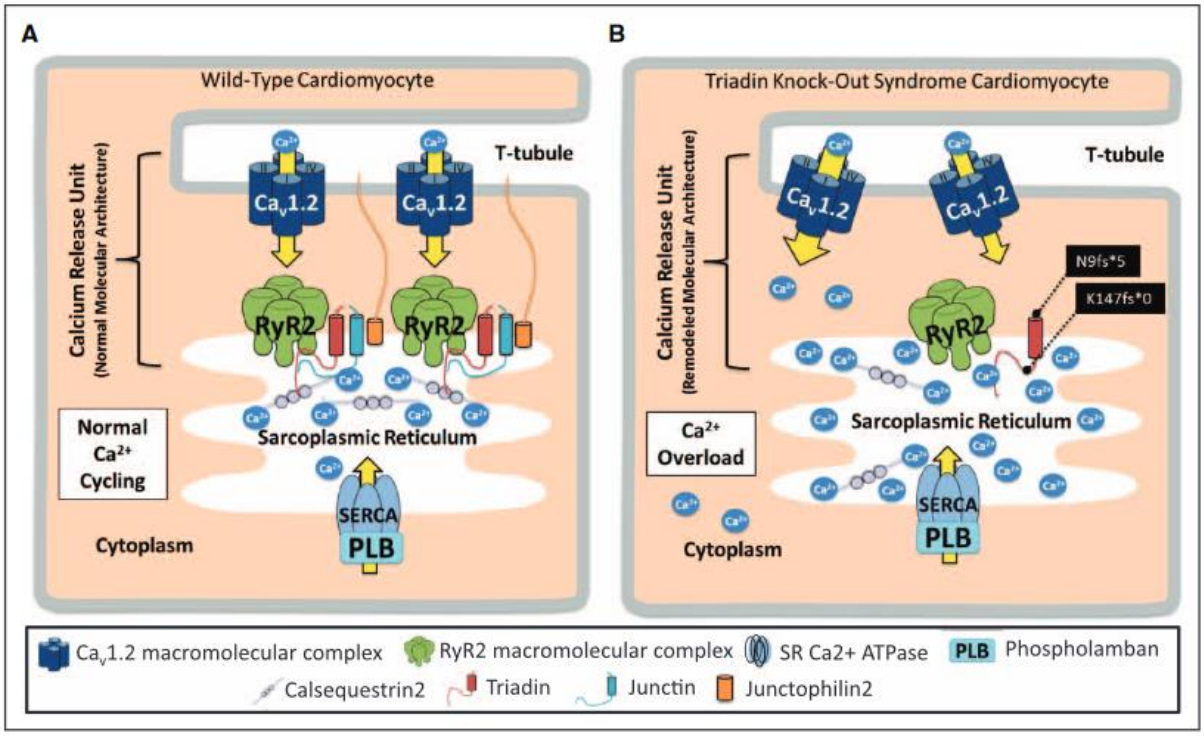

Figure 6 | The molecular basis of the triadin knockout syndrome. A In a functioning cardiac dyad, all involved components are correctly localized and ryanodine receptors juxtaposed to CaV1.2 resulting in a normal calcium cycling. **B** The remodelled calcium release unit in Triadin Knock-Out Syndrome cardiomyocytes shows loss of juxtaposed localisation of RyR2 and CaV1.2, loss of normal junctin and junctophilin expression/function as well as a miss-localisation of calcium and calsequestrin in the SR, resulting in disturbed calcium handling and a calcium overload within the SR. (Taken from Giudicessi & Ackermann, 2016)

1.3. Long non-coding RNAs: Multi-talents of gene regulation

The human nucleus contains approximately 2 meter of linear DNA, tightly folded into a three-dimensional structure. It has long been assumed that this DNA only harbours uni-directional genetic information, transcribed into mRNA and subsequently translated into proteins, called the central dogma of molecular biology (Crick, 1961). However, recent decades of scientific exploration have rendered this dogma obsolete with the discovery of various classes of non-coding RNAs (ncRNAs; Yanofsky, 2007). Despite lacking coding potential, these ncRNAs play diverse roles in various kinds of biological processes. In fact, less than 3% of the whole genome encodes for mRNAs while more than 80% is transcribed but displays no coding potential (Figure 7A; Amaral et al., 2008; Derrien et al, 2012; Djebali et al., 2012). Non-coding RNAs can be categorized into distinct groups depending on their length and structural identity like tRNAs, rRNAs and the two major groups dividing small non-coding RNAs and long non-coding RNAs (lncRNAs). The extensively studied group of the small non-coding RNAs, generally smaller than 200 nucleotides, encompasses well-conserved classes such as microRNAs (miRNAs), small nuclear RNAs (snRNAs), small nucleolar RNAs (snoRNAs), piwi-interacting RNAs (piRNAs) and small interfering RNAs (siRNAs) (Ghildiyal & Zamore, 2009; Mendel & Olson, 2012). Over the past decade the focus of scientific research has shifted towards the second group, presented by the long non-coding RNAs. LncRNAs, exceeding 200 nucleotides, are transcribed by polymerase II and mostly spliced, 5'-capped and polyadenylated. Despite their primary sequence often lacking conservation, their mode of action extends across various species (Taft et al., 2010; Rinn & Chang, 2012; Uchida & Dimmeler 2015).

The human GENCODE statistic counts nearly 20,000 lncRNA genes and more than 58,000 lncRNA transcript loci in the human genome to date (GENCODE Release 44). Given such high numbers of long non-coding genes and transcripts, further categories are used, mainly depending on their genomic localization in relation to protein-coding genes (Figure 7B; Wu et al., 2017; Ghildiyal et al., 2018):

- **Intergenic:** between two protein-coding genes with no overlap and a certain distance. Also called long intergenic non coding RNAs (lincRNAs)
- **Sense:** commonly share transcription from the same promoter as a protein-coding gene
- **antisense:** in opposite direction to a protein-coding gene with individual promoter

- **intronic:** transcribed from introns of protein-coding genes
- **enhancer RNAs**: emerge from enhancer regions within or outside of protein-coding genes (eRNAs; elncRNAs)
- **circular:** usually arise from splicing of protein-coding genes and form covalently enclosed circular rings (circRNAs)

The long-time underestimation of lncRNAs can be attributed to their low expression levels as well as limited conservation. Consequently, lncRNAs were often dismissed as background noise in many studies, particularly those associated with regulatory-regions as elncRNAs, promoter ncRNAs, intronic lncRNAs and bidirectional lncRNAs. Fortunately, the continual advancements in next-generation sequencing techniques, especially in RNA and long-range sequencing, steadily unveils new classes of long non-coding RNAs. These technological developments expand the possibilities for studying molecular functions of lncRNA *in vitro* and *in vivo* (Guttman & Amit et al., 2009 Mattick & Rinn, 2009; Xie et al., 2014; Uchida & Dimmeler 2015; Chen et al., 2023).

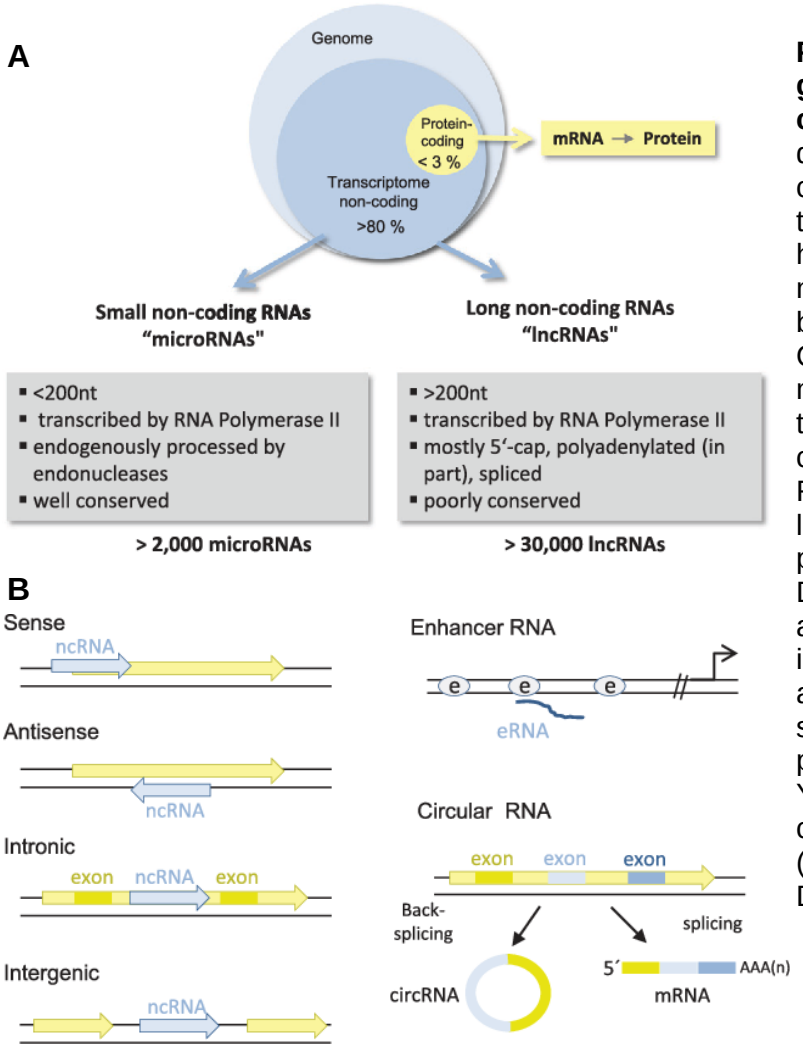

Figure 7 | The non-coding genome and its classification. A Pie chart displaying the distribution of coding- vs non-coding transcripts. Over 80 % of the human genome is considered non-coding with many of them being long non-coding RNAs. Grey boxes summarize the most important features of the two non-coding classes. **B** The classification of non-coding RNAs relates to their genomic localisation in relation to protein-coding genes. Depicted here are sense-, antisense-, intronic-, intergenic-, enhancer- as well as circular-lncRNAs. Not shown are bidirectional and promoter associated lncRNAs. Yellow boxes indicate protein-coding genes. E, enhancer. (Taken from Uchida & Dimmeler 2015)

1.3.1. Mechanism and functions of *trans*- and *cis*-acting lncRNAs

In contrast to mRNAs and miRNAs, lncRNAs exhibit diverse mechanisms for regulating gene expression and have emerged as crucial gene regulators. While miRNAs typically decrease gene expression by binding to a target mRNA sequence, leading to degradation, lncRNAs possess the capability to either suppress or activate gene expression at the DNA, RNA and protein level (Wapinski & Chang, 2011). LncRNAs are able to regulate gene expression via modulation of chromatin structure and function, transcriptional activation or repression as well as by interfering with RNA splicing, stability and translation (Rin & Chang, 2012; Wang & Chang, 2011). Despite the vast potential of lncRNAs, most annotated ones are yet to undergo functional studies and due to their diverse functions, a clear categorization based on their molecular function has not been established yet. A widely accepted classification involves the proximity of the genetic loci of the long non-coding RNA to their target gene. ***Cis*-acting lncRNAs** regulate target genes within the same loci or the same chromosome, whereas ***trans*-acting lncRNAs** impact genes at distal genomic loci or operate within different cell compartments (Schonrock, Harvey & Mattick, 2012; Anderson & Anderson, 2022). *Cis*-acting lncRNAs regulate gene expression, in most cases, by interacting with regulatory gene elements (enhancer, promoter region) or recruiting of additional regulatory proteins (e.g. chromatin remodeller/modifier; Figure 8B). Nonetheless, *cis*-acting lncRNAs can also achieve gene regulation through simple transcription in a sequence-independent manner. In contrast, *trans*-acting lncRNAs, being detached from their chromosomal locus, possess numerous possibilities for gene regulation. Their actions are typically dependent on RNA sequence and conformation, and many mechanisms include RNA-Protein interactions to establish inter-chromosomal interactions, inhibit or facilitate binding to a target DNA region or influence translation efficiency within the cytoplasm (Figure 8A; Liu & Lim, 2018; Statello et al., 2021; Mattick et al., 2023).

Gene regulation by long non-coding RNAs. Numerous lncRNAs are known to date which facilitate gene regulation *in cis* as well as *in trans* by interacting with chromatin modifiers and recruiting them to target-gene promoters or gene bodies. This recruitment can be activating as well as suppressing for the target gene transcription. In this regard, the first described and one of the most intensively studied lncRNAs is the X-inactive specific transcript (*Xist*) lncRNA. Drawing attention in 1991 in the context

of dosage compensation, *Xist* was demonstrated to cover the entire inactive X-chromosome in females of higher vertebrate. Ongoing studies revealed, that *Xist* is able to recruit the polycomb repressive complex 2 (PRC2) to initiate the heterochromatinization of the whole chromosome and thereby almost completely represses the transcriptional activity *in cis* (Brockdorff et al., 1991; Colognori et al., 2019; Wang et al., 2021).

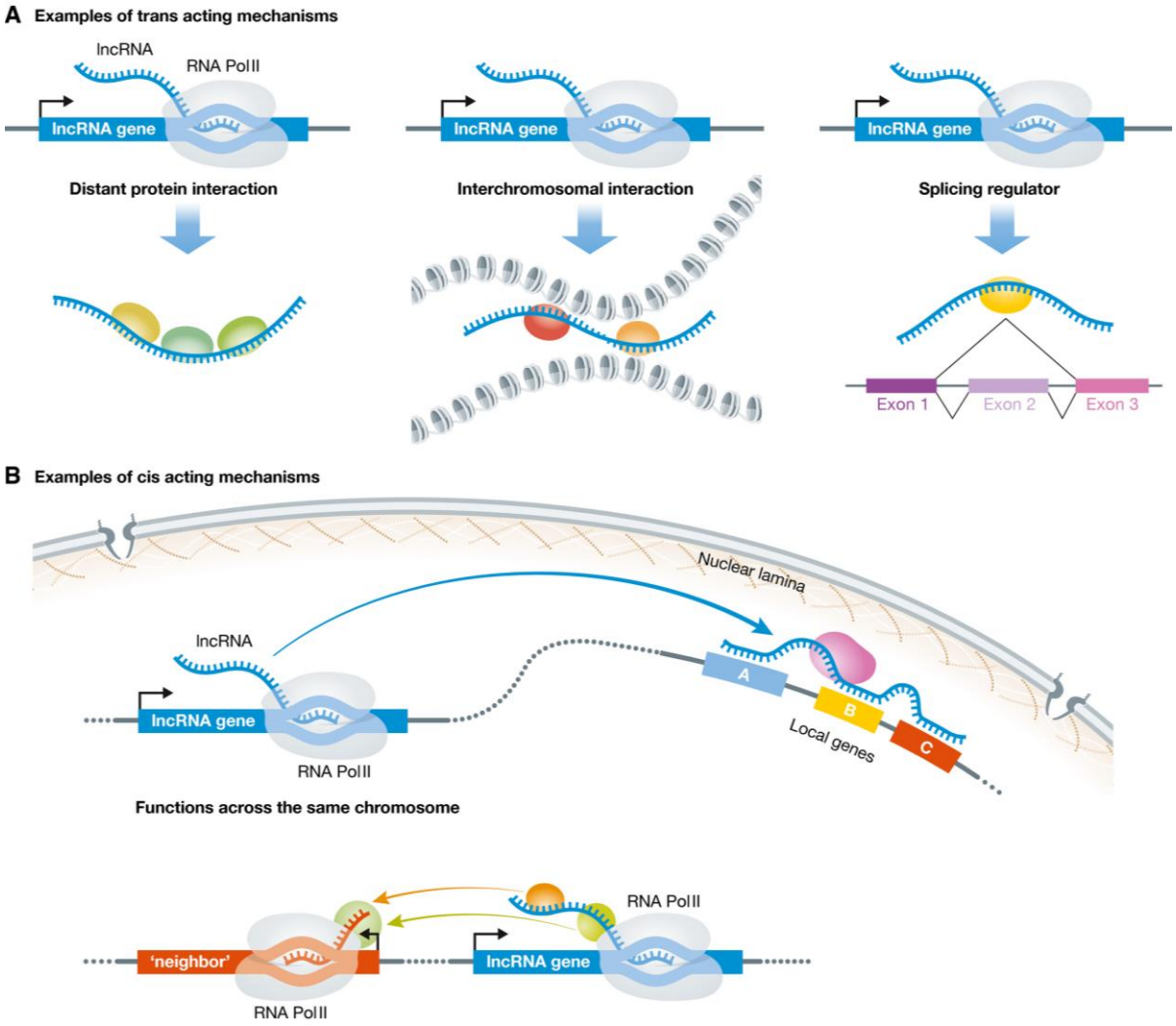

Figure 8 | The molecular mechanisms of lncRNA functions. A trans-acting lncRNA mechanisms affect genes at distal loci or can even modulate gene expression outside of the nucleus. Depicted mechanisms shown here include distal protein interactions (e.g. *HOTAIR*, *lncMyh*), interchromosomal interactions (e.g. *FIRRE*) and splicing regulation (e.g. *MALAT1*, PNCTR). **B** cis-acting lncRNA mechanisms regulate gene expression on the same chromosome or within the same gene locus. Mechanisms across the same chromosome can regulate gene expression by for example recruitment of proteins (e.g. *XIST*, *COOLAIR*). LncRNAs can also regulate neighbouring genes in-cis through their own process of transcription by changing the chromatin organization (e.g. *TARID*), promoter accessibility (e.g. Airn) or regulate splicing (e.g. *ZEB2-AS1*, *Brd1as*). (Taken from Liu & Lim, 2018)

To enable cell-specific functions at distinct stages, *In-trans* acting long non-coding RNAs not only recruit protein complexes but can also alter their composition. One example presents the skeletal muscle specific RNA *lncMyh* (myosin heavy chain gene cluster associated), which directly interacts with the chromatin remodeler complex Ino80 in myoblasts and myotubes, thereby modulating its molecular composition (Schutt et al., 2020). Another intriguing mechanism of lncRNAs to regulate chromatin has drawn attention in recent years, involving the formation of RNA:DNA hybrids known as R-loops. R-loops can form either in-cis or in-trans via the interaction between an lncRNA and DNA. For example, the antisense long non-coding RNA *RASSF1* (*ANRASSF1*) forms an RNA:DNA hybrid *in cis,* directing PRC2 to the promoter region of the protein-coding gene RASSF1A, while lncRNA *APOLO* recognizes specific motifs at the promoter region of target genes, where it binds and forms R-loops *in trans*. (Beckedorff et al., 2013; Ariel et al., 2020).

Gene regulation on the act of non-coding transcription. Despite the fact, that there are numerous lncRNAs working in a sequence- and recruitment-specific manner, non-coding RNAs can also function only via their mode of transcription. These lncRNAs only influence their own genetic region and the actual RNA product is dispensable, making them *a priori cis* acting lncRNAs. The modes of regulation include the change in general chromatin organization, a transcriptional interference or if the RNA polymerase II encounters regulatory elements while travelling along the DNA. The resulting gene regulation can be either activating or repressing (Kornienko et al., 2013).

The vast majority of *a priori cis* acting long non-coding RNAs modulate gene expression via transcription mediated silencing, also referred to as transcriptional interference (Martens, Laprade & Winston, 2004). In this case, the transcription of the non-coding gene leads to a repression or inactivation of the corresponding protein-coding gene. The underlying mechanism is in many cases still unclear but there have been several theories postulated. One commonly accepted model describes transcriptional interference as a consequence either of an influence on the promoter/enhancer accessibility or of the RNA polymerase II transcription elongation, splicing or polyadenylation (Pelechano & Steinmetz, 2013). For transcriptional interference to occur, the only necessary feature needed are overlapping promoter or intergenic regions harbouring intersecting DNA regulatory regions. Thereby the genomic localization of the non-coding RNA and the protein-coding gene can be on

the same strand, but in the majority of cases, the non-coding RNA is located opposite to its target protein. These lncRNAs constitute their own subclass namely long non-coding antisense RNAs or natural antisense transcripts (NATs), with exons partially overlapping (Lapidot & Pilpel, 2006; Pelechano & Steinmetz, 2013; Srijyothi et al., 2018). For instance, the antisense lncRNA *Airn* (antisense to insulin-like growth factor 2 receptor (*Igf2r*)) has been intensively studied in mouse ESC, where it regulates genomic imprinting only via its transcription. The transcriptional overlap combined with a strong *Airn* promoter compared to a rather 'sensitive' *Igf2r* promoter is sufficient for silencing *Igf2r*. In contrast to other imprinted genes, no methylation or different repressive chromatin state is necessary, but a constant expression of the lncRNA *Airn* (Latos et al., 2012; Santoro et al., 2013; Andergassen et al., 2019; Andergassen & Rinn, 2022). Transcriptional interference can also go beyond simple gene silencing by promoter shielding as in the case of *Airn*. The simultaneous transcription of an intergenic antisense transcript can result in alternative splicing of the sense transcribed protein-coding gene by different mechanisms. In the case of human zinc finger E-box-binding homeobox 2 gene (*ZEB2*), its antisense RNA *ZEB2-AS1* induces the retention of an intron containing an internal ribosome entry site by protecting the 5' splice site. The alternatively spliced mRNA increases its translation efficiency and thereby the protein abundance (Figure 9C; Beltran et al., 2008).

While the *ZEB2* transcribing polymerases avoid interferences, the consequence of opposing RNA polymerases typically results in a collision, eventually leading to transcription termination (Figure 9A). This scenario enables one polymerase to serve as a 'roadblock' for the incoming polymerase, effectively regulating gene expression and isoform abundance. The initiation of transcriptional interference through roadblock formation involves a regulatory DNA element or interaction partner that extends polymerase occupancy time, leading to elongation repression (Shearwin, Callen & Egan, 2005; Kornienko et al., 2013). In studies involving *Saccharomyces cerevisiae*, the expression of the non-coding antisense transcript regulator of meiosis 2 (*RME2*) induces transcription termination of the *IME4* gene via a 450 bp internal region inducing elongation repression and thereby blocking sense transcription (Figure 9B; Gelfand et al., 2011). When elongation repression, followed by sense transcription termination, occurs at additional termination sites of the protein-coding gene, it can result in the generation of new isoforms (Figure 9D). The mechanism, where antisense lncRNA transcription leads to differential isoform expression, is implicated across various

species and appears to be a common regulatory mechanism for controlling alternative splicing. In mouse and human studies, multiple differentiation stages demonstrate a correlation between isoform abundance and non-coding antisense transcription. Examples include *Zmynd8as* and *Brd1as*, where antisense transcription of the non-coding genes correlates with the abundance of short isoforms of the sense protein-coding genes (Morrissy et al., 2011; Onodera et al., 2012; Pelechano & Steinmetz, 2013; Pisignano & Ladomery, 2021).

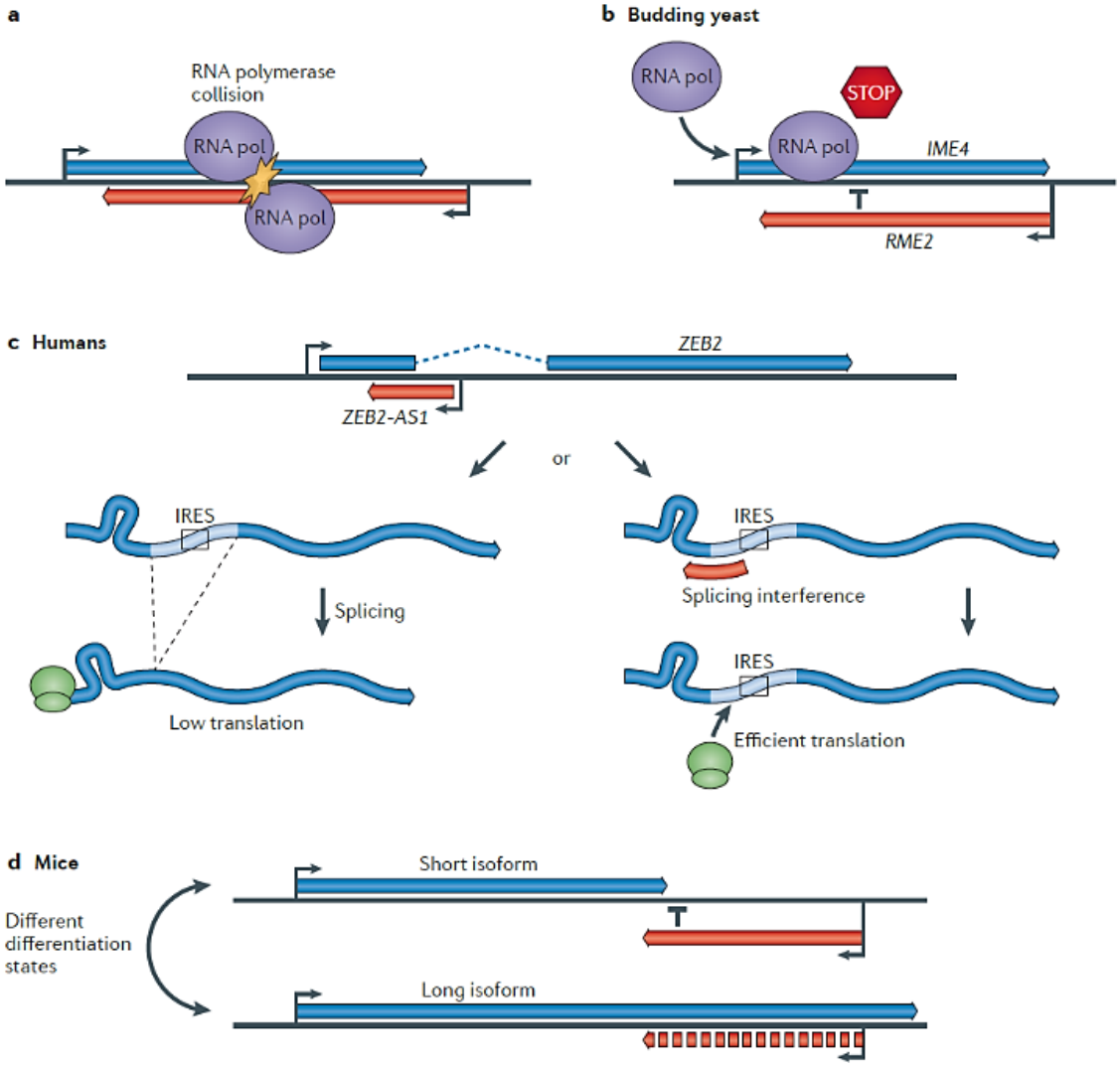

Figure 9 | Co-transcriptional effects of non-coding antisense transcripts. A opposing RNA polymerase II transcription can lead to collisions. **B** the transcription of the non-coding RNA *RME2* on the antisense strand leads to an elongation repression of the sense protein-coding gene IME4 and thereby to transcriptional interference. An internal sequence within the *RME2* direction is needed to stop sense-transcription. **C** in humans, *ZEB2-AS1* induces intron retention of its protein-coding gene by covering a 5' splice site, resulting in increased translation efficiency. **D** Transcriptional interference by the expression of intergenic antisense transcripts can result in the generation of new isoforms by limiting the length of the sense transcript. Upon loss of the antisense transcript, the long isoform can be re-established, as demonstrated in mice. (Taken from Pelechano & Steinmetz, 2013)

1.3.2. Long non-coding RNAs in cardiac function and disease

The occurrence of lncRNAs in a tissue- , cell- and stage-dependent manner has led to the assumption that they play time- and location dependent functions, opening new scientific research fields (Cabili et al., 2011). In this regard, the lncRNA dependent regulatory networks of the heart controlling development and adaptations represent a highly interesting field. By using deep-sequencing approaches numerous cardiac-specific lncRNAs have been identified, revealing differential expression during cardiovascular development and disease (CVD) (Wamstad et al., 2012). Many of these lncRNAs have highly specific promoter and enhancer motifs, possibly contributing to the spatial- and time dependent expression profiles (Vučićević et al., 2015; Mattioli et al., 2019). One extensively studied lncRNA in cardiac development is *Fendrr* (Fetal-lethal noncoding developmental regulatory RNA), which is highly expressed in the posterior mesoderm, the progenitor of the ventral body wall and the heart. Deletion of *Fendrr* leads to embryonic lethality around E13.5, due to heart failure. By interaction with the PRC2 and TrxG/MLL complexes, *Fendrr* regulates several transcription factors responsible for cardiac mesoderm differentiation and is therefore a pivotal regulator of chromatin signature in the developing heart (Grote et al., 2013). Another example is the lncRNA *Braveheart* (*BVHT*), expressed in cardiac mesoderm and adult cardiomyocytes. *In vitro* deletion of *BVHT* leads to a severe differentiation defect in neonatal cardiomyocytes, making the lncRNA a critical regulator of cardiac lineage commitment (Klattenhof et al., 2013). While the interest in lncRNA function has traditionally focused on developmental aspects, recent studies have expanded this interest to various pathways in the heart. These pathways encompass metabolism, differentiation and proliferation, contraction and conduction as well as hypertrophy and other aspects of CVD (Figure 10). For instance, the lncRNA *ANRIL* (*CDKN2B-AS1*) regulates important genes involved in glucose- and fatty-acid metabolism such as *ADIPOR1*, *VAMP3* and *TMEM258*, demonstrating the extensive function of this lncRNA in the cardiovascular system. Subsequently, *ANRIL* expression is used as a biomarker for coronary artery disease as well as for left ventricular dysfunction after myocardial infarct (MI) (Bochenek et al., 2013; Vausort, Wagner & Devaux, 2014; Devaux et al., 2015).

Given that the hearts main function is to generate the force required to pump blood throughout the body, two of the most intriguing systems influenced by lncRNAs refer

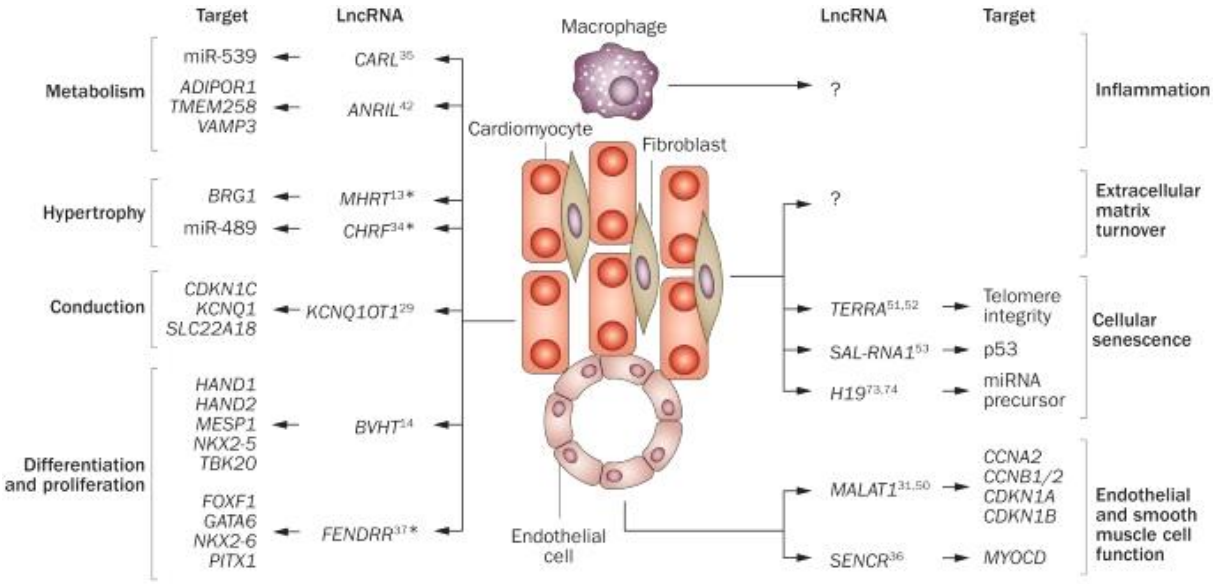

Figure 10 | Regulatory pathways of lncRNAs in different cardiac cell-types. Long non-coding RNAs are expressed in various kinds of cell types and regulate distinct molecular pathways, like metabolism, hypertrophy, sensecence and proliferation as well as differentiation in the heart. lncRNAs marked with an asterix * have been proven to regulate these processes in vivo. (Taken from Devaux et al., 2015)

to contraction and conduction. An example lncRNA presents *KCNQ1OT1* (*potassium voltage-gated channel subfamily KQT member 1 opposite strand 1*), which modulates the chromatin methylation of its sense protein coding gene *KCNQ1 in-cis* and distant genes like *SLC22A18* and *CDKN1C in-trans*. Dysregulation of this lncRNA has been linked to heart failure and has been implemented as a biomarker for left ventricular dysfunction (Figure 10; Mohammad et al., 2010; Korostowski et al., 2012). A more recently discovered long non-coding RNA involved in regulating contractility is *ZNF593-AS,* which is significantly downregulated in the expression profiles of patients with dilated cardiomyopathy (DCM). Notably, it is one of the lncRNAs that is primarily localized in the cytoplasm, where it binds the mRNA of *RyR2* and contributes to its stabilization. Overexpression of *ZNF593-AS* has been shown to restore aberrant calcium release of CMs after transverse aortic construction-induced cardiac dysfunction and therefore improves cardiac function in DCM (Fan et al., 2021). These two lncRNAs underscore the importance of lncRNA function in cardiac contractility and emphasize their potential as biomarkers and therapeutic targets to enhance cardiac function in diseased states. Ongoing screenings in human failing hearts continue to unveil a growing array of differentially expressed lncRNAs, with yet-to-be-explored molecular mechanisms and functions (Kohlmaier et al., 2023). One such long non-coding RNA demonstrates *AS-Trdn*, which will be further elucidated in the next section.

1.3.3. The lncRNA *AS-Trdn* regulates the isoform balance of the protein coding gene triadin in the heart

As previously detailed in section 1.2.1, triadin, a transmembrane protein crucial for regulating the sarcoplasmic reticulum calcium-release complex, undergoes differentially splicing between skeletal and cardiac muscle. Through deep RNA sequencing as well as microarray analysis of human failing and non-failing hearts, an antisense long non-coding RNA intergenic to triadin was discovered and termed *AS-Trdn* in mouse or *HRAT13* (heart related antisense transcript 13) in humans (Zhang et al., 2018). This lncRNA is exclusively expressed in the heart and exhibits exceptionally high conservation, mirroring the overall highly conserved triadin (Figure 11 A - C). Given these characteristics, *AS-Trdn* emerges as a highly interesting lncRNA and will therefore be the focal point of this scientific work.

AS-Trdn already gained attention in previous studies due to its differential expression in human heart failure. In a first study in 2018 by Zhang et al., *AS-Trdn* expression was positively correlated with the expression of the short cardiac specific isoform of triadin in the heart, in mice as well as in humans (Figure 11 B & C). This observation raised the question if *AS-Trdn* is responsible for the isoform abundance of trisk32 in the heart and whether dysregulation leads to a cardiac phenotype. Building on the findings related to other antisense lncRNAs, such as *Zmynd8as* and *Brd1as,* linked to isoform regulation upon transcription, *AS-Trdn* was further investigated in relation to triadin expression. Using the SP-dCas9-VPR system in HL-1 cells to overexpress *AS-Trdn* from its own promoter, the scientists significantly increased the abundance of the cardiac specific triadin isoform, confirming the initial hypothesis. The underlying mechanism by which expression of *AS-Trdn* induces alternative splicing of the short *Trdn* isoform and the physiological importance of the suggested regulation remained elusive, but a potential transcriptional interference by the two opposing RNA polymerases was postulated (Figure 11 C; Zhang et al., 2018). More recently, a second group focused on the function of the spliced *AS-Trdn* transcript in mouse cardiomyocytes and human induced Pluripotent Stem Cells derived cardiomyocytes (hIPSC-CMs). By genomic deletion of the second and third exon of the lncRNA, they sufficiently achieved a full loss of the spliced lncRNA expression in both models (Figure 12 A & B). The loss of *AS-Trdn* transcript led to impaired cardiac function, evidenced by a reduced ejection fraction of the heart and premature death in KO mice starting at

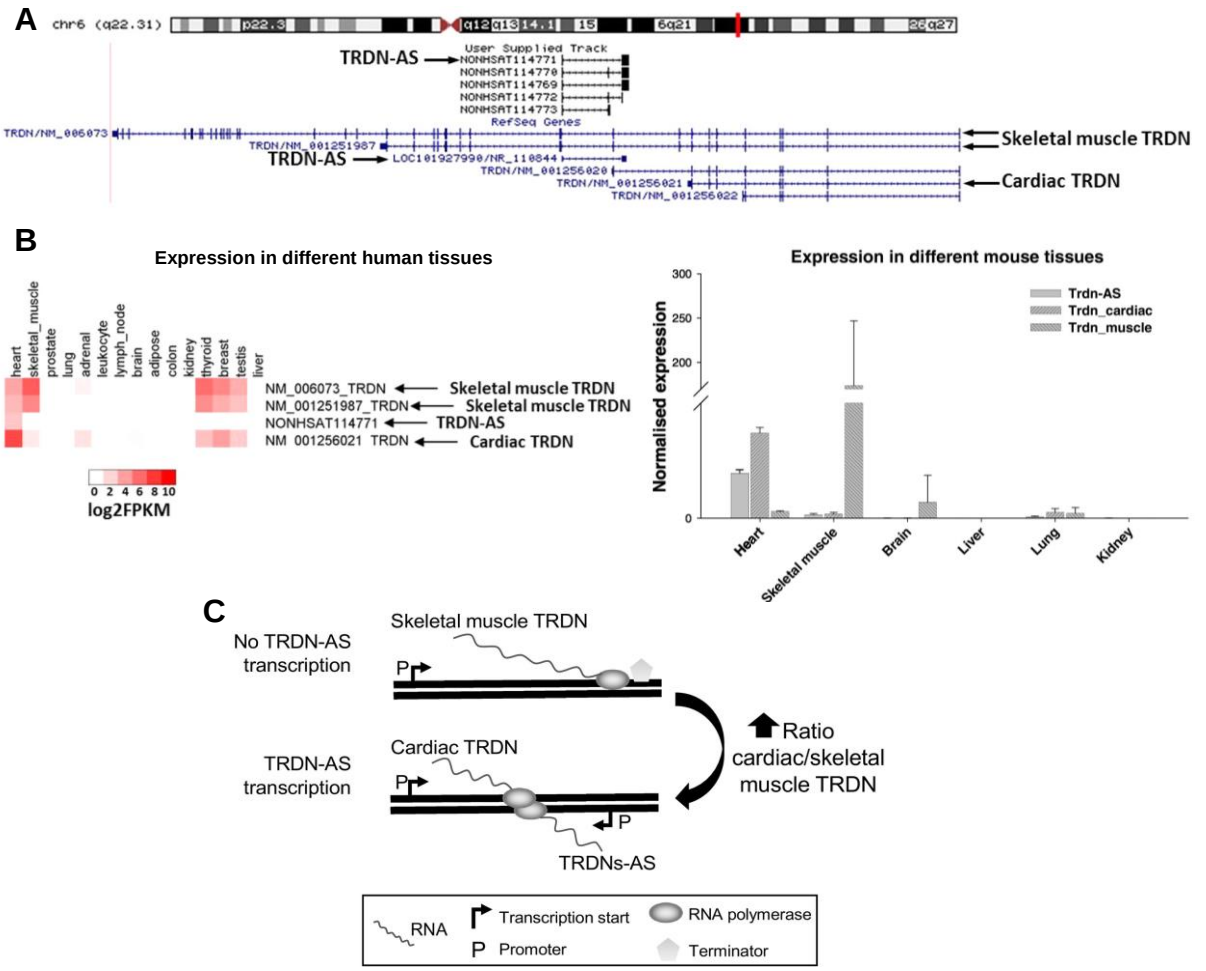

Figure 11 | *AS-Trdn* is a cardiac specific lncRNA responsible for triadin isoform abundance in the heart. A Genomic localisation of the protein-coding gene triadin, its isoform variants and the antisense lncRNA *AS-Trdn* in in the human genome (GRCh37/hg19). **B** expression profile of the triadin isoforms and *AS-Trdn* in 15 human organs (RNAseq dataset) and in 6 mouse tissues as assessed by qPCR (normalized to GAPDH). **C** postulated mechanism of the transcriptional interference mechanism by *AS-Trdn*. In absence of *AS-Trdn* transcription, the *Trdn* locus is fully transcribed, giving rise to skeletal muscle *Trdn*. Upon transcritpion of *AS-Trdn*, the transcribing polymerases are unable to bypass each other, leading to premature transcription termination and the formation of the sort cardiac *Trdn* isoform. (Taken from Zhang et al., 2018)

6 months of age. Calcium measurements using the IonOptix-system revealed no differences in isolated WT and KO cardiomyocytes under steady state conditions, but treatment with isoproterenol inducing an increase in calcium cycling was attenuated by KO cells. Consequently, mice were monitored using ECG, but no obvious differences were detected under normal conditions. However, treatment with isoproterenol induced a higher number of premature ventricular contractions and ventricular tachycardia in KO mice, demonstrating that *AS-Trdn* is important for cardiomyocytes calcium homeostasis under stress conditions. Nonetheless, these effects are a secondary consequence of altered triadin expression, as the loss of the spliced lncRNA led to a

reduced trisk32 abundance on RNA as well as on protein level, while expression of trisk51 and trisk95 stayed unchanged (Figure 12 C - F), resembling a loss of TRDN phenotype (Zhao, Riching and Knight et al., 2022).

Taken together, this study shows that deletion of *AS-Trdn* transcript, without disturbing of the lncRNA transcription has no effect on the long triadin isoform expression, supporting the transcriptional interference hypothesis proposed by Zhang et al.

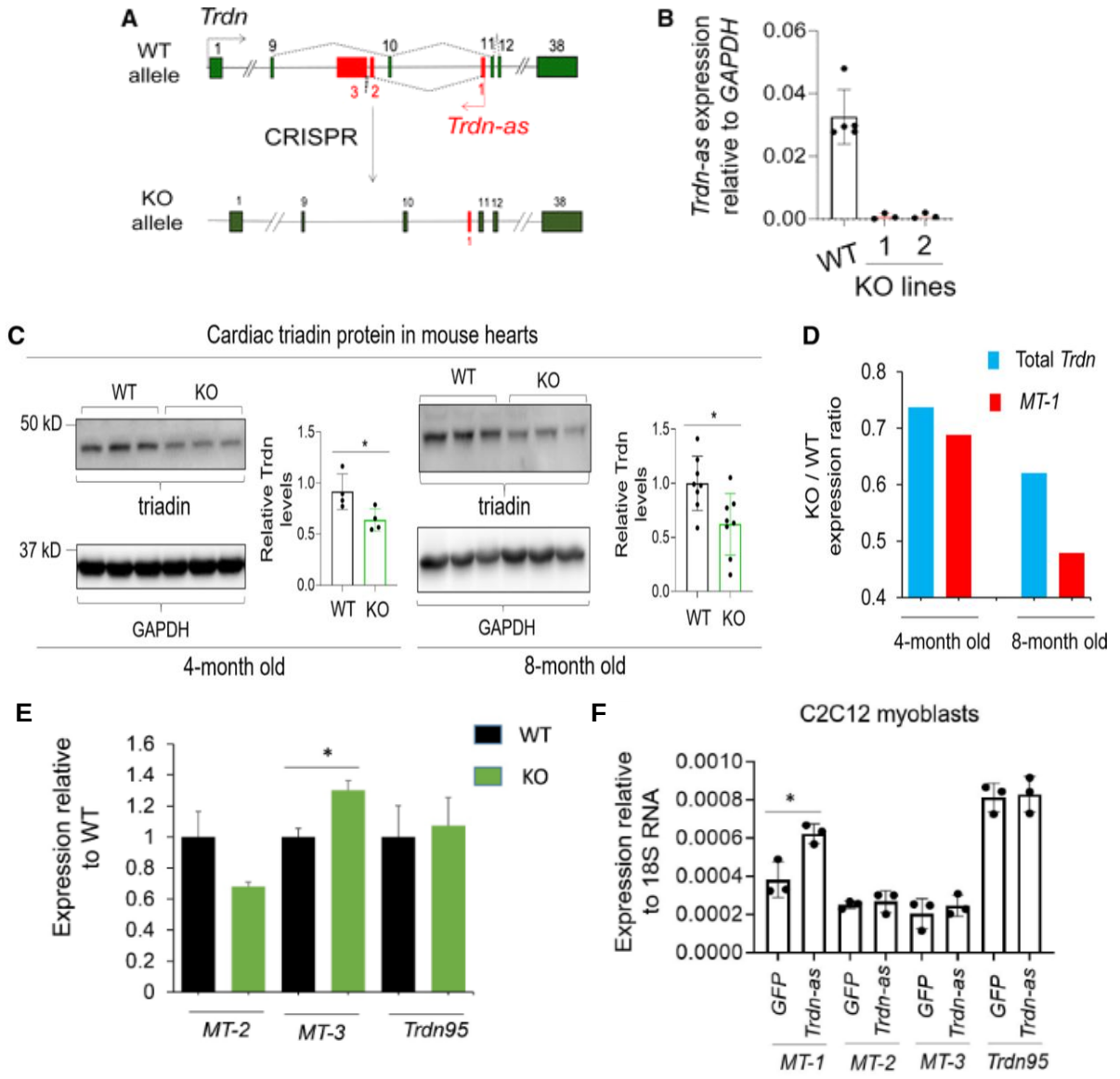

Figure 12 | *AS-Trdn* transcript regulates trisk32 isoform splicing but has no effect on trisk95. A genomic deletion of *AS-Trdn* using CRISPR gene editing**. B** Quantification of *AS-Trdn* deletion efficiency in 2 different strains using qPCR normalized to GAPDH. **C - E** Western-Blot and qPCR analysis of Trdn isoform expression in WT and KO hearts at different ages indicates a drcrease in cardiac Triadin upon loss of *AS-Trdn* but no change in the abundance of the long Trdn isoforms (MT-2/MT-3, short isoform splice variants; Trdn95, trisk95). **F** *AS-Trdn* overexpression in C2C12 myoblast cells increases the abundance of trisk32 (MT-1) but no difference in other Trdn isoforms was detected. (Taken from Zhao, Riching and Knight et al., 2022)

1.4. Aim

The aim of this study was to elucidate the mechanism of *AS-Trdn* in regulating triadin isoforms in the heart. Therefore, a polyA cassette was specifically inserted into the first exon of the antisense lncRNA locus to establish an *AS-Trdn* KO mouse line. This approach has been used before in multiple lncRNA studies (e.g. *Firre*, *Uph, lncMyh*) and has been successful in inducing premature transcription termination and therefore loss of the lncRNA without major structural alteration of the genomic organisation. After successful repression of *AS-Trdn* transcription, as confirmed by RNAseq, the triadin isoform abundance was investigated on RNA as well as on protein level. The aim was to investigate the impact of the transcription termination of *AS-Trdn* on triadin isoform expression and to understand the physiological relevance of the different triadin isoforms for *in vivo* heart functionality and contractility, calcium homeostasis and sarcoplasmic reticulum structure.

2. Material and Methods

2.1. Materials

All used chemicals, reagents and solutions are mentioned in the corresponding section in the text as well as method specific buffers and antibodies. Below the used mouse and cell lines, common buffers and software are listed.

Table 1 | Generated mouse lines

Full name	Description	Internal abbreviation
***AS-Trdn* KO**	Insertion of a PolyA cassette into the first exon of *AS-Trdn*	**971**
***AS-Trdn* PolyA DS 1**	Insertion of a PolyA cassette 1 kb downstream of *AS-Trdn* exon 3	**1173**
***AS-Trdn* PolyA DS 2**	Insertion of a PolyA cassette 1 kb before Trdn exon 9 in antisense direction	**1178**
Cas9-SPH-Pax7Cre^{ERT2}	expression of a Cas9-SPH system under control of a Pax7-Cre^{ERT2}	**dCASSPHP7E**
***AS-Trdn* DS del**	deletion of polyA 2 & 3 between exon 8 and 9 of Triadin	**1185**

Table 2 | Cell lines & primary cells

Name	Origin
C2C12	subclone of immortalized myoblasts
cardiomyocytes	neonatal as well as adult cardiomyocytes are isolated in house
hIPSC	provided by Gheo Idrissou from TU Munich
mESC	mouse embryonic stem cells are isolated in house
satellite cells	primary satellite cells are isolated in house

Table 3 | Common buffers

Abbreviation	Reagents
PBS 20x	2.7 M NaCl; 100 mM KCl; 200 mM Na2HPO4; 14.1 mM NaH_2PO_4 x H2O; 40 mM KH_2PO_4
PFA 4 %	40 mg/ml paraformaldehyde (PFA) in PBS pH 7.4
modified RiPA	50 mM Tris/HCL; 150 mM NaCl; 1% NP40; 0.25% Na-Deoxycholate; adjust pH to 7.4 with HCL
sample loading buffer	25% Ficoll; 100 mM EDTA pH 8.0; bromophenol blue
Tail-Lyse-buffer	100 mM Tris-HCl pH 8.0; 5 mM EDTA; 200 mM NaCl; 0.2% SDS
TBS 10x	500 mM Tris; 1.5 M NaCl; pH 7.4
TE 1x	10 mM Tris-HCl pH 8.0; 1 mM EDTA, pH 8.0
$T_{1/10}E$	10 mM Tris pH 8; 0.1 mM EDTA

Table 4 | Software

Software name	Developer
Access, Excel, PowerPoint, Word	Microsoft
Adobe Reader	Adobe Systems Incorporated
CAT	Computer Administriertes Tierhaus (MPG)
Dataquest ART 4.0	Data Sciences International
EndNote	Clarivate Analytics
Ensemble Genome Browser	European Bioinformatics Institute (EMBL-EBI)
GraphPad Prism® 9	GraphPad Software Inc. (USA)
ImageJ	National Institutes of Health (USA)
ImageLab	Bio-Rad Laboratories, Inc.
Integrated Genome Browser (IGV)	Broad Institute
IonWizard	IonOptix LLC
Medis Suite V4.0	Medis Medical Imaging Systems B.V
SeqBuilder/SeqMan Pro 17	DNASTAR Lasergene
StepOne Software v2.3	ThermoFisher
ZEN - ZEISS Efficient Navigation	Carl Zeiss AG

2.1.1. Public available NGS Data sets

Next-generation-sequencing (NGS) has emerged as one of the most important tools in today's scientific world. In order to analyse the *AS-Trdn* locus expression and chromatin marks with different NGS data sets, public available data sets were downloaded from encode (https://www.encodeproject.org/) or NCBI (https://www.ncbi.nlm.nih.gov/geo/query/acc.cgi) and either analysed using the IGV program or by uploading into the UCSC genome browser (http://genome.ucsc.edu/). All used public available data sets are marked within the dissertation with corresponding encode or GEO accession numbers.

2.2. Methods

2.2.1. Animal husbandry

All mice are kept centrally in the MPI BN animal facility in accordance to the animal welfare regulations and are monitored daily by trained animal caretakers to ensure species-appropriate animal husbandry. Mice are kept in separately ventilated cages from Techniplast (Aero Cage-Mouse IVC, Italy) at ~ 22°C air temperature and ~ 45 % relative air humidity. To ensure a “real-life” day/night rhythm, lights are turned off at 6 pm and turned on again at 7 am with 1 hour of dawn and dusk in between.

2.2.1.1. Animal experiments, sacrifice procedure and organ harvest

All animal experiments were performed as approved in TVA B2/2010 and B2/1224. Animals were sacrificed after a short isoflurane narcosis using cervical dislocation and afterwards the thorax was opened for atrial perfusion with PBS pH 7.4. Mouse hearts and *tibialis anterior* muscle (TA) were dissected and either kept in 4 % PFA/PBS for histological approaches or snap frozen in liquid nitrogen for molecular biology methods.

2.2.2. Mouse-line generation and cloning

2.2.2.1. Generation of AS-Trdn polyA mouse-lines using CRISPR/Cas9

To generate a constitutive KO mouse model for the long non-coding RNA *AS-Trdn* the well-established CRISPR/CAS9 system was used. Therefore specific gRNAs (guide RNAs) were designed using the UCSC mouse Crispr track (https://genome.ucsc.edu/cgi-bin/hgTrackUi?db=criGri1&g=crispr) to target the Cas9 endonuclease to the *AS-Trdn* locus. Upon recognition of the so called PAM sequence, Cas9 induces a double strand break within the genomic sgRNA binding site and thereby triggers the endogenous repair mechanism of the transfected cell. By using a combination of the Crispr system together with repair oligos (Table 6), an insertion of a certain target sequence can be achieved by homologous recombination (Knock-In (Cong et al., 2013; Ran et al., 2013)). In case of the *AS-Trdn* polyA line, my former colleague Dr. Maria Weiss used the Cas9n system and a 200 bp ss-oligo harbouring two times the polyadenylation signal (polyA) sequence “AAATAAA” for insertion into

the start of the first Exon of *AS-Trdn*. This leads to an early transcriptional stop of the RNA polymerase II and thereby to a loss of the *AS-Trdn* transcript. This mutant was used for all main experiments. Additional polyA lines #1173/78 have been generated by myself during the concourse of the PhD thesis work in a similar way.

The Crispr system used in our lab to generate polyA insertions and complete genomic deletions is based on the Addgene plasmid px459 pSpCas9(BB)-2A-Puro. This vector harbours the whole Cas9wt system without a gRNA and in a first step, this plasmid is digested using BbsI to generate specific overhangs for the insertion of the gRNAs. The restriction enzyme BbsI generates two overhangs with distinct sequences, “CACC” and “AAAC”, which can be used to insert the gRNAs by attaching one sequence 5’ to the designed sense oligo and one to the antisense oligo. The resulting vector can afterwards be transfected in the requested cell line and positive clones can be selected by PCR and sequencing. The exact experimental procedure will be explained in the following paragraph.

The designed sgRNAs (Table 6) were cloned into the Cas9wt vector, for which first, the corresponding sense and antisense oligonucleotides (Oligos) were hybridized. Oligos were dissolved in 10 µl ddH2O and 8 µl of each was mixed with 2 µl of annealing buffer (50 mM Tris/HCl; 1 M NaCl; 10 mM EDTA pH 8.0) and 2 µl of ddH2O. The reaction tube containing the annealing mixture was added to 98°C of boiling water and remained there until the water reached back to room temperature (RT). To insert the annealed gRNAs into the Cas9wt vector, the target vector was digested with the restriction enzyme BbsI, by incubating 10 µg of the plasmid with 2 µl BbsI and 5 µl of the corresponding 10x buffer in a total volume of 50 µl. After incubation at 37 °C for 3-4 hours, 10 µl of sample loading buffer was added to stop the reaction and the whole mixture was loaded for separation onto a 1 % ethidium bromide gel, to ensure linearization. After Gel-extraction of the linearized plasmid using the NucleoSpin® Gel and PCR Clean-up Kit (Macherey Nagel #740609.240C), ligation of the vector and the previously annealed gRNAs was performed at 16°C ON using a T4-Ligase (Promega GmbH, Madison, WI, USA) as shown in table 5.

Table 5 | T4-ligase reaction set-up

	1:10	1:100	empty control
Vector	1 µl	1 µl	1 µl
gRNA (1:10)	1 µl	-	-
gRNA (1:100)	-	1 µl	-
H2O	6 µl	6µl	7 µl
T4-Ligase	1 µl	1 µl	1 µl
10x T4-Ligase-Buffer	1 µl	1 µl	1 µl

On the following day, the ligation mixture was desalted on a dialysis membrane and added to 50 µl of bacterial suspension (XL1-blue; Dh10α). After transferring the whole mixture to a suitable cuvette (Bio Rad cuvettes; 1 mM), the electroporation was performed in an electroporation chamber at 1.8 kV, 200 Ω, and 25 µFD. Immediately afterwards the bacteria were resuspended in 900 µl of SOC medium, transferred to a new reaction tube and incubated for 1h at 37 °C and 300 rpm. The bacterial suspension was afterwards shortly centrifuged at 1000 g for 1 min, most of the supernatant removed and the remaining bacteria were spread out on agar plates and incubated ON at 37 °C. To check for proper insertion of the gRNAs, single colonies were picked and inoculated ON in 3 ml of LB-Medium and antibiotics for mini-preparation. On the next day, 2 ml of the suspension was centrifuged at 14000 rpm for 30 sec and the supernatant discarded. The pellet was resuspended in 300 µl of P1 (50 mM Tris/HCl, pH 8,0; 10 mM EDTA, pH 8.0) by vortexing and another 300 µl of P2 (200 mM NaOH; 1 % SDS) was added and mixed by cautious inverting of the tube. Cells were lysed for 5 min at RT before stopping the reaction by adding 300 µl P3 (3 M potassium-acetate pH 5.2), again cautious inverting and a 3 min incubation at RT. The lysate was centrifuged for 15 min at 14000 rpm, 4 °C and 850 µl of the supernatant transferred to a new reaction tube. To precipitate the plasmids, 600 µl of isopropanol (~ 80 % of the volume) was added to the supernatant and after multiple rounds of inverting the mixture was again centrifuged for 15 min at 14000 rpm, 4 °C. The dried pellet was resolved in 20 µl of T1/10E containing 0.5 % RNase A on a 55°C shaker for 30 min. Confirmation of the insertion was done using Sanger-sequencing by an external company.

The bacterial clones containing the positively sequenced plasmids were further inoculated for maxi-preparation using the NucleoBond® Xtra Maxi plasmid DNA

purification kit (Macherey-Nagel) after the manufactures guide. Finally the plasmids were used for transfection into mES cells together with the ordered polyA containing repair-oligos, which was either carried out by Sonja Krüger (971) or myself (1173;1178,1185). The exact procedure for mESC transfection and cell culture can be found in section 2.2.6.3. Positive mESC clones were used to generate the mouse lines 971, 1173 and 1178 and (Table 1).

Table 6 | CRISPR/Cas9 sgRNAs, repair Oligos and corresponding plasmids

Oligo suffix	Sequence 5´>3´	Purpose & plasmid #
MA356	caccGCTATAAGCTTGGACTCCATGGG	*AS-Trdn* PolyA p971
MA357	aaacCCCATGGAGTCCAAGCTTATAGC	
TB1005	TGACTTTTCTATTAAGCTATTAGATATAAGCACTTGTTATTATTATTCTAAATGACTAGACTTACCAGAAgaattcTGGTTACAAATAAAGCAATAGCATCACAAATTTCACAAATAAAGCATTTTTTTCACTTCATGGAACCATACATGATTTTGCATAGCATTCAGACATACTACAACCTTGGTGTACCCAAGAACTC	*AS-Trdn* PolyA PolyA Oligo
TG50	caccgTGATTCCAGAAAAACACTGA	*AS-Trdn* DS 1 p1173
TG54	aaacTCAGTGTTTTTCTGGAATCAc	
TG126	A*T*ATTGGTGTGATTAAAAACCTTTCTTCATTGCAGAGGTAGAAGCCAAAGTTAAGTAACTgaattcTGGTTACAAATAAAGCAATAGCATCACAAATTTCACAAATAAAGCATTTTTTTCAGAATCACAAAAGACCATAAATAAGAAAATCTAAATATTTTAGAAAGATAAGACTCAGTATTTGAGAAGTGCTGTATG*T*T	*AS-Trdn* DS 1 PolyA Oligo
TG78	caccgTTTGACAGTACCTTGTAACA	*AS-Trdn* DS 2 p1178
TG80	aaacTGTTACAAGGTACTGTCAAAc	
TG128	T*G*TTGAAGCAGATGACTCTTTTAAAAGTCTAGGAGATAAAGCTTTGAGGAGATTTTCCTGgaattcTGGTTACAAATAAAGCAATAGCATCACAAATTTCACAAATAAAGCATTTTTTTCACTGTCAAAAGAAGCTTCAGTTAATCTCTACTTTATACCAGCCTTGGCAAAGCTGACTGGACAATGGCAAGAGCATCA*G*T	*AS-Trdn* DS 2 PolyA Oligo
TG87	caccgCTAGAATACAGACTAGCCAA	*AS-Trdn* DS del p1185
TG95	aaacTTGGCTAGTCTGTATTCTAGc	

2.2.2.2. Generation of AS-Trdn Downstream deletion mutants

The aim of this study was to investigate the molecular function of the long non-coding RNA *AS-Trdn* in the heart and in this regard multiple genomic deletions of the endogenous locus have been generated. For this approach, the CRISPR/Cas9 system was used, but instead of the Cas9wt plasmid a mutated version called Cas9n was used. The induced mutation turning an aspartate into an alanine (D10A) leads to a mutation in the catalytic subunit of RuvC. Compared to the Cas9wt, this mutant version can only induce single-strand breaks. This significantly reduces the likelihood of off-target effects, as the putatively induced single-strand breaks can be repaired without error. To induce a larger genomic deletion, 2 different gRNAs were used, flanking the targeted region for deletion. The plasmids harbouring the gRNAs were co-transfected into mES cells like described in section 2.2.6.3. and the successful deletion quantified by Sanger-seq. Again, positive cell clones were used to generate the mouse-line 1185 (Table 1).

2.2.3. Molecular methods

2.2.3.1. Isolation of genomic DNA and genotyping

Isolation of genomic DNA was either carried out using tail biopsies or ear punches of 2-3 week old mice. Both tissues were lysed overnight (ON) at 56°C in tail-lysis buffer (100 mM Tris/HCl pH 8.0; 5 mM EDTA; 200 mM NaCl; 0.2% SDS) with 10 mg/ml Proteinase K. On the next day the DNA was precipitated by adding 0.8 Vol. Isopropanol and several rounds of inverting. The precipitated DNA was pelleted by centrifugation (1400 rpm, 15 min, at 4°C), washed once using 70% EtOH and was afterwards air-dried at room temperature (RT) until all EtOH was evaporated. The dry pellet was resolved in 100 µl of T1/10E (10 mm Tris/HCl pH8.0; 0.1 mm EDTA pH 8.0) at 55°C ON and stored at 4°C.

The isolated DNA was used for PCRs with specifically designed primers with expected band sizes to determine the genotype of different mice. In the following tables the different Primer combinations for each genotyping, the standardized PCR program as well as the used PCR Mastermix are listed.

Table 7 | PCR Mastermix

Reagents	Volume [µl]
2 × Taq Plus Master Mix II #P213	10
Primer 1	1
Primer 2	1
(Primer 3)	1
DNA	1
Fill up with ddH2O	25 total

Table 8 | PCR standardized program

Step	Temperature	Time	
Initial denaturing	95 °C	3 min	
Denaturing	95 °C	30 sec	35 cycles
Annealing	58 °C	30 sec	
Elongation	72 °C	30 sec	
Final elongation	72 °C	5 min	35 cycles
Hold	10 °C	∞	

Table 9 | Mouse-line specific genotypings

Mouse-strain specific PCR	Primer combinations	expected band sizes (bp)	
		WT	KO
971 (*AS-Trdn* KO)	MA434 / MA435	454	605
1173 (*AS-Trdn* DS 1)	TG216/TG217	346	406
1178 (*AS-Trdn* DS 2)	TG130/TG153	150	210
1185 (*AS-Trdn* DS del)	TG102/TG105/TG146	382	269

Table 10 | Sequences of primers used for genotyping

Primer	Sequence 5´>3´
MA434	TTAGTCTGGGAAAGTGACAAATGGC
MA435	TTGGACCTGGTGACATTCATGTGGC
TG216	CCTGCGTTTGCTGCATGGCCTGTTG
TG217	CCTTTCTTCATTGCAGAGGTAGAAG
TG130	GAACCAGATGTTGAAGCAGATGACTC
TG153	CTGATGCTCTTGCCATTGTCCAGTC
TG102	GTAATGGGTCCTATACATGCATTCTG
TG105	CAAGTGCATTGTATCTGTTAGGGTC
TG146	CATTAATACTTAAATAAAGGTGAGTC

2.2.3.2. RNA isolation and fractionation for RT-qPCR and RNAseq

For total RNA isolation, N_2 snap-frozen tissues or fresh cells were transferred to Trizol (1 ml/50-100 mg sample), and homogenized in a mixer mill (mM301; Retsch GmbH) for 5 min with iron beads at RT. Afterwards phase separation was achieved by adding 0.2 ml chloroform/1 ml Trizol, 30 seconds of vortexing and 15 min centrifugation with 12,000 g and 4 °C. The upper aqueous phase was transferred to a new 1.5 ml Eppendorf tube and the RNA was precipitated for 10 min at RT by adding 0.5 ml Isopropanol/1 ml Trizol. Subsequently the RNA was pelleted by another centrifugation for 10 min at 12,000 g and 4 °C, washed once with 70 % EtOH and air-dryed. Depending on the initial tissue or cells the RNA pellet was taken up in an appropriate amount of ddH_2O.

For Next-Generation sequencing approaches, RNA was isolated using the Qiagen miRNeasy Mini Kit (Cat. No. 217004) according to the manufactures protocol.

To determine the subcellular localisation of *AS-Trdn*, nuclear and cytoplasmic RNA was isolated from cardiomyocytes and C2C12 cells. Therefor the cells were washed twice with ice cold PBS and transferred in 1 ml PBS to a fresh 1.5 ml reaction tube. After 10 min centrifugation with 1000 g at 4°C, the pellet was resuspended in 200 µl buffer A (10 mM Tris/HCL pH8.0; 140 mM NaCL; 1.5 mM MgCl2; 0.5% Nonidet P-40) and incubated on ice for 5 min with flicking from time to time. After another round of centrifugation with 1000 g for 3 min at 4 °C, the supernatant contains the cytoplasmic RNA which was transferred to a fresh reaction tube containing 700 µl Trizol. The remaining pellet was washed two more times using buffer A with centrifugation in between (3 min, 1000 x g, 4°C). In a final step to extract the nuclear RNA, the pellet was resuspended in 200 µl buffer B (Buffer A + 1% Tween-40 and 0.5% deoxycholic acid), centrifuged again with 1000 g for 3 min at 4 °C and the supernatant discarded. The pellet was resuspended in 700 µl Trizol and afterwards the nuclear as well as the cytoplasmic RNA was extracted using the protocol described above.

2.2.3.3. Quantitative reverse transcription PCR (RT-qPCR)

To quantify the expression of different target RNAs, a quantitative reverse transcription PCR was used, which consists of a two-step approach. In a first step the isolated RNA is reverse transcribed to cDNA using the Primescript RT Reagant Kit with gDNA eraser (TaKaRa #RR047A) after the manufactures recommendation. In a second step, the generated cDNA was diluted 1:10 in ddH2O for Real-time PCRs using gene specific primers (Table 11). Therefore the Blue S´Green qPCR Kit (#F410-L/F415-L; Biozym) was used in combination with a StepOne Plus System (#4376600; Thermo Scientific). All steps were followed as recommended by the manufacturer and for each sample 2-3 replicates were quantified, as well as a –RT and water control.

Table 11 | Sequences of RT-qPCR primer

Primer	Sequence 5'>3'	Target
AK90	GTTGTAGTATGTCTGAATGCTATGC	*AS-Trdn*
AK101	GTCCAAGCTTATAGCTAGGCAGCAC	
AK95	GAGATGCCAGCTGTGCATGAGCAG	*Cardiac Trdn*
AK97	CAGGCTTGTTGGCTTGGATCTC	
AK99	GCCACCACCATCATTGACACCTTCC	*Skeletal Trdn*
AK100	GCCTGGTTCTTTGCCTTTCCCATC	
CS681	AGGAGGCCATCGTTGAAGTCAGCTT	*Neat1*
CS682	CCATTCATGCATCCGCAAAGAATGA	
JD106	ACCACAGTCCATGCCATCAC	*Gapdh*
JD107	CATGCCAGTGAGCTTCCCGT	
TG040	CTAGGTATAAATGGATGTACCGGTG	*AS-Trdn* DS OE
TG042	GATGAAGCCCCGAAGGGACCCTGTC	

2.2.3.4. Isolation of proteins, membrane isolation and western blotting

For protein isolation different tissues and organs were harvested and directly snap-frozen in liquid nitrogen. The still frozen tissues/organs were broken up to small pieces with a mortar on dry ice and an appropriate amount of modified RiPA was added, followed by sonication using an ultrasonic wand (30 power/5 cycle/20 sec). The suspension was centrifuged at 14000 rpm for 5 min at 4 °C and the supernatant was transferred to a fresh reaction tube. 20 µl of the protein extract was removed to determine the protein concentration, whilst the remainder was boiled with DTT (4 µl/100 µl RiPA) for 1 min at 99 °C and frozen at -80 °C.

Since Triadin is a very well-known transmembrane protein of the sarcoplasmic reticulum, membrane isolations were carried out to determine changes in membrane composition and Triadin abundance. To isolate membrane proteins from frozen hearts, the tissue was again minced on dry ice and afterwards taken up in 700 µl of homogenising buffer (125 mM NaCl; 20 mM Tris/HCl, pH 8.0; 4,5 mM EDTA pH 8.0; 1x Complete). The suspension was sonicated (30 power/5 cycle/20 sec) and afterwards the cell debris centrifuged two times at 1000 g for 5 min at 4 °C. The supernatants were fused and in order to collect the membranes, put in an ultracentrifuge at 50,000 rpm (135,240 g) for 1 hour at 4 °C (rotors TL-100, centrifuge

tubes 9091-90203 kontron polyallomer TH (50), 13,5 ml). Afterwards the supernatant was discarded and the cell pellet dissolved in 200 µl sample buffer (RiPA; 4 mM pefablock; 1x Complete). 20 µl were again taken for measuring protein concentration while the remainder was frozen at -80 °C.

Before western-blotting of the extracted proteins was carried out, concentrations of the samples were measured using the BioRad DC protein assay kit (#5000111, Biorad). Therefore 3 replicates of each protein lysate were measured at 720 nm against a protein standard with known concentrations. The evaluation was performed using the MultiscanTM FC microplate photometer (#51119000, ThermoScientific). Subsequently the proteins were diluted with RiPA to a final concentration of 10 µg, laemmli-buffer was added 4:1 and loaded on a 4 – 12 % gradient BisTris gel (NuPage Novex BisTris gels, Invitrogen #NP0321BOX) in a western-blot chamber (X-cell SureLockTM Mini-Cell, El0001). The inner part of the chamber was filled with fresh MES-buffer (50 mM MES; 0.1% SDS; 50 mM Tris/HCL; 1 mM EDTA) while the outer parts were filled with used MES-buffer. As a reference, 5µl of the pre-stained protein ladder from Applichem was used (#A8889, Applichem; 10 – 245 kDa). For the first 15 min the gel was run at 75 V to ensure proper invagination of the samples into the gel and then run for another hour at 180 V on ice. Afterwards the gel was released from the chamber and transferred to a nitrocellulose membrane (GE Healthcare, ProtranBA85) in transfer buffer (20% methanol; 0.5 M Bicine; 0.5 M BisTris; 20.5 mM EDTA pH 8.0). The blotting chamber was set up as follows: 3 layers of sponges, one 3 mm Whatmann paper (#3030704), the protein containing gel, nitrocellulose membrane, another Whatmann paper and sponges until the chamber closes tightly. Blotting was carried out at 30 V for 2 – 3 h and afterwards the membrane was taken out and incubated in RedAlertTM (Merck #71078) for overall protein staining. The membrane was documented using a scanner and afterwards cut into the desired parts for antibody staining or dried for later use.

For antibody staining of the blotted proteins, the membrane was either incubated in 5% BSA (#A7284; Sigma Aldrich) in TBS-T (1 x Tris Buffered Saline, 1 % Tween20) or in 5% milk/TBS-T for 1 hour on a shaker. In a following step, the membrane was washed 3 times for 10 min with TBS-T and the primary antibody (Trisk32, custom-made, Isabel Marty; ab247008, Abcam; ab231058, Abcam) was added in 3% BSA/TBS-T for incubation ON at 4 °C on a shaker. On the next day, the membrane

was again washed 6 times for 5 min to remove unspecifically bound antibodies and incubated with the secondary HRP-antibody (Horse-raddish-preroxidase-coupled-antibody (goat-anti-rabbit, 1858415, Pierce) for 1 hour at RT on a shaker. Subsequently, the membrane was washed again six times for 5 min with TBS-T on a shaker and before imaging for one full hour. The HRP-antibody signal was detected using the Pico (#35065) or Femto kit (#34095) in a ChemiDoc imaging system (BioRad #1708280).

2.2.3.5. Immunoprecipitation

To investigate protein-protein interactions, immunoprecipitation (IP) was carried out for Triadin in heart and tibialis anterior muscle (TA). For each IP sample, 30 µl of slurry beads (G-sepharose, #P3296-5ML, Sigma Aldrich) were used and in a first step washed twice in RIPA buffer, with centrifugation at 12500 rpm for 30 sec at 4 °C in between. Subsequently, the beads were incubated with blocking solution consisting of 3 % BSA in RIPA for 1 hour on a rotating wheel at 4 °C. At the same time, 2 mg of the protein lysates were incubated with the slurry-beads in the same way, to avoid unspecific binding of the beads. Afterwards all samples were centrifuged again at 12500 rpm for 30 sec at 4 °C and the blocking solution was discarded. In a next step the pre-cleared protein lysate is added to the pre-blocked slurry beads and either 2 µg of Triadin (ab231058, Abcam) or IgG (2729S, Cell Signaling) antibody was added for incubation ON on a rotating wheel at 4 °C. The following day, samples were washed three times for 10 min on a rotating wheel with RIPA and finally taken up in 200 µl RIPA. To validate the IP, 20 µl was mixed with 10 µl of laemmli buffer, cooked for 10 min at 99 °C and used for western-blotting (section 2.2.3.4).

2.2.3.6. Cleavage under targets and release using nuclease (Cut&Run)

Cut&Run (CnR) is a is a next-generation-sequencing approach that couples the cleavage of an MNase to an antibody, to target a protein of interest and analyse the DNA binding sites. Compared to the formerly used ChIPseq, Cut&Run is highly sensitive, works with small sample sizes (~ 30,000 cells/sample) and additional fixation is not needed. To investigate the mechanism of *AS-Trdn*, different Cut&Run approaches were used. On one side a commonly available kit from Cell Signalling Technologies (CUT&RUN Assay Kit; #86652; Cell Signaling Technologies) was used

after the manufacturers instruction and on the other side a newly established method called MapR (Mapping of native R-loops using a MNase coupled to a catalytic inactive form of RNase H) was used to detect R-loops (section 2.2.3.8).

In both cases prior to performing the Cut&Run, WT and KO mice were sacrificed and hearts were directly snap-frozen in liquid nitrogen. Afterwards CM nuclei were isolated using sucrose to enhance Cut&Run sensitivity due to high cytoplasmic amounts of cardiomyocytes. Therefore, frozen mouse ventricles were thawed in 3 ml of lysis buffer (5 mM CaCl2; 3 mM MgAc; 2 mM EDTA, pH 8.0; 0.5 mM EGTA, pH 8.0: 10 mM Tris/HCl, pH 8.0) and were dissected using the Milteny gentleMACS Dissociator for 1 min twice. For further digestion of the heart lysate, 3 ml of lysis buffer containing 0.4 % Triton X-100 was added and the lysate kept on ice for 10 min. After 5 min incubation, lysates were pushed at least 10 times through a 30 gr. syringe to disturb remaining cell aggregates. The suspension was filtered through a 40 µm cell strainer (BD Bioscience) and after washing the filter with 2 ml of lysis buffer, the lysate was centrifuged at 1000 g for 5 min at 4 °C. While centrifuging, 15 ml falcons were prepared with 1 ml of 1M sucrose buffer (3 mM MgAc, 10 mM Tris/HCL, pH 8.0). The cell pellet was resuspended in 500 µl of nuclei buffer (PBS; 5 % BSA; 0.2 % 0.5 M EDTA, pH 8.0; 0.2 % NP40) and slowly pipetted onto the sucrose. After centrifugation (1000 g; 5 min; 4 °C) the cell debris and the sucrose was removed and the remaining nuclei pellet resuspended in 500 µl of nuclei buffer. Afterwards nuclei pellets were used for either Cut&Run assays using the Cell Signaling Technologies kit or for MapR experiments. The used antibodies for Cut&Run can be seen in table 12.

Table 12 | antibodies used for Cut&Run

Name	Manufacturer	Cat#
RNA pol II CTD phospho Ser2 antibody (mAb)	Active Motif	61083
Pcf11 (mAb)	Santa Cruze	sc-514158
TCEA3 Monoclonal Antibody (4E11; mAb)	ThermoFisher	H00006920-M08

2.2.3.7. Identification of native R-loops using MapR

To investigate the role of R-loops (RNA:DNA hybrids) in relation to the mechanism and function of *AS-Trdn*, I established the new sequencing method MapR (Mapping Native R-Loops Genome-wide Using a Targeted Nuclease Approach; Figure 13) which was published in 2020 by Yan and Sarma in combination with a modified version by Jauregui-Lozano et al. (2022) for cardiomyocytes in our lab. MapR is based on the coupling of a catalytically inactive form of RNase H with the micrococcal nuclease (MNase), whereby targeted genomic regions are cut and released from the nucleus and can be sequenced afterwards. The whole experiment was set-up in three individual steps:

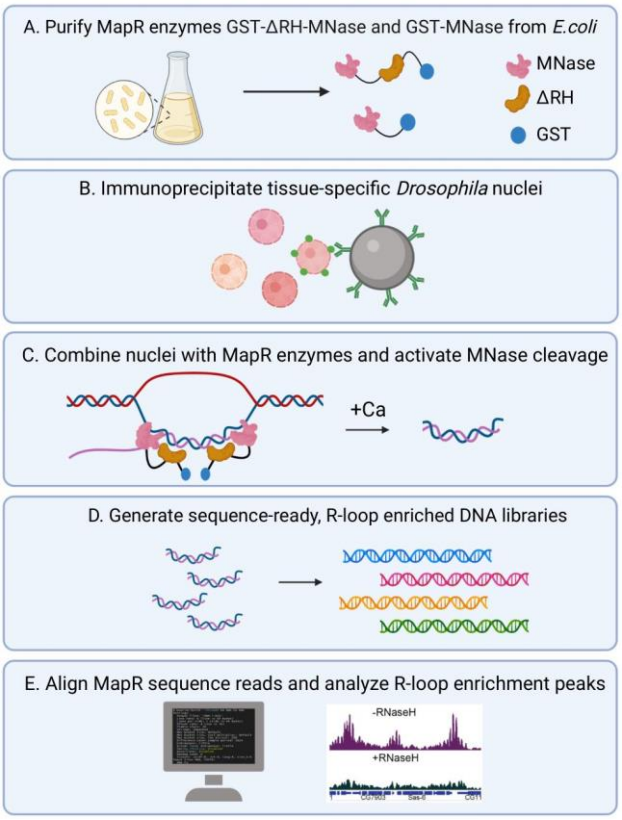

Figure 13 | Modified MapR workflow. A The fusion proteins GST-RNAseHΔ-MNase and GST-MNase are purified from BL21 (DE3) E. coli. **B.** Immunoprecipitation of tissue specific nuclei, in this example Drosophila nuclei, prior to MapR is performed. In this study, cardiomyocytes specific nuclei were isolated using a PCM1 antibody. **C** The isolated and bead-bound nuclei are incubated with the fusion proteins and upon addition of calcium, the nuclease starts cleaving the R-loop containing DNA regions. These fragments diffuse out of the permeabilized nuclei and can be used for DNA isolation. **D** After DNA-isolation using the supernatant, sequence-ready and R-loop enriched DNA libraries are prepared. Samples can now be sent for NGS **E** MapR sequences are aligned to the mouse reference genome and R-loop enrichment peaks are analysed by comparing WT, KO and RNase H treated samples. (From Jauregui-Lozano et al., Bio-protocol 2022)

Fusion protein purification: In a first step, the GST-tagged inactive RNase H coupled MNase fusion protein (GST-RNaseHΔ-MNase) and the control fusion protein without the inactive RNase H (GST-MNase) were purified. Therefore two plasmids were purchased from Addgene (GST-MNase, #136291; GST-RH▲-MNase, # 136292; Addgene), harbouring the sequences for the fusion proteins and transformed into BL21 (DE3) *E. coli* (#C600003; ThermoFisher). The purification of the GST-tagged proteins was performed like described by Jauregui-Lozano et al. (2022). 500 ml of IPTG induced bacteria culture were used for purification with PierceTM glutathione magnetic

agarose beads (#78601; ThermoFisher). After the fusion proteins were purified, dialysis was performed using the Slide-A-Lyzer™ G3 dialysis cassettes (#A52971; ThermoFisher) with 2 L BC100 buffer (50 mM Tris/HCL, Ph 7.6; 2 mM EDTA, pH 8.0; 100 mM KCl; 10 % Glycerol; 0.1 mM DTT; 0.2 mM PMSF) for one hour at 4 °C and after changing to 3 L of fresh BC100 ON at 4°C. Purification was evaluated by SDS page with 10 µl of dialyzed proteins containing 25 % glycerol and InstantBlue® Coomassie Protein Stain (#ab119211; Abcam).

Nuclei isolation and binding to beads: For a better outcome of the whole MapR approach, nuclei of WT and KO cardiomyocytes were isolated like described in section 2.2.3.7. The isolated single nuclei were further purified for CM specific nuclei by binding to PCM1 antibody coupled magnetic beads (DynabeadsTM protein G; #10003D; Invitrogen) like described by Jauregui-Lozano et al. (2022). Therefore 3 nuclei isolations of each genotype were pooled.

MapR: After successful isolation and bead-binding, the CM nuclei were resuspended carefully in 1 ml of dig-wash buffer (20 mM HEPES-NaOH, pH 7.5; 0.5 mM spermidine, pH 7.0; 150 mM NaCl; 0.02 % digitonin; 1 x Complete) followed by constant rotation for 5 min at 4 °C. Using the magnetic stand, the supernatant was removed and the wash step was repeated two more times. After the last wash step, the bead-bound nuclei were resuspended in 150 µl dig-wash buffer and the fusion proteins GST-RNaseHΔ-MNase and GST-MNase were added to a final concentration of 1 µM. Subsequently, the nuclei were incubated for 1 h with constant rotation at 4 °C followed by two rounds of washing with 500 µl dig-wash buffer. Nuclei were cautiously resuspended in 1 ml of low salt rinse buffer (20 mM HEPES-NaOH, pH 7.5; 0.5 mM spermidine, pH 7.0; 0,05 % digitonin; 1 x Complete) and afterwards incubated in 200 µl of ice-cold calcium containing incubation buffer (3.5 mM HEPES pH 7.5; 10 mM $CaCl_2$; 0.05% Digitonin; 1 x complete) on wet ice for 1 min. After discarding the supernatant, EGTA-stop buffer (170 mM NaCl; 20 mM EGTA, pH 8.0; 0.05% digitonin; 50 µg/ml RNase A; 25 µg/ml linear acrylamide) was directly added to the nuclei and incubated for 30 min at 37 °C. The DNA-fragment containing supernatant was removed using the magnetic rack and transferred to a fresh reaction tube. The DNA clean-up was done using the ChIP DNA clean & concentrator kit (#D5205; Zymo Research) after the manufacturer's protocol and send for Next-generation sequencing.

2.2.4. Histological methods

2.2.4.1. Cryo- and paraffin sectioning

In order to perform immunohistological stainings with cryo-sections, mice were killed using cervical dislocation and hearts were perfused with 1 x PBS followed by a second perfusion with 4 % paraformaldehyde (PFA). Hearts were harvested in cold 4 % PFA for 1 hour and afterwards put through 15 % sucrose, 30 % sucrose and Tissue Tek (Surgipath, FSC 22 Clear #3801480) over night. After embedding of the hearts in Tissue Tek, 10 µm four-chamber sections were cut using a cryotome (Leica GmbH; CM3050).

To prepare paraffin sections, hearts were collected as described for cryo sections. After incubation in 4 % PFA, hearts were dehydrated over an ascending ethanol series (70%, 80%, 90%, 95 %, 100%, isopropanol, ON, 4 °C) and then transferred to toluol for about 1 week to clear the tissue. At last hearts were incubated with paraffin in a heating chamber at 56 °C ON, embedded in paraffin and sectioned to 8-10 µm using a microtome (RM 2125RT; Leica GmbH).

2.2.4.2. Haematoxylin/Eosin staining according to Gill

Haematoxylin/Eosin staining (H&E staining) is used for better visualization of tissue sections, whereby nuclei are stained blue using haematoxylin solution (Gill's No. 3) and muscle fibres as well as cytoplasm are stained red using eosin solution. For this purpose, paraffin sections were cleared in xylene twice for 5 min. Afterwards, a descending ethanol series (100 %, 90 %, 80 %, 70 %) was performed to rehydrate the sections. The nuclei were stained for 10 min using haematoxylin solution, followed by two times dipping in AquaDest and subsequent rinsing with tap water (approx. 10 min). This results in the so-called bluing of the nuclei, whereby the higher pH value causes a colour change from reddish-brown to blue-violet. To prevent discoloration, the sections were dipped ten times in ethanol/HCL and washed thoroughly with tap water. Staining with the eosin working solution (0.01 % eosin G, 0.05 % acetic acid) was carried out for 7 min with subsequent ascending ethanol series and 10 min clarification in 100 % xylene. The stained sections were embedded with Entellan® and cured overnight before microscopic analysis.

2.2.4.3. Immunohisto- and Immunocytochemistry

For immunohistochemistry and immunocytochemistry, cryosections of WT and KO hearts as well as isolated WT and KO cardiomyocytes were used. In the case of cryosections, slides were thawed and dried for 30 min at RT before staining. In a first step, fixation was repeated using 4% PFA for 10 min followed by permeabilization of the membrane by washing three times with 0.3% Triton/PBS for 10 min. After rinsing with PBS for 5 min whilst slow shaking, a one-hour incubation with Blocking Solution (0.01% Triton X-100/PBS, Blocking One (Hikari, Nacalai tesque) was performed. After washing again with PBS for 5 min whilst slow shaking, the slides were incubated with Alexa488-coupled WGA (Invitrogen, W11261) in Solution A (Hikari, Nacalai tesque) or in 0.05% BSA/0.005% Triton X-100/PBS for cells ON at 4 °C. To remove all unbound primary antibody, the sections/cells were washed three times for 10 min in 0.01% Triton/PBS. In a last step, slides/cells were rinsed using 0.01% PBS for 5 min and covered with a small amount of Fluoromount G and a cover glass. The stained cells either remained in PBS or were covered with Fluoromount G and were used for imaging under a Z1 inverted fluorescent microscope (Zeiss GmbH).

2.2.4.4. Single-molecule Fluorescence in-Situ Hybridization (smFiSH)

To analyse the subcellular localisation of the *AS-Trdn* transcript, single-molecule RNA Fluorescence-in-Situ-Hybridization (smFiSH) was performed on isolated WT and KO cardiomyocytes. For this approach, the Stellaris RNA FiSH system (Biosearch Technologies) was used and therefore a pool of 30 RNA FiSH probes were designed in anti-sense direction to the lncRNA using the Stellaris design tool. Briefly, cells were cultured in a 12 well chamber slide with removable silicone chambers (ibidi #81201) and fixed in 3.7% PFA/PBS for 15 min at RT. After cells were rinsed twice with PBS, they were permeabilized with 70% ethanol for 1 hour at 4 °C. At this point cells can either be stored at 4 °C in 70% EtOH or stained directly. The ethanol was aspirated off and cells were washed once with 1 ml of wash buffer A (Cat# SMF-WA1-60) for 5 min at RT. Then a humidified box was assembled in which the chamber slide was incubated with 100 µl of hybridization buffer (Cat# SMF-HB1-10) and 125 nM (1µl) of RNA FiSH probe. Hybridization was done in a heating chamber at 37 °C for at least 16 h in the dark. Subsequently, cells were washed twice with wash buffer A for 30 min at 37 °C in the dark and for the last 10 min Dapi (1:1000) was added to stain the nuclei. Cells were

washed for 5 min at RT in wash buffer B (Cat# SMF-WA1-20) and afterwards the silicone chamber was removed, cells sealed using ProLong Gold Antifade Mounting reagent (#P10144; Thermo Fisher) and covered with a coverglass. Slides were kept at RT in the dark for 2 days before imaging under a Z1 inverted fluorescent microscope (Zeiss GmbH).

2.2.4.5. Transmission electron microscopy (TEM)

Transmission electron microscopy was used to investigate the ultrastructural differences between WT and KO hearts. Therefore whole hearts were harvested, perfused with 1 x PBS and fixed in 1.5% PFA (Sigma #6148-1KG), 1.5% glutaraldehyde (Sigma #G5882), and 0.15 M HEPES (Sigma #H3375) in MilliQ at 4 °C for at least 24 hours. Staining using 1 % osmium tetroxide solution, epoxy resin and ultrathin sectioning was carried out by Dr. Ulrich Gärtners lab at the EM facility of the medical department at Justus-Liebig-University Gießen. Imaging was done by myself on a Zeiss EM 902.

2.2.5. Physiological methods

2.2.5.1. Magnetic resonance imaging (MRI)

Magnetic resonance imaging (MRI) is a non-invasive medical imaging technique that is used to investigate inner-anatomical changes in a three dimensional manner. Therefore the MRI uses strong magnetic field gradients and radio waves to generate detailed images of internal structures based on their difference in atomic movements upon excitation. This technology is commonly used to detect inner-body diseases, for diagnosis and medical treatment monitoring (NIH website; www.nibib.nih.gov/science-education/science-topics/magnetic-resonance-imaging-mri).

In this study, MRI technology was used to investigate the consequences of the loss of *AS-Trdn* on heart physiology and contraction of *mus musculus*. The measurements themselves were performed by the MPI BN MRI service group under the direction of Dr. Astrid Wietelmann on a 7.0 T (300 MHz for H1) MRI scanner (Pharmascan 70/16, Bruker, Ettlingen, BRD). A circularly polarized birdcage resonator (MPI workshop) with an inner diameter of 2.5 cm was used as transmitting and receiving coil. To trigger the ECG and the respiratory signal, the "self-gating" method Intragate from Bruker BioSpin was used, which determines the cardiac phase from a navigator echo preceding each image line in k-space (Larson, White et al. 2004). During the measurement, the mouse was fixed and anesthetized with 1.5 to 2.0 % isoflurane in 0.5 l/min air and 0.5 l/min oxygen via an inhalation mask during the whole MRI measurement continuously. Body temperature was maintained at 37°C with a thermostatically regulating water flow system.

To analyse the cardiac function of WT and KO mice, 8 different animals (n = 4) were individually measured. By measurement of the individual heart slices using an analysis software (Mass4Mice, Medis, Leiden, NL) different ventricular parameters such as end-diastolic and end-systolic volumes (EDV, ESV), stroke volume (SV), ejection fraction (EF), cardiac output (CO) and fractional shortening (FS) were determined:

Stroke volume (SV) [ml] = end-diastolic volume (EDV) – end-systolic volume (ESV)

Ejection fraction (EF) [%] = SV/EDV x 100

Cardiac output (CO) [ml/min] = SV x heart rate = (beats/ min *mL) = mL/min

Fractional shortening (FS) [%] = (end-diastolic diameter (EDD) - end-systolic diameter (ESD) / end-diastolic diameter (EDD)) x 100

2.2.5.2. Telemetric measurements using ECG-transmitter

Telemetric measurements using implanted electrocardiogram-transmitters allows tracking of electrical signals from the heart under normal physiological conditions and thereby enables us to investigate abnormalities in heart physiology in WT and KO mice. Implantation of the transmitter was performed under isoflurane anaesthesia on a 37 °C heating plate by my supervisor Thomas Böttger. In short, the two electrodes for signal transmission were passed through the abdominal wall and placed subcutaneously on the left side at the level of the anterior limb and on the right side of the thorax about one finger far from the armpit.

The transmitter was sutured to the abdominal wall with a non-absorbable suture as well as the remaining skin wound. As pain therapy, 0.1 mg/kg buprenorphine was applied s.c. before anaesthesia and 1.6 ml/l metamizole was administered in drinking water postoperatively for one week. After one week recovery, animals were kept in single cages on electrical receiver plates and ECG as well as heart rate measurements were collected for 1 day every 10 min for 1 min using the Dataquest A.R.T. 4.0 program with a recording rate of 500 Hz and a frequency filter of 100 Hz.

Using different adrenergic stimuli is a widely used experimental method to study the stress response of the body in order to diagnose disease related alterations. In this study the β-adrenergic receptor agonist Isoproterenol (#16504; Sigma Aldrich) was used, which is a drug used to treat bradycardia. Here, we used this drug to stimulate the β-adrenergic signalling of WT and *AS-Trdn* KO hearts to investigate the difference in stress response and the cardiac parameters upon stimulation. Therefore, 1 µg/ml Isoproterenol was injected i.p. and the telemetric measurement was started 10 min prior to injection in a continuous manner.

For Data analysis of ECG-traces and heart rate measurements the software LabChart was used. The default ECG settings for mice were used with a maximum RT interval of 140 ms, and the ECG signals of 30 s each were averaged. Heart rate variability was calculated by the software on the before described parameters. Heart rate ON was calculated by averaging the heart rate from 8:00 pm to 6:00 am and isoproterenol response heart rate was calculated by averaging the heart rate from 5 min after i.p. injection to 30 min in total compared to the average heart rate ON.

2.2.5.3. Calcium imaging using the IonOptix system

To study the Calcium transients of single isolated WT and KO adult cardiomyocytes (aCM), the IonOptix system in combination with the ratiometric calcium dye Fura was used in this study. Therefore CMs were isolated and plated on 25 mm x 25 mm coverslips coated with 10 µg laminin/well. Cells were washed once with experimental buffer (EB: 117 mM NaCl; 2.8 mM KCl; 0.6 mM $MgCl_2$; 1.2 mM KH_2PO_4; 1.2 mM $CaCl_2$; 10mM HEPES; 20mM Glucose; pH 7.3) and afterwards incubated with Fura-2/AM (#F1221; ThermoFisher Scientific). Fura can be excited at 340 nm and 380 nm and the ratio between those is directly related to the calcium amount and cycling inside the cell. Since it is highly light sensitive, Fura-2/AM was dissolved in DMSO until a concentration of 1 mg/ml was reached and afterwards aliquoted and stored at -20 °C in the dark. These stocks were used in a 1:500 dilution in EB for a 15 min incubation on the cells in the dark at RT whilst slow shaking. Afterwards cells were rinsed twice with EB and after 20 min of slow shaking monitored using the IonOptix system at 20 V, 1 Hz and 5 msec duration (Figure 14). Multiple cells/mouse were measured and analysed using the IonWizard software (IonOptix). Therefore all events of the measured cells in one run where averaged to calculate sarcomere length, sarcomere relaxation and calcium transient parameters like peak height, time to peak, time to baseline. To study spontaneous effects, all measured cells were screened for extra peaks within 1 Hz or calcium oscillations lasting longer than 5 Hz and taken for statistical comparison between WT and KO cardiomyocytes.

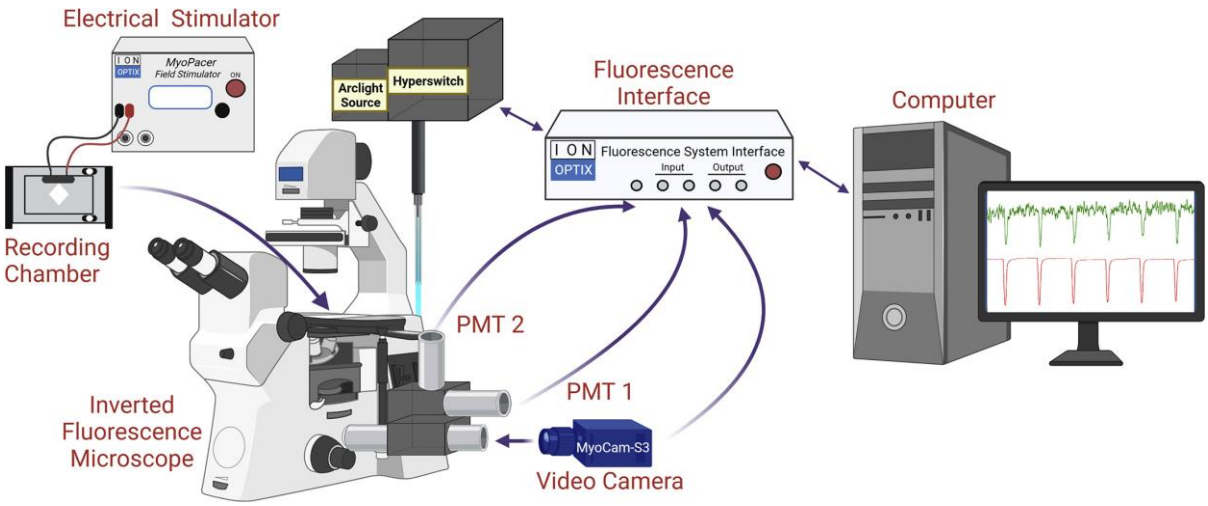

Figure 14 | Schematic drawing of the IonOptix measurement system for sarcomere contraction and intracellular calcium cycling. (adapted after Lyu, Yankun, et al. 2022)

2.2.6. Cell culture

2.2.6.1. Culture, transfection and harvest of immortalized cell lines

Culturing of immortalized cell lines is a commonly used laboratory strategy to study molecular mechanisms *in vitro*. C2C12 cells belong to a commonly used immortalized myoblast cell line, which has a proliferative state but can also undergo differentiation into myotubes and simple myofibers. C2C12 cells were cultured in proliferation medium (DMEM high glucose (#11965-092; ThermoFisher Scientific); 10 % foetal calve serum (FCS); 1 % penicillin-streptomycin-glutamine (PSG)). Upon reaching a confluence of ~ 70 %, C2C12 cells were split by rinsing once with PBS and detaching of the cells using 2 x trypsin (Sigma Aldrich #T4549) in PBS for 10 min at 37 °C. The reaction was stopped by adding 3 ml of medium and cells were centrifuged at 1250 rpm for 5 min. After taking the cell pellet up in an appropriate amount of medium, cells were plated in the desired well format and maintained at 37 °C and 10 % CO2. If transfection of cells was desired, cells were transfected not later than 1 h after splitting using Lipofectamine3000 (#L3000075; ThermoFisher) after the manufactures recommendation.

Upon reaching a confluence of ~ 90 % cells will start fusing and thereby differentiating. At this point the medium was changed to differentiation medium containing 2 % horse serum (HS) instead of FCS and kept in culture for one week until myofibers start contracting.

To harvest the cells for RNA or protein isolation, C2C12 cells were washed once with PBS and covered with an appropriate amount of either Trizol® or RIPA buffer and scraped off. Using a 1 ml pipette, cells were resuspended multiple times and transferred to a 2 ml safe lock tube and kept at -80 °C until further use.

2.2.6.2. Culture and transfection of mESC and cardiac body differentiation

Mouse embryonic stem cells (mESC) are pluripotent stem cells, which are isolated from the developing inner mass of the blastocyst and can be maintained in cell culture, differentiated into various cell lineages and used to generate genetically modified mouse strains (Waisman et al 2019). Therefore mESC represent a very useful *In vitro* model to study basic molecular mechanisms. In this study αMHC-Neo-PGK Hygro in V5,6 mESC were used to study the molecular function of the long non-coding RNA *AS*-

Trdn in *in vitro* differentiated cardiac bodies (CBs). Therefore the CRISPR/Cas9 system was used to induce greater genomic deletions or Knock-Ins in the mESC genome before differentiation into cardiac bodies. If the mutant cell lines revealed promising results, these clones were further used for mouse line generation by the MPI BN transgenic mouse facility under direction of Susanne Kreutzer.

Inactivation of MEFs: In order to culture mESC cells, mouse embryonic fibroblasts (MEFs; FDR4) are necessary as a so-called “feeder-layer” in order for the stem cells to form colonies and stay in an undifferentiated state. Therefore the MEFs had to be isolated first (carried out by Sonja Krüger) and afterwards the proliferation was inactivated using Mitomycin C (#M4287-2MG, Sigma Aldrich), to avoid overgrowing of the feeder cells over the mESCs. Mitomycin C is a known cell cytostatic which impairs cell growth by inhibiting DNA synthesis. To perform mitomycin treatment, cells were grown on 15 cm dishes in Feeder Medium (DMEM high glucose (#11965-092; Thermo Scientific); 15 % FCS; 1 % PS; 1 % non-essential amino acids; 0.7 % β-mercaptoethanol) until a density of 100 % was reached. Afterwards, 2 mg of Mitomycin C was dissolved in 190 ml of DMEM high glucose medium and 10 ml FCS and 20 ml of the solution was incubated on the cells for 4 hours at 37 °C and 10 % CO_2. Subsequently cells were washed twice using 1 x PBS and trypsinized using 0.25 % TE/HEPES for 5 min at 37 °C. Each 15 cm plate was split into 3 reaction tubes and centrifuged for 5 min at 1250 rpm at RT. Each pellet was taken up in 900 µl of 1 x freezing medium (80 % FCS; 10 % DMEM high glucose; 10 % DMSO) and frozen at -80 °C for one week before moving to the long-time storage in liquid nitrogen.

mESC culture, transfection and selection*:* One day before thawing the mESC, feeder cells were seeded as dense as possible (ideally 90 – 100 %) on a gelatine (0,2 % in ddH2O; autoclave) coated 12-well plate in mESC proliferation medium (PM; Table 13). mES cells were thawed and directly resuspended in fresh PM, centrifuged at 1250 rpm for 5 min, taken up in 1 ml of medium and seeded onto the well. Medium was changed every two days during the proliferative phase and colonies were starting to form already after one day. As soon as the colonies started to become three-dimensional, mESC were split into the desired format. In case of transfection, stem cells were split on a 6-well plate. Therefore new gelatine coated and MEF covered plates were prepared one day in advance. On the day of splitting, mESC plates were washed once with 1 x HEPES buffer (120 mM NaCl; 5.4 mM KCl; 440 µM KH2PO4;

300 µM Na2HPO4-2H2O; 5.5 mM glucose; 30 µM phenol red; 20 mM HEPES: pH 7.3; autoclave) and cell detaching was started by addition of 1 ml 0,25 % TE/HEPES for 5 min at 37 °C. The cell aggregates were singulated by multiple rounds of pipetting, before stopping the reaction by adding 2 ml of PM. Cells were briefly centrifuged at 1250 rpm for 5 min, taken up in 5 ml of PM and mES cells counted under a microscope. 400,000 stem cells were seeded on the beforehand prepared fresh 6-well plate in 5 ml PM. After 1 h settlement, transfection using Lipofectamine3000 and different plasmids containing the CRISPR/Cas9 system was performed. The different mESC strains which were generated during the course of this study can be found in table 14. The cells were left in the incubator until a first medium change the next morning. On the same day in the evening, cells were transferred to a 10 cm dish and after 30 h of incubation, the puromycin (2 µg/ml) selection was started by changing the medium to PM containing the antibiotics. The selection was stopped 48 hours later by changing the medium back to normal PM and cells were left in the incubator until three-dimensional colonies became visible. From these colonies, single colonies were picked into a 96-well plate containing gelatine and FDR4-MEFs. One week later each colony was split 1:2 on two fresh 96-well plates, where one plate was used for freezing by addition of 1 x freezing medium and oil and the other plate was used for DNA isolation and PCR analysis. Positive clones were further confirmed by Sanger sequencing and could at any time be re-thawn from the corresponding frozen 96-well plate.

Table 13 | mESC media composition

Name	Composition
mESC proliferation medium	415 ml DMEM high glucose; 5 ml PS; 5 ml non-essential amino acids; 3,5 µl β-mercaptoethanol; 50 µl Lif (10^7 U/ml); 75 ml FCS
mESC differentiation medium	440 ml DMEM high glucose; 5 ml PS; 5 ml non-essential amino acids; 3,5 µl β-mercaptoethanol; 50 ml FCS

Cardiac body differentiation: In this study, specific mESC were used to generate cardiac like aggregates called “cardiac bodies”. These cells contain the myocardial specific α-Myosin-Heavy-Chain promoter (αMHC) for G418-induced expression of cardiac specific transcripts, thereby pushing the cells to generate CBs. To induce cardiac body differentiation, positive clones were regrown on a 10 cm dish in PM until colonies again became three-dimensional. Cells were trypsinized and one million cells resuspended in 10 ml of differentiation medium (DM) in a CERO suitable tube. The tubes were placed in a rotating 3D cell culture incubator (CERO 3D; Omni Life Science GmbH & Co.KG) and the program for mESC differentiation was started according to the manufacturer’s recommendation. On days 3, 5 and 7 after the start of differentiation, 5 ml of the medium was changed to fresh DM. After 7 days, embryonic bodies became visible and cardiac body selection was started by replacing as much of the medium as possible with DM containing 0.4 mg/ml G418. The selection was continued for 5 – 7 more days, depending on the number of beating bodies. In a last step, cardiac bodies were transferred to a fresh reaction tube, centrifuged at high speed and the supernatant discarded. The pellet was either taken up in Trizol (RNA isolation), RIPA (protein isolation) or snap-frozen for later use.

Table 14 | generated mESC stable lines

clone suffix	full name	transfected plasmids and/or oligo
1173	*AS-Trdn* PolyA KI DS 1	p1173 x TG126
1178	*AS-Trdn* PolyA KI DS 2	p1178 x TG128
1180	*AS-Trdn* intronic PolyA del 1	p1180 x p1182
1182	*AS-Trdn* intronic PolyA full del	p1182 x p1184
1185	*AS-Trdn* intronic PolyA del 2	p1185 x p1187

2.2.6.3. Isolation, culture and transfection of neonatal and adult cardiomyocytes

Neonatal cardiomyocytes (neoCM) were isolated using the Miltenyi Neonatal Heart Dissociation Kit (#130-098-373; Miltenyi Biotec) and the Miltenyi Neonatal Cardiomyocyte Isolation Kit (#130-100-825; Miltenyi Biotec). Therefor WT and *AS-Trdn* KO hearts from at least 10 pubs aged P0 - P1 were dissected and kept in PBS on ice. The hearts were dissociated using a gentleMACS Dissociator (Miltenyi Biotec) in the enzyme mix as recommended from the manufacturer. After successful isolation of single neonatal cardiomyocytes, cells were plated on fibronectin (1:100stock/PBS; Sigma-Aldrich; #F1141) coated 24-well plates at a density of 70 % in DMEM high glucose medium containing 10 % FCS and 1 % PS. One day after seeding, the medium was changed and cells were transfected using 5 µM of different Dharmacon siRNA pools and DharmaFECT transfection regents (#T-2001-03; Horizon Discovery Ltd.) as described by the company. To ensure sufficiency of the siRNA KD, another 5 µM of the siRNA pools were added to the cells on the next morning, after another round of medium change. The transfected neoCMs were harvested 48 h after the first transfection by washing two times with PBS and addition of 1 ml of Trizol®. NeoCMs were scraped off the plates, transferred to a fresh reaction tube and either used for direct RNA isolation or for freezing at -80°C until further use.

Adult cardiomyocytes were isolated by our technical assistant Kerstin Richter. In a first step, WT and KO mice were injected i.p. with 100 µl heparin and 100 µl/10 g body weight ketamine/xylazine (4 ml NaCl 0.9 %; 0.5 ml ketamine; 0.25 ml xylazyen). After dissection of the whole lung and heart, excess tissue was removed to reach the aorta. A cannula was inserted until halfway through the aortic arch and firmly bound using a fine thread. Sufficient flow-through was tested by rinsing the heart with 1 ml of perfusion buffer (113 mM NaCl; 4.7 mM KCl; 0.6 mM Na_2HPO_4; 0.6 mM KH_2PO_4; 1.2 mM $MgSO_4$ x 7 H2O; 12 mM $NaHCO_3$; 10 mM $KHCO_3$; 30 mM taurine; 10 mM HEPES; 10 mM 2,3-Butanedione monoxime; 5.5 mM glucose) before removing all of the lungs. The heart was then fixed on a Langendorf apparatus and after removing all excess air, flushed with 15 ml of perfusion buffer. Subsequently after ~ 8 ml of perfusion buffer had passed through, 15 ml of enzyme buffer (perfusion buffer, Liberase DH 0.25 mg/ml, Trypsin 0.27 mg/ml, 23.2 µM $CaCl_2$) was added. The perfusate was collected and reused for perfusion until the heart was soft enough to fall of the cannula. The heart was carefully minced in enzyme/perfusion buffer and transferred to a fresh 50 ml canonical tube for settlement. The supernatant was removed and the cells cautiously resuspended in 10

ml of stop buffer (perfusion buffer; 5 % FCS; 12.5 µM $CaCl_2$). For cell culture and IonOptix experiments, cells were afterwards treated with an ascending $CaCl_2$ series (50 µl 10 mM; 50 µl 10 mM; 100 µl 10 mM; 30 µl 100 mM; 50 µl 100 mM) with 5 min incubation in between, before cells were separated on a 100 µm cell strainer. After a short 1 min centrifugation at 500 rpm RT, cells were resuspended in a suitable amount of culture Medium (M199; 5 mM Creatine x H2O; 2 mM L-Carnitine x H2O; 5 mM taurine; 25 mM HEPES; 5 % FCS; 1 % PS; 1 % ITS supplements; 10 µM AraC: pH 7.3 with NaOH) and plated on laminin (4 µg/ml PBS) coated slides. Adult cardiomyocytes were afterwards used for IonOptix experiments, staining or RNA/Protein-extractions.

2.2.6.4. Isolation and culture of mouse primary satellite cells

To isolate murine satellite cells (SC), mice were killed by cervical dislocation and as much muscle mass as possible was collected in 50 ml DMEM/1% PS. Afterwards the collected muscle was processed to a homogeneous mass using the McIlwain-Tissue-Chopper (TC752) followed by several washing steps with 50 ml medium and 1200 g centrifugation to remove excess fat and tendons. To obtain a suspension of single cells, the muscle mass was incubated for 1 hour with dispase (BD #354-235) and collagenase type II (Worthington #LS004185) in 20 ml DMEM/1% PS in a 37°C horizontal shaker. The muscle suspension was then forced several times through a 20 ml syringe to disrupt remaining larger pieces of muscle. A homogenous suspension should now be present that no longer contains any lumps. Inactivation of the dispase /collagenase was achieved by adding 10% FCS and filling up to 50 ml DMEM/1% PS. Afterwards the suspension was briefly centrifuged at 600 g and the supernatant filtered successively through 100 µm, 70 µm and 40 µm cell strainer into new 50 ml falcons each case. The suspension was centrifuged again at 1000 g for 10 min and the supernatant was aspirated. After one time washing using DMEM/2% FCS/1% PS and centrifugation at 1200 rpm for 5 min, the pellet was resuspended in 200 µl cell sorting buffer (CSB: 1x PBS, 1 mM EDTA pH 8.0, 25 mM HEPES pH 7.0, 1 % FCS) and CD45, CD31, Sca-1 and α-integrin FITC antibodies (1:100 each) were added. After a one hour incubation on ice, cells were replenished with medium and centrifuged at 1200 rpm for 5 mi. The supernatant was removed and the cells again taken up in 200 µl CSB and 30 µl of anti-APC micro beads were added. After a 25 min incubation in the fridge, cells were replenished in DMEM/FCS/PS medium and centrifuged at 1200 rpm for 5 min.

After removal of the supernatant, cells were resuspended in10 ml medium and filtered by MACS (magnetic cell separation), which involves specific sorting of cells based on their surface characteristics. In this case, sorting is by depletion meaning the negative fraction or flow-through contains the satellite cells. The negative fraction is centrifuged for 5 min at 120 rpm and resuspended in 700 µl DMEM/FCS/PS medium and transferred to a sorter tube. Now the cells can be sorted by FACS for further purification

After successful FACS sorting, satellite cells were centrifuged at 1200 g for 5 min and taken up in a suitable amount of SC Medium (DMEM GlutaMAX (Dulbecco's Modified Eagle Medium); 20 % fetal calve serum (FCS); 2 % Penicillin/Streptomycin (PS); 0,1 % basic fibroblast growth factor (bFGF)) and plated on cell culture plates coated with matrigel (1:50 in SC medium). Coating has to be prior for 20 min at RT and another 20-30 min at 3°C. Depending on the experimental approach SCs were either transfected after 2 days or transferred to differentiation medium (DMEM GlutaMAX; 2 % Pferdeserum, 1 % PS) at 70% confluence.

2.2.6.5. Endogenous overexpression of AS-Trdn using dCas9-SPH in satellite and C2C12 cells

The CRISPR/CAS9-SPH overexpression system was used in isolates satellite cells to overexpress the lncRNA from the endogenous promoter (Balboa *et al* 2015). In this approach cells were split on a 24 well plate at a density of 90 % and kept at 37 °C. Within one hour, cells were transfected with the plasmids containing the Cas9-SPH system together with *AS-Trdn* promoter specific sgRNAs, which were designed using the UCSC CRISPR targets track together with the publication from Balboa *et al* 2015. The sgRNA sequences and plasmids used are listed below (Table 15 & 16). The two plasmids and one of the sgRNAs was transfected in a 9:1 manner (e.g. 900 ng plasmids/100 ng sgRNA/well), where plasmids were used in an equal manner. To directly induce the differentiation of the used cell system, cells were transfected in differentiation medium containing 2 % HS. Transfection was carried out using Lipofectamine2000 like described in 2.2.6.2. After 24 hours of incubation, another 100 ng of each sgRNA was added and incubated for another 24 h before harvesting the cells in Trizol® for RNA isolation and RT-qPCR analysis to check for a sufficient overexpression (section 2.2.3.2 - 3). As a negative control, either a non-specific sgRNA was used (Dr. Maria Weiss) or no sgRNA was transfected to exclude off-target effect.

Table 15 | *AS-Trdn* promoter sgRNA sequences

internal #	sgRNA sequence plus 5' and 3' overhang
TG224	GTGGAAAGGACGAAACACCgTAGAGTTCTTGGGTACACCAGTTTTAGAGCTAGAAATAG
TG225	GTGGAAAGGACGAAACACCgGTGACATTCATGTGGCAGTGGTTTTAGAGCTAGAAATAG
TG226	GTGGAAAGGACGAAACACCgTGTCAACAGATATTTGGACCGTTTTAGAGCTAGAAATAG
TG227	GTGGAAAGGACGAAACACCgATTAACTCAAAATAGAATGGGTTTTAGAGCTAGAAATAG
TG228	GTGGAAAGGACGAAACACCgGGTCATTCAGTACTTCAAAGGTTTTAGAGCTAGAAATAG
TG229	GTGGAAAGGACGAAACACCgTTCTGTCCTAGGCAACCTTGGTTTTAGAGCTAGAAATAG
TG230	GTGGAAAGGACGAAACACCgTGGACCTGGTGACATTCATGGTTTTAGAGCTAGAAATAG
TG231	GTGGAAAGGACGAAACACCgATTCAGACATACTACAACCTGTTTTAGAGCTAGAAATAG
TG232	GTGGAAAGGACGAAACACCgCCCAGAAGTTGTCAGCCTATGTTTTAGAGCTAGAAATAG
TG233	GTGGAAAGGACGAAACACCgATTCATAATAGTAGCAAATAGTTTTAGAGCTAGAAATAG

Table 16 | Cas9-SPH containing plasmids

internal #	plasmid description	cat #
p1238	dSV40-NLS-dCas9-HA-NLS-NLS-10xGCN4	Addgene #107310
p1239	EF1α-scFv-p65-HSF1-T2A-EGFP-WPRE-PolyA	Addgene #107311

2.2.7 Statistical analysis

If not stated otherwise, significance was calculated using an unpaired, two-sided students T-test on normally distributed data. If the data didn't show normal Gauß-distribution, the Mann-Withney-Test was assigned. All calculations were carried out using the GraphPad Prism program. For ECG analysis over a certain time frame, a two-way anova analysis was used to calculate significance. P-values were marked as followed: ns, not significant $p > 0.05$; *, significant p-value < 0.05; **, significant p-value > 0.01; ***, significant p-value < 0.001; ****, significant p-value < 0.0001.

3. Results

3.1. Molecular analysis of *AS-Trdn* lncRNA mechanism & function

3.1.1. Genomic locus and sequence analysis of a heart specific antisense lncRNA in human and mice

The long non-coding RNA with accession number AK085762 (D830005E20Rik; ENSMUSG00000112707) was initially described in a study by Zhang et al. as antisense and intergenic to the protein-coding gene triadin, subsequently renamed *AS-Trdn* or *Trdn-AS* (Zhang et al., 2018). In *Mus musculus* this lncRNA is located on the minus strand of chromosome 10, positioned between exon 9 and 11 of triadin. It consists of three exons, resulting in a total spliced-transcript length of 1844 bp and a total genomic locus size of 34 kb (Figure 15 A). *AS-Trdn* is a well conserved lncRNA expressed in various species, including humans, specifically in cardiac muscle. The human orthologue (ENSG00000235535; HRAT13) is located on chromosome 6, demonstrating the same antisense orientation and intergenic location to the *Trdn* locus, between exon 9 and 11. Similar to the mouse lncRNA, its transcript comprises three spliced exons with a total length of 2384 bp and a total genomic locus size of 32 kb. The only distinction between human and mouse *AS-Trdn* is the inverted orientation of the whole locus, where *Trdn* is located on the minus- while *AS-Trdn* is located on the plus-strand. A comparison of the human and mouse spliced transcript revealed a sequence identity of 42.1 – 48.7 %, determined using two different homology comparison tools (VectorBuilder; EMBOSS-Water; Figure 15 A, B).

To confirm the non-coding nature of *AS-Trdn*, the coding potential was assessed using the web-based Coding Potential Calculator 2 (CPC2). With a Fickett TESTCODE score of 0.33, a complete putative ORF of 148 AA and a coding probability of 0.45, *AS-Trdn* was verified as non-coding (Figure 15 C). The Fickett score identifies non-coding transcripts based on a combinational calculation of their nucleotide composition and codon usage, with a coding cutoff at 0.44 for *Mus musculus* (Kang et al., 2017). Using publicly available RNA sequencing data from various developmental stages, *triadin* was found to be expressed from a very early time point (< 10.5), while *AS-Trdn* expression commenced at E13.5, exhibiting stable and high expression from P0 onwards (Figure 16 A). To investigate the cardiac specific expressiom of *AS-Trdn* in adult mice, in-house Microarray datasets of isolated heart-cells and 11 other tissues were utilized (AG Böttger, unpublished data). *AS-Trdn* was exclusively and highly

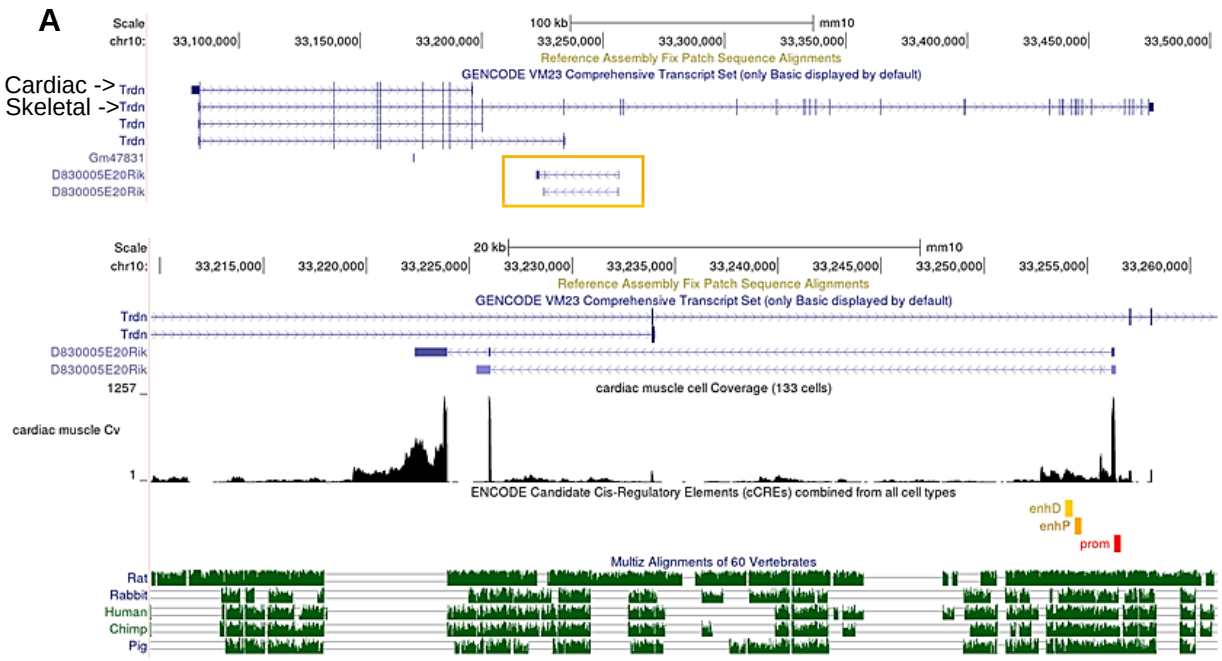

B

Platform	VectorBuilder		EMBOSS-Water	
Organism	Human	Mouse	Human	Mouse
Sequence length	2384	1844	2384	1844
Alignment length	2694		2650	
Identity	1312 (48.70%)		1115 (42.1%)	
Gaps	1160 (43.06%)		1227 (46.3%)	

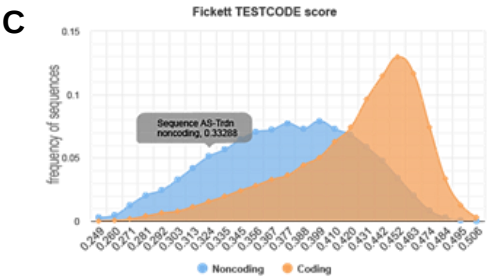

Figure 15 | Genomic localization and sequence analysis of the long non-coding RNA *AS-Trdn*. A UCSC Genome browser view of the triadin and *AS-Triadin* locus (D830005E20Rik), with triadin isoforms (upper panel) and detailed view on *AS-Trdn* (lower panel). RNA sequencing and cis-regulatory element tracks of cardiac muscle cells show expression coverage of the antisense lncRNA and the promoter as well as two enhancer regions. The regulatory regions, exon 1 and 2 are highly conserved among different species as shown by the multi alignment track in green. **B** Homology calculations of the main human and mouse *AS-Trdn* transcript shows sequence identity between 42.1 and 48.7 % (VectorBuilder; EMBOSS-Water). **C** *AS-Trdn* sequence analysis proofs it as non-coding by a Fickett TESTCODE score of 0.33.

detectable in the heart, specifically in cardiomyocytes, compared to multiple other lncRNAs and tissues (Figure 16 B). To further elucidate the subcellular localization of *AS-Trdn*, quantitative reverse transcription PCR (RT-qPCR) and RNA fluorescence in-situ hybridization (RNA-FiSH) were performed. The RT-qPCR demonstrated high detection of *AS-Trdn* in nuclear compared to cytoplasmic fractions of adult cardiomyocytes, while *GAPDH* control displayed almost equal distribution in both fractions (Figure 16 C). The RNA FiSH on isolated adult and neo cardiomyocytes displayed distinct expression of *AS-Trdn* in the nucleus of adult CMs while no expression was detected in neoCMs. A probe against the polyA-tail of mRNAs was

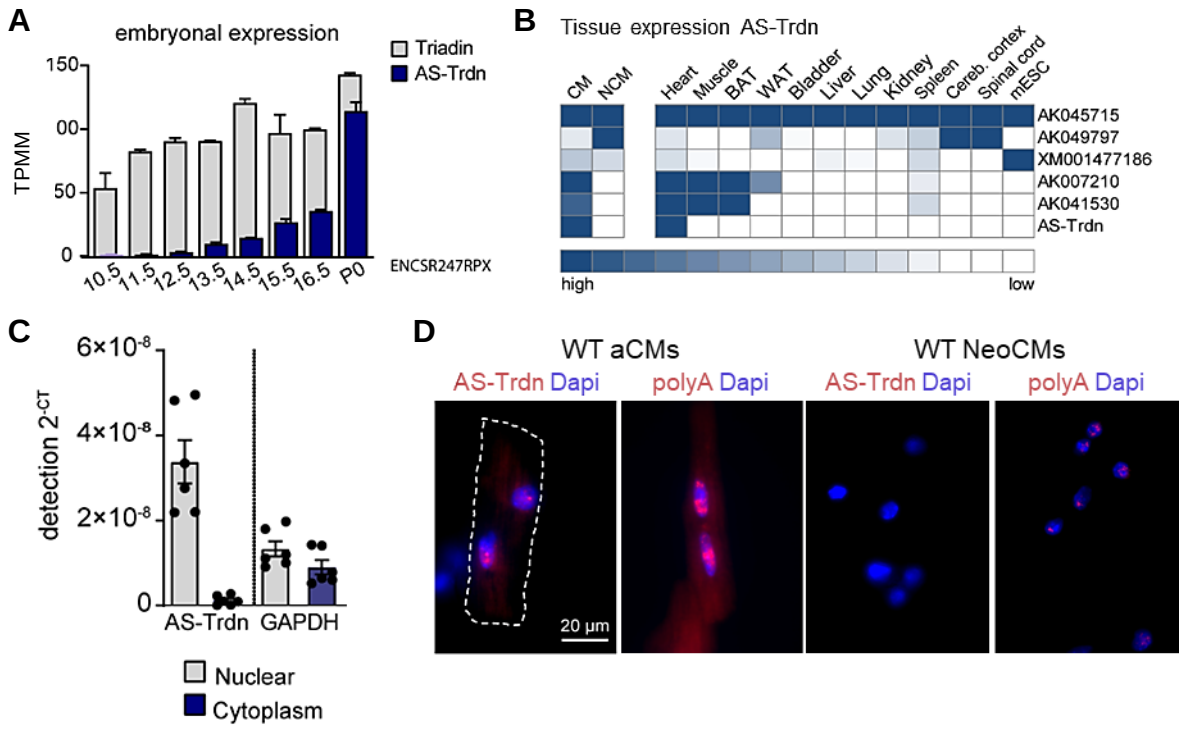

Figure 16 | *AS-Trdn* is a heart exclusive and nuclear enriched lncRNA. A Expression analysis of *AS-Trdn* and *triadin* using a publicly available RNAseq data set of different embryonic mouse stages. TPM, transcript per million. n = 2 of each stage. **B** Tissue expression analysis of in-house microarray data-sets demonstrates cardiomyocyte specific expression of *AS-Trdn* compared to multiple tissues and lncRNAs in mice. **C** qRT-PCR of *AS-Trdn* in fractionated cardiomyocytes. *AS-Trdn* expression is detected in nuclear fractions of adult CMs while being undetected in the cytoplasm. *GAPDH* is used for comparison. n = 6 CMs. **D** RNA FiSH of *AS-Trdn* in adult cardiomyocytes (aCMs) and neonatal cardiomyocytes (NeoCMs), compared to polyA mRNA in control. *AS-Trdn*, red, Quasar 570; T30, red, Quasar 570; Dapi, blue. n = 3. **A & C** Mean ± SEM.

used as a control in both cases, showing a strong, mainly nuclear localization in adult and neonatal cardiomyocytes. Relatively, the expression of *AS-Trdn* was focused in distinct regions in the nucleus while the polyA signal was detectable in greater extend throughout the whole nucleus (Figure 16 D).

3.1.2. Loss of *AS-Trdn* induces long *Trdn* isoform expression

To investigate the molecular and physiological function of *AS-Trdn*, a Knock-In (KI) mouse line was established, incorporating a genomic polyA insertion to stop antisense polymerase elongation. Therefore, the CRISPR/CAS9 system was employed to insert a 2 x polyA sequence in antisense direction into the first exon of the lncRNA. The KI mouse line was originally generated by Dr. Maria Weiss during her PhD work as part of a screening approach and is well established (Figure 17 A; Weiss, 2020). Given that the Knock-In is designed to eliminate the expression of its target gene, the *AS-Trdn* polyA KI line will be subsequently referred to as *AS-Trdn* KO or KO. The successful insertion of the polyA cassette was confirmed by PCR, with one primer on exon 1 and a second primer on the polyA sequence. KO DNA probes revealed a band sized 605 bp on gel electrophoresis upon successful insertion. To validate the efficient deletion of *AS-Trdn* RNA upon polyA insertion, RT-PqCR was performed on isolated WT and KO hearts and compared to *tibialis anterior* muscle as a control, where *triadin* but not *AS-Trdn* is expressed (TA). In both KO hearts and in TA muscle, no expression of the lncRNA was detected, while WT hearts exhibited normal expression levels. This data confirmed the successful loss of *AS-Trdn* expression upon polyA insertion (Figure 17 B).

Given *AS-Trdn*'s role in regulating the isoform abundance of triadin in the heart, the expressional changes of triadin isoforms upon loss of the lncRNA were examined using primers localized within the unique 3' UTR of cardiac *Trdn* exon 8 and skeletal *Trdn* exon 38 (trisk32 and trisk95 respectively). In WT hearts, cardiac *Trdn* was detected significantly stronger compared to a minor detection of the long skeletal muscle isoform. The results of the *AS-Trdn* KO hearts revealed a significant reduction in cardiac *Trdn*, while the expression of the skeletal muscle specific *Trdn* isoform was drastically increased (Figure 17 C). To confirm and visualize the loss of *AS-Trdn* transcription and, consequently, the induced expression of the long *triadin* isoform, whole transcriptome RNAseq was performed. The RNAseq was performed in-house on 3 WT and 3 KO hearts using paired-end sequencing and strand specific mapping to distinguish sense- (+) and antisense-strand (-). The sequencing of the KO hearts revealed a full loss of *AS-Trdn* expression, whereas the WT samples displayed clear read coverage along the *AS-Trdn* locus. Interestingly, *AS-Trdn* displayed widespread transcript coverage over the whole annotated locus and beyond, reaching until exon 9 of the triadin locus (Figure 17 D). Examining the whole triadin locus, an approximately

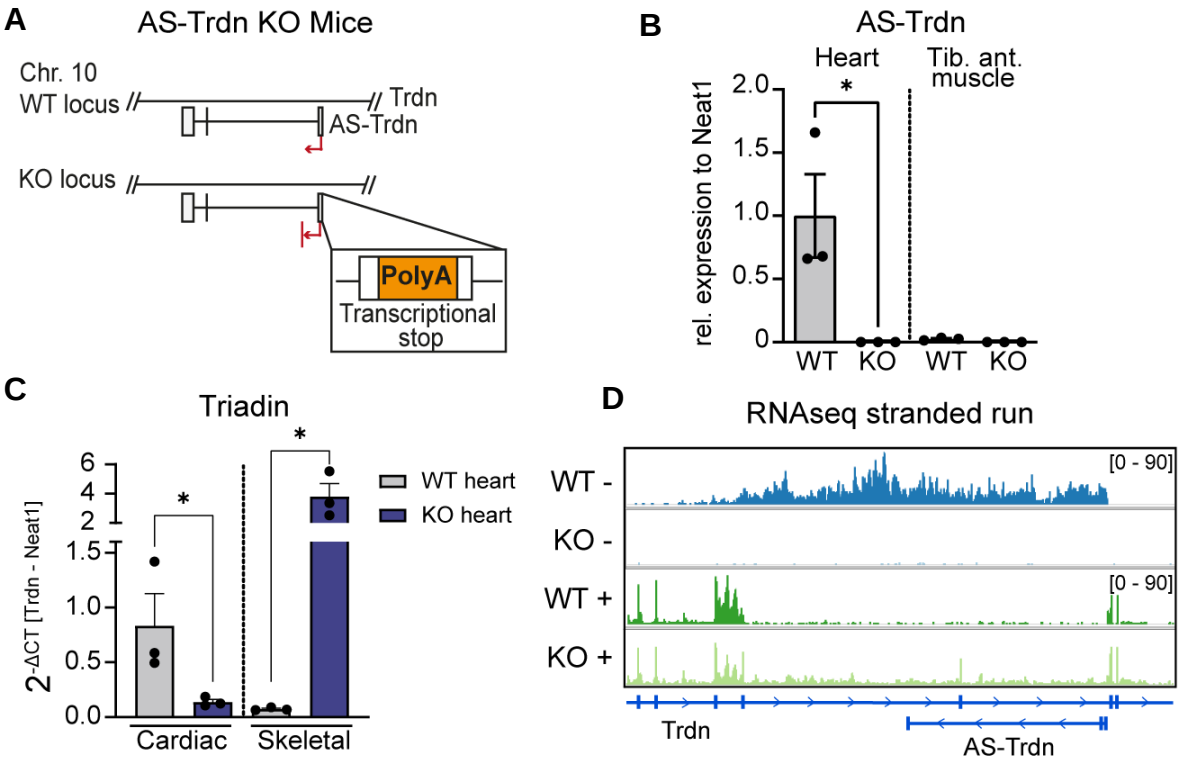

Figure 17 | *AS-Trdn* KO strategy and evaluation. A Schematic drawing of the AS-Trdn KO strategy. PolyA insertion into the first exon of *AS-Trdn* leads to an early transcription termination. **B** qRT-PCR of *AS-Trdn* in WT and KO heart and *tibialis anterior* muscle confirms significant loss of the lncRNA expression. n = 3. **C** qRT-PCR of triadin isoform expression in *AS-Trdn* WT and KO. Cardiac triadin expression is significantly lost in KO hearts, while expression of skeletal muscle triadin is significantly increased. n = 3. **D** Visualization of the stranded RNA sequencing of WT and KO hearts confirms the loss of antisense transcription on the antisense (-) strand without disturbance of the sense (+) transcription. B & C Mean ± SEM.

50 % increased expression of the skeletal muscle *triadin* exons was detected in KO compared to WT hearts. Simultaneously, Splicing between exon 9, 10 and 11 was strongly detectable in *AS-Trdn* KO hearts, which were only very minor detectable in WT samples and represent the first skeletal muscle specific triadin exons (Figure 18 A). By analysing the differential splice junctions of WT and KO hearts, the newly established splicing along the *AS-Trdn* locus from *triadin* exons 9 to 10 and 11 until the last exon of the long *triadin* isoform could be confirmed. In WT hearts on the other side, even though expression of exons from the long Trdn isoform were detected, again almost no splicing along the *AS-Trdn* locus was observed (Figure 18 A & B). To further validate this observation, a bioinformatics calculation tool called JunctionSeq was employed. This sequence analysis tool is utilized to illustrate the differential usage of exons and splice junctions in RNAseq experiments. By plotting the results comparing WT and KO hearts, the observed increase in the expression of exons 9 and 10 was confirmed. This change was the most prominent difference between WT and *AS-Trdn*

KO hearts, followed by a comparatively slight increase in the subsequent exons of skeletal *triadin* (Figure 18 B). Given that the RT-qPCR results and the JunctionSeq analysis revealed a switch in *triadin* isoform abundance upon loss of *AS-Trdn*, the finding of decreased but ongoing expression of long *triadin* reads, while almost no splicing along the *AS-Trdn* locus was detected in the WT situation, was surprising. To clarify the triadin isoform abundance and consequent protein expression, a western blot analysis of WT and *AS-Trdn* KO heart membrane isolations was conducted, using antibodies specifically binding to the cardiac or skeletal muscle TRDN isoform. The cardiac specific antibody, recognizing a peptide coded within the cardiac unique extended 8th exon, was provided by Dr. Isabel Marty from Grenoble institute in France. For the long skeletal muscle specific triadin protein, a commonly available antibody was used. Western blot analysis confirmed the findings of the RT-qPCR as well as the JunctionSeq analysis, indicating that cardiac TRDN is the only isoform expressed in WT hearts, while the *AS-Trdn* KO hearts exhibited high expression of the skeletal muscle specific triadin isoform (Figure 18 C).

Since *AS-Trdn* is a highly conserved long non-coding RNA, the question arises whether the same molecular mechanism regulating triadin isoforms is also applicable in human samples or human cell lines. To address this question, Gheo Bio Maria Idrissou from Technical University Munich replicated the *AS-Trdn* KO in human Induced Pluripotent Stem Cells (hIPSC). A RNA polymerase II ChIPseq dataset of human heart tissue was examined to locate the transcriptional start side of human *AS-TRDN.* Based on this analysis a sgRNA as well as a polyA harbouring repair oligo was designed to delte expression of human *AS-TRDN* (Figure 19 A). The construct as well as the repair oligo harbouring the polyA site were subsequently transfected into hIPSC cells by Gheo Idrissou and insertion of the repair oligo into the target site was identified by PCR and confirmed by Sanger sequencing of the PCR product. One *AS-TRDN* KO clone and one negative clone serving as a control were then differentiated into an early form of cardiomyocytes (hIPSC-CMs). These hIPSC derived cardiomyocytes formed a beating monolayer after 48 days of differentiation, presenting fibre development with sarcomere structures (Figure 19 B). To determine if the *AS-TRDN* KO in hIPSC was sufficient and exhibited the same effect on *TRDN* isoform abundance as demonstrated in mice, RT-qPCR was assessed for *AS-TRDN*, cardiac and skeletal *triadin*. The polyA insertion resulted in a significant and complete loss of *AS-TRDN* transcript as well as a significant decrease in cardiac *triadin* expression (Figure 19 C).

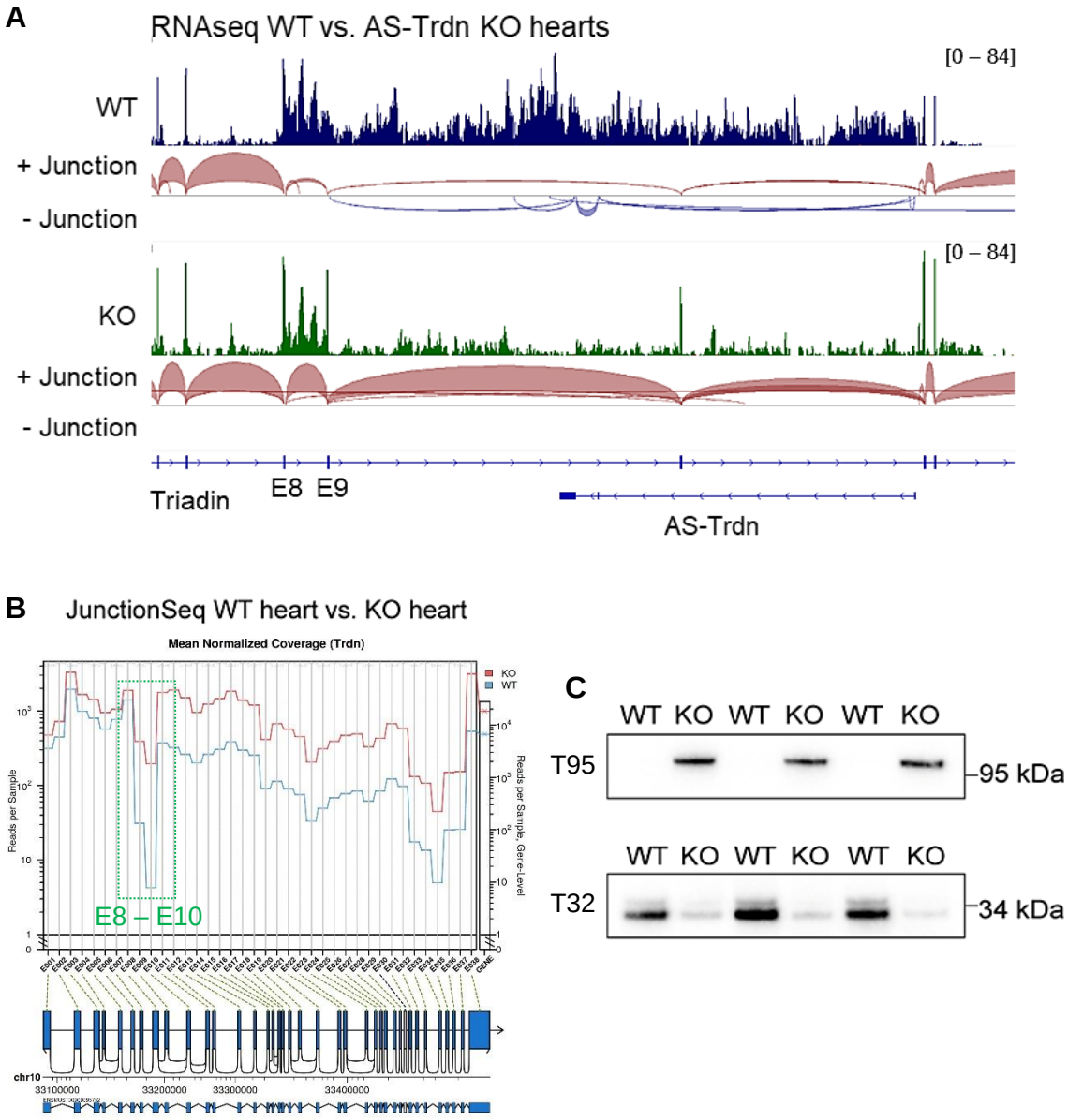

Figure 18 | Loss of *AS-Trdn* transcription leads to expression of the long skeletal muscle isoform of triadin in the heart. A RNAseq of WT and *AS-Trdn* KO hearts reveals loss of *AS-Trdn* coverage, splicing and consequent expression of triadin exons upstream of the lncRNA locus. Sense (+) and antisense (-) junctions are displayed below the coverage tracks. n = 3. **B** JunctionSeq analysis demonstrating the splicing of the *triadin* isoforms in WT and KO hearts. The WT situtation reveales ongoing expression of long isoform reads of *triadin* until exon 38, while the unctions between exon 8 and 9 and 10 show a major decrease. **C** WB analysis of WT and KO membrane isolations using cardiac (T32) and skeletal muscle (T95) TRDN isoform specific antibodies. n = 3.

Simultaneously, the expression of the skeletal muscle specific *triadin* isoform increased, although lacking statistical significance. Nonetheless, by calculating the relative ratio between cardiac and skeletal *triadin* mRNA to examine the change in isoform tendency of each sample, the KO hIPSC revealed a significant shift towards the long skeletal muscle isoform upon loss of antisense transcription (Figure 19 D). These investigations demonstrated, that *AS-TRDN* expression is needed to induce cardiac *TRDN* formation in mouse as well as human heart cells.

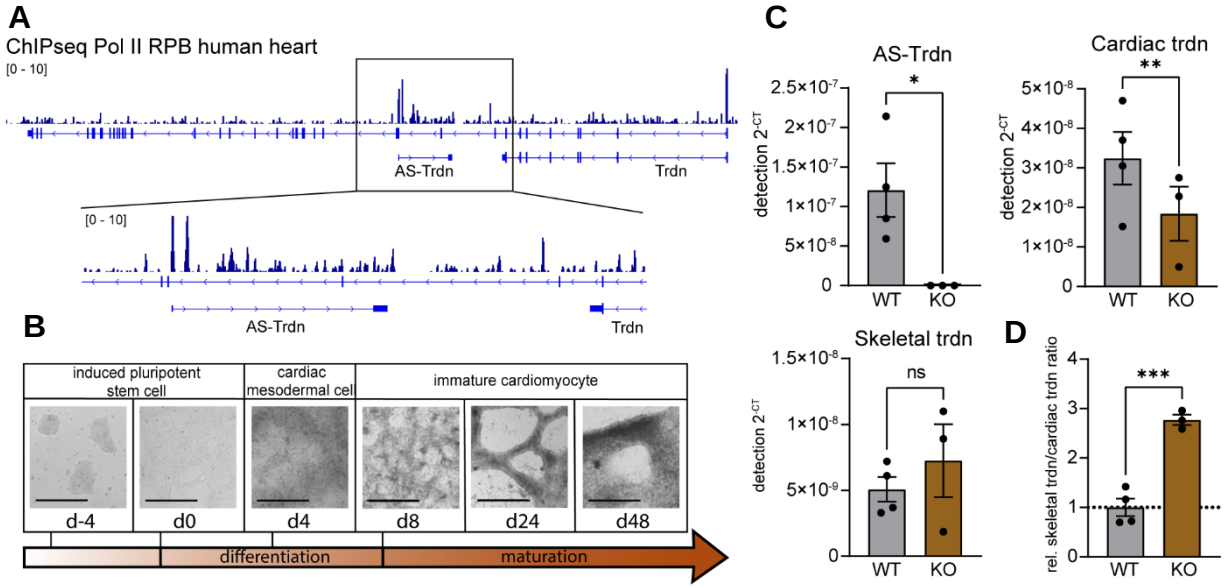

Figure 19 | Loss of *AS-TRDN* transcription induces skeletal muscle triadin isoform expression in hIPSC cardiomyocytes. A RNA Polymerase II ChIPseq of human heart samples revealed transcriptional start side of *AS-TRDN* at exon 1 (ENCODE accession #ENCSR336YRS). **B** Schematic representation of hIPSC-CM differentiation and maturation progress. After 48 days, hIPSC form immature cardiomyocytes, which show sarcomeric structre and synchroneous beating. **C** qRT-PCR of hIPSC-CM WT and KO RNA revealed complete loss of *AS-TRDN* as well as significant decrease in cardiac *triadin* expression. Skeletal muscle *TRDN* was increased in KO hIPSC-CM even though not significantlly. Cardiac Trdn, paired two-tailed student's t-test. **D** Calculating the relative ratio between skeletal and cardiac *triadin* mRNA abundance revealed a significant tendency towards the long skeletal muscle isoform in KO hIPSC-CMs. n = 4 WT/3 KO. Mean ± SEM.

3.1.3. *AS-Trdn* transcription is driven by GATA4 and expands the annotated 3'-termination site

AS-Trdn is a nuclear localized lncRNA, as confirmed in previous results, expressed on the antisense strand of the protein-coding gene Triadin in the heart. Analysing the WT and *AS-Trdn* KO heart RNA sequencing results, ongoing RNA transcription beyond the annotated 3'-UTR of *AS-Trdn* was detected. To investigate this observation also in human heart, the expression of *AS-TRDN* was analysed using publicly available RNAseq data of human left ventricle samples (ENCODE accession #ENCSR000AHH). This analysis confirmed a prolonged transcription of *AS-TRDN* extending beyond the annotated exon 3 until approximately exon 9 of triadin and revealing a total transcription elongation of *AS-TRDN* for ~ 32 kb (Figure 20 A).

To provide further validation for these transcripts, RT-qPCR was assessed at two different loci within the intronic region of *AS-Trdn* exon 3 and triadin exon 9 using again mouse RNA probes. These results were compared to *AS-Trdn* KO mouse and TA samples, where no antisense transcription exists. Indeed, the RT-qPCR displayed significant expression of both regions (*AS-Trdn* downstream 1 and 2 (AS-T DS1 and DS2)) in WT hearts while no expression was detected in KO hearts and *tibialis anterior* (Figure 20 B). Addressing concerns about potential contaminations or artefacts, the *AS-Trdn* locus was further investigated using long-range sequencing. NanoporeSeq, a next-generation sequencing technique capable of sequencing non-fragmented RNAs and thereby analysing full-length transcripts, was employed. Dr. Ralf Gilsbach from university hospital Frankfurt (now Heidelberg) shared his mouse WT heart sequencing results, allowing the investigation of the full-length *AS-Trdn* transcript. Excluding all transcripts of the sense strand, the mapping revealed, that the spliced *AS-Trdn* transcript possesses at least 4 exons instead of 3, with the last exon overlapping exon 9 of the protein-coding gene. A high abundance of the intronic transcripts evaluated prior using RT-qPCR were observed, thereby confirming the previous results and suggesting that the actual *AS-Trdn* transcript and therefore the transcription goes beyond the annotated 3'-UTR, terminating at the side of the last exon of the cardiac *Trdn* isoform (Figure 20 C). Analysing the NanoporeSeq data revealed an additional, previously not annotated exon of the *Trdn* gene upstream of *AS-Trdn*. This newly found sense exon is located only approx. 500 bp upstream of the first *AS-Trdn* exon and is only detected in cardiac but not skeletal muscle, suggesting that the promoter of AS-Trdn is bidirectional (Figure 20 D). This bidirectional promoter might drive the

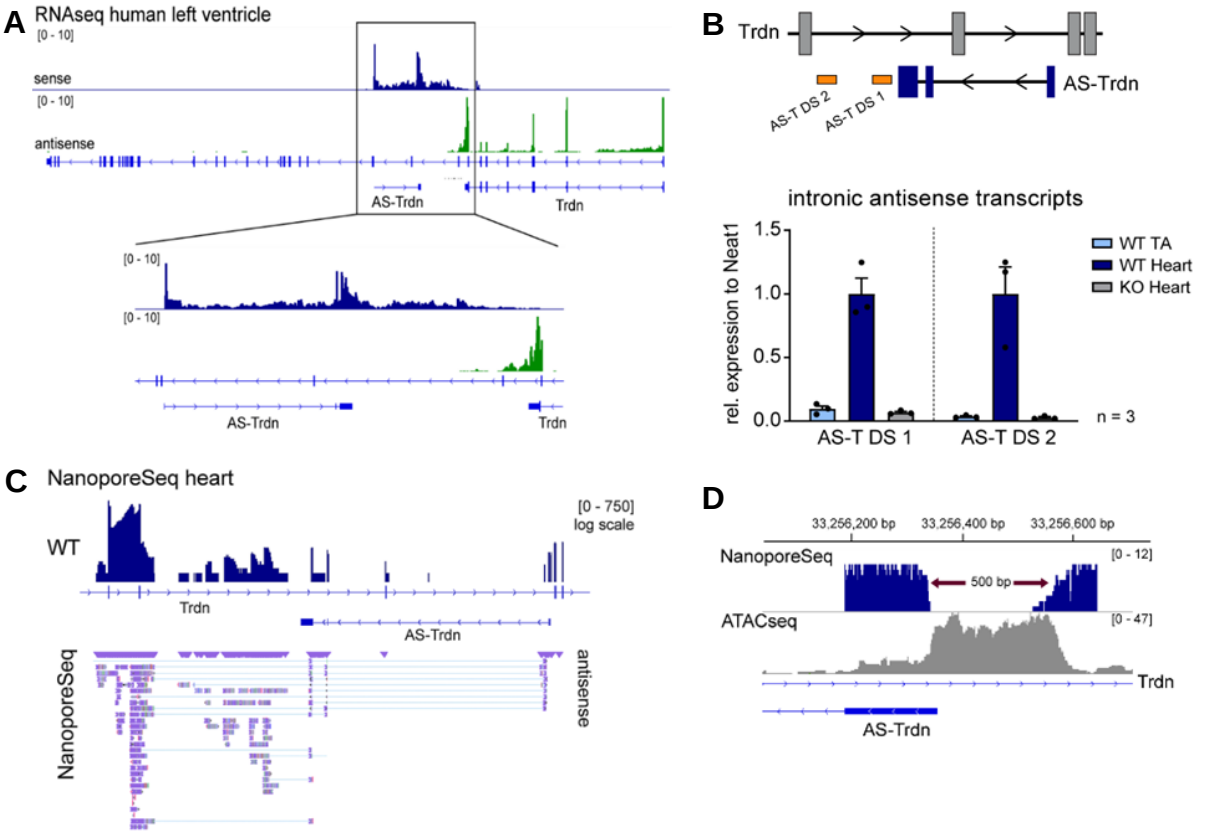

Figure 20 | Long-range sequencing reveals new *AS-Trdn* termination site and potential bidirectionality of its promoter. A Stranded RNAseq of human left ventricle confirms ongoing antisense transcription beyond the annotated *AS-TRDN* termination site (ENCODE accession #ENCSR000AHH). **B** Schematic drawing of the designed *AS-Trdn* downstream primer combinations to check for expression in qRT-PCR. Both intronic transcripts show high abundance in WT heart samples, while almost no expression was detected in WT TA and KO heart samples. n = 3. Mean ± SEM. **C** Long-range sequencing of the *AS-Trdn* locus was analysed using NanoporeSeq data of WT mouse hearts, provided by Ralf Gilsbach. The transcript of *AS-Trdn* exhibits 4 spliced exons instead of 3 and shows a high abundance of unspliced RNA fragments in the intronic region downstream of exon 3. **D** Zoomed in view of the *AS-Trdn* promoter region, as indicated by ATACseq (ENCODE accession #ENCSR451NAE), reveals new exon on the sense strand in close proximity to the first *AS-Trdn* exon.

expression of *AS-Trdn* as well as the expression of the *Trdn* exons located in sense downstream of *AS-Trdn,* including the newly found exon. To test this hypothesis, a luciferase assay was designed, using a dual-reporter system. The *AS-Trdn* promoter, evaluated using publicly available ATACseq data of mouse hearts (ENCODE accession #ENCSR451NAE), was cloned independently or together with the potential enhancer regions into a vector situated between a *renilla* and a *firefly* luciferase reporter (Figure 21 A). The two constructs were subsequently transfected into HEK293 cells were neither Triadin nor *AS-Trdn* are expressed. After an overnight incubation, the relative luminescence was measured and compared to two control transfections. The measurements revealed significant antisense (*firefly*) as well as sense (*renilla*)

expression of the reporter in both constructs, while no signal was detected in the two control samples. This confirms that the *AS-Trdn* promoter exhibits bidirectional transcription, confirming the original hypothesis (Figure 21 B). In a next step to elucidate the heart exclusive expression of *AS-Trdn* further, the enhancer function within the *AS-Trdn* locus was investigated. Therefore, ChIPseq datasets and a transcription factor binding site prediction were employed to discover potential heart specific transcription factors binding to either the promoter or enhancer region. Serum response factor (SRF) as well as ep300 were identified as strongly binding to the promoter and in case of SRF also to the enhancer region of *AS-Trdn*. These factors are known co-factors of multiple heart specific transcription factors. Two of them are GATA4 (GATA Binding Protein 4) and TEAD1 (TEA domain transcription factor 1), each having multiple potential binding sites within the promoter as well as the enhancer region (Figure 21 C, D). To validate the potential involvement of these transcription factors, both constructs were transfected in HEK293 cells and co-transfected with plasmids containing the sequence for either *Gata4* or *Tead1*. After an overnight incubation, again luminescence was measured to validate expressional changes. While TEAD1 showed no effect on either sense or antisense transcription, GATA4 significantly increased sense and antisense transcription of *AS-Trdn* using the promoter construct and even further increased it by addition of the enhancer region (Figure 21 E, F).

In conclusion, the data clearly demonstrate, that *AS-Trdn* transcription exceeds the annotated 3'-UTR and thereby overlaps with the transcriptional termination side of cardiac Triadin. Using luciferase assays, the heart-specific transcription factor gata4 was demonstrated to be a main driver of *AS-Trdn* expression upon binding to the promoter as well as to the enhancer region. The resulting bidirectional transcription of the *AS-Trdn* promoter explains the remaining expression levels of the triadin exons downstream of *AS-Trdn*. With the newly identified exon, this transcription may give rise to an independent heart-specific transcript, which might encode a truncated TRDN-related protein. The experimental planning as well as the sequencing analysis were performed by myself, while the experimental procedure of cloning, cell transfection and the luciferase assays were carried out by Sara Hettrich in the course of her master thesis.

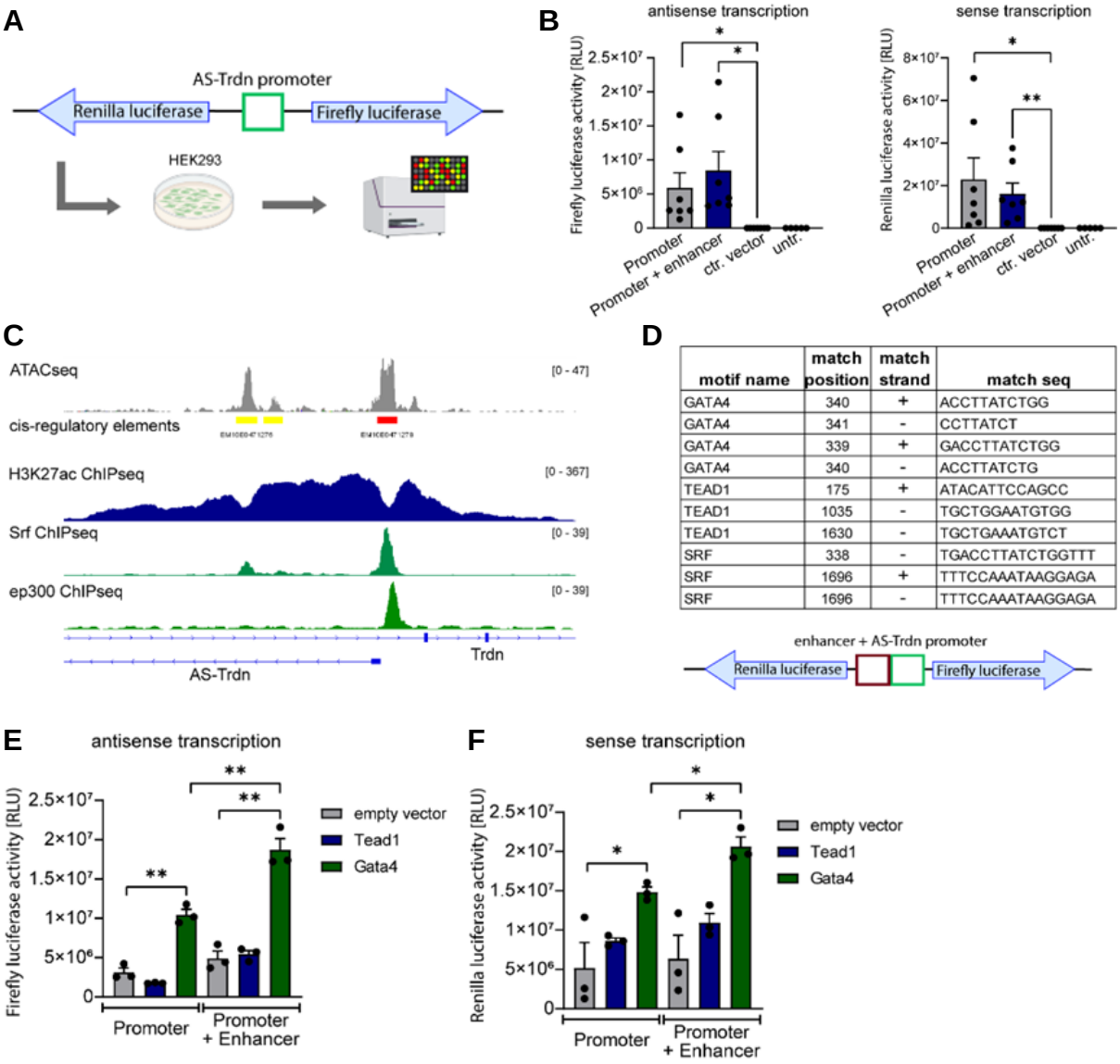

motif name	match position	match strand	match seq
GATA4	340	+	ACCTTATCTGG
GATA4	341	-	CCTTATCT
GATA4	339	+	GACCTTATCTGG
GATA4	340	-	ACCTTATCTG
TEAD1	175	+	ATACATTCCAGCC
TEAD1	1035	-	TGCTGGAATGTGG
TEAD1	1630	-	TGCTGAAATGTCT
SRF	338	-	TGACCTTATCTGGTTT
SRF	1696	+	TTTCCAAATAAGGAGA
SRF	1696	-	TTTCCAAATAAGGAGA

Figure 21 | *AS-Trdn* promoter exhibits bi-directionality and is driven by GATA4. **A** Schematic drawing of the cloning strategy to insert the *AS-Trdn* promoter in a dual luciferase reporter vector and subsequent transfection into HEK293 cells, followed by luminescence measurement using the MITRAS system. **B** Luciferase assay quantification by relative measurement of renilla and firefly luminescence of the transfected reporter vectors harbouring the *AS-Trdn* promoter region, promoter and enhancer region, an empty vector (ctr.) or an untransfected control (untr.). The results display a significant expression of both reporters compared to the controls. n = 7 **C** IGV representation of the *AS-Trdn* promoter and enhancer region, as evaluated by open chromatin structures indicated by the ATACseq track, and binding of the transcription factors SRF and EP300 as indicated by ChIPseq experiments of adult mouse hearts (SRF, NCBI GSM2944730; EP300, ENCODE accession #ENCSR777VNA). **D** Transcription factor binding site prediction shows potential binding sites for GATA4, TEAD1 and SRF on sense and antisense strand. Match position under 400 indicates potential binding site at promoter region and >400 at enhancer region. **E, F** luciferase assay quantification of the reporter vectors co-transfected with *Gata4* and *Tead1* expression plasmids. GATA4 shows a significant increase upon promoter as well as enhancer co-transfection, in sense and antisense direction. n = 3. Mean ± SEM.

3.1.4. *AS-Trdn* expression leads to transcriptional interference via roadblock formation

The studies by Zhao, Riching and Knight et al. demonstrated, that genomic deletion of exon 2 and 3 of *AS-Trdn* had no effect on the formation of the long skeletal muscle specific isoform of triadin. They agreed to the postulated mechanism of transcriptional interference by opposing polymerases, which was suggested by Zhang et al. in 2018, but were not able to elucidate it (Zhang et al., 2018; Zhao, Riching and Knight et al.. 2022). To investigate the transcriptional effect of *AS-Trdn* on the formation of triadin short (cardiac) and long (skeletal muscle) isoform, the aim was to generate an *AS-Trdn* KO mouse line with immediate transcriptional termination by insertion of a polyA cassette into the first exon of the lncRNA. In the previous results, the loss of *AS-Trdn* transcription could be confirmed in KO mice and led indeed to the formation of the long triadin isoform in the heart on RNA as well as on protein level. In order to prove the transcriptional interference by the antisense lncRNA further, a “proof of concept” experiment was performed on skeletal muscle cells, where *AS-Trdn* is not expressed but skeletal muscle triadin. In this regard, satellite cells were isolated from muscle tissues of mice using FACS and transfected with two different constructs. In a first approach, a pCMV-*AS-Trdn* plasmid was used to overexpress the lncRNA from an exogenous locus, evaluating the spliced-transcript function of the lncRNA. In a second approach the CAS9-SPH system was used in combination with a sgRNA targeting the promoter region of *AS-Trdn*. Upon binding of the Cas9-SPH construct, the expression of the lncRNA from its endogenous locus is initiated (Zhou et al., 2018; Figure 22 A). With these two approaches, the aim was to distinguish between the transcript dependent and transcriptional dependent function of *AS-Trdn* by evaluating the expression profile of the different *Trdn* isoforms. First, the successful overexpression of *AS-Trdn* was quantified using RT-qPCR. The transfection of pCMV-*AS-Trdn* induced a massive expression of the lncRNA, with numbers exceeding every *in vivo* situation, while the expression level reached with the Cas9-SPH system approximately matched *in vivo* levels, but were still lower compared to expression in the heart. As a control, cells were either transfected with a GFP-control plasmid or a sgRNA targeting *mitolnc*, an lncRNA which is involved in metabolic regulation in the heart, or left untransfected. None of the controls displayed detectable expression of *AS-Trdn* (Figure 22 B). To examine the changes in *triadin* isoform expression, Taqman probes targeting either the 5’ region of *triadin* or the 3’ region of the long *Trdn* isoform were

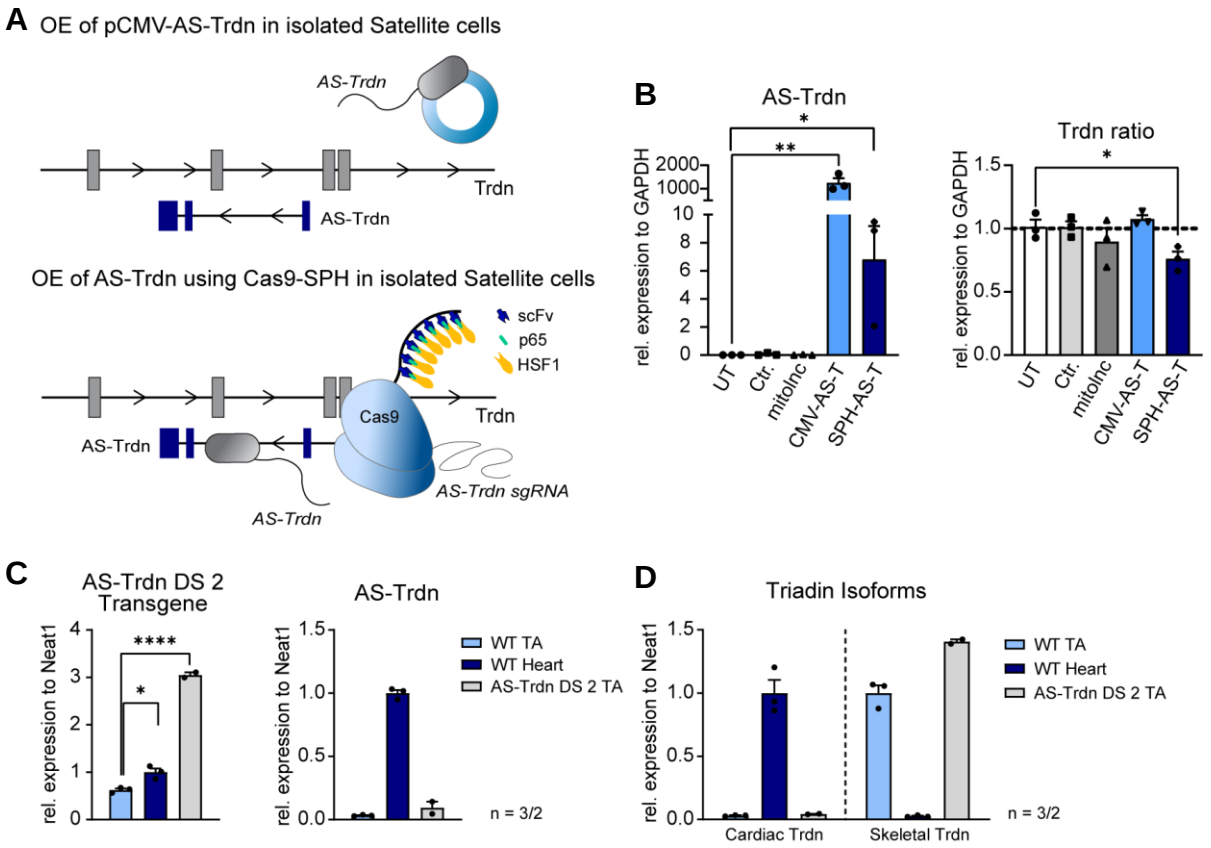

Figure 22 | Transcriptional activation of *AS-Trdn* leads to cardiac *triadin* isoform generation in satellite cells. A Schematic drawing of the experimental procedure to test the function of *AS-Trdn* in isolated satellite cells. Two different approaches were performed: the overexpression (OE) of *AS-Trdn* using a CMV promoter driven plasmid (exogenous) and the overexpression upon endogenous activation of the *AS-Trdn* promoter region. **B** RT-qPCR of the transfected and differentiated satellite cells shows significant induction of *AS-Trdn* expression upon both approaches, whilst only CAS9-SPH OE of *AS-Trdn* resulted in a significant change in *trdn* isoform expression. *Trdn* ratio was measured as *Trdn* long/*Trdn* all = > 1 (> skeletal muscle isoform) or < 1 (> cardiac isoform). n = 3. **C** Quantitative RT-PCR evaluation of the transgenic OE of the *AS-Trdn* DS2 transcript was significant in TA muscle, whilst *AS-Trdn* expression levels remained unchanged. **D** *Triadin* isoform abundance displayed no changes on RT-qPCR upon transgenic OE of the *AS-Trdn* DS 2 transcript as compared to WT TA and WT heart. **B-D** Mean ± SEM.

used, due to very low RNA concentrations. By calculating the ratio of the resulting expression levels, a tendency towards the short (<1) or the long (>1) *triadin* isoform can be evaluated. The results revealed no changes in *triadin* isoform abundance in the control transfections as well as upon overexpression of *AS-Trdn* from an exogenous locus (pCMV-*AS-Trdn*). Nevertheless, upon transcriptional activation of the *AS-Trdn* endogenous locus, the *Trdn* ratio was reduced by 25 %, indicating a partial switch in favour of the cardiac specific isoform (Figure 22 B). These results demonstrate, that transcriptional activation of the *AS-Trdn* locus is sufficient to induce cardiac *Trdn* formation, while the transcript itself seems to be dispensable. Since the RNAseq as

well as the NanoporeSeq results of WT mouse hearts revealed a new downstream transcript of *AS-Trdn*, the possibility can't be ruled out, that this RNA fragment has an antisense siRNA effect on the 3'-UTR of the *triadin* mRNA or influences the locus with a so far unknown mechanism. To test this hypothesis, a transgenic mouse line expressing the newly identified downstream part of *AS-Trdn* was generated and the change in *triadin* isoforms was assessed using again RT-qPCR of *tibialis anterior* muscle. The transgene was significantly expressed in TA muscle compared to WT TA and heart, while no change in the expression of *AS-Trdn* lncRNA was detected (Figure 22 C). Despite sufficient expression, the downstream transcript had no effects on the expression level of the cardiac or skeletal muscle isoform of t*riadin*, as RT-qPCR results demonstrated (Figure 22 D).

In order to investigate a possible polymerase interference, the first aim was to visualize the mode of transcription of both polymerases. Therefore, CUT&RUN experiments using an antibody against the serine 2 phosphorylated RNA polymerase II (Pol II pSer2) were performed on WT and *AS-Trdn* KO cardiomyocytes. These results were compared to a publicly available ChIPseq data set targeting the large subunit of RNA polymerase II (Pol II RPB) from WT mouse as well as the already introduced ChIPseq data set of human hearts. All data sets showed the common *AS-Trdn* promoter proximal stalling of the RNA Pol II as well as the stalling at the proximal enhancer region of *AS-Trdn*. Interestingly, the mouse as well as the human RNA polymerase II analysis revealed an additional identical stalling site downstream of *AS-Trdn*, shortly before exon 9 of triadin (Figure 23 A-C). Since the KO CUT&RUN analysis displayed no peak at this site, it can be assumed, that this peak belongs to the polymerase transcribing the antisense strand, but it cannot be ruled out that it also belongs to the sense-transcribing polymerase. Investigating the sequence composition of the identified termination or stalling site, an increase in GC content of about ~ 20 % was observed (Figure 23 C). To investigate if this GC rich sequence is causing the RNA Pol II stalling/termination or just common polyA signals, two different approaches were performed. At first, two polyA KI mouse lines were generated to stop transcription at earlier stages downstream of *AS-Trdn* exon 3. Unfortunately, even though the insertion was successful, no changes in *AS-Trdn* expression could be determined, indicating the polyA sequences were not recognized as stop signals (Appendix). In the second approach, three intronic polyA sites between exon 8 and 9 of triadin were identified using a public available polyA atlas and consequently deleted in mESC using

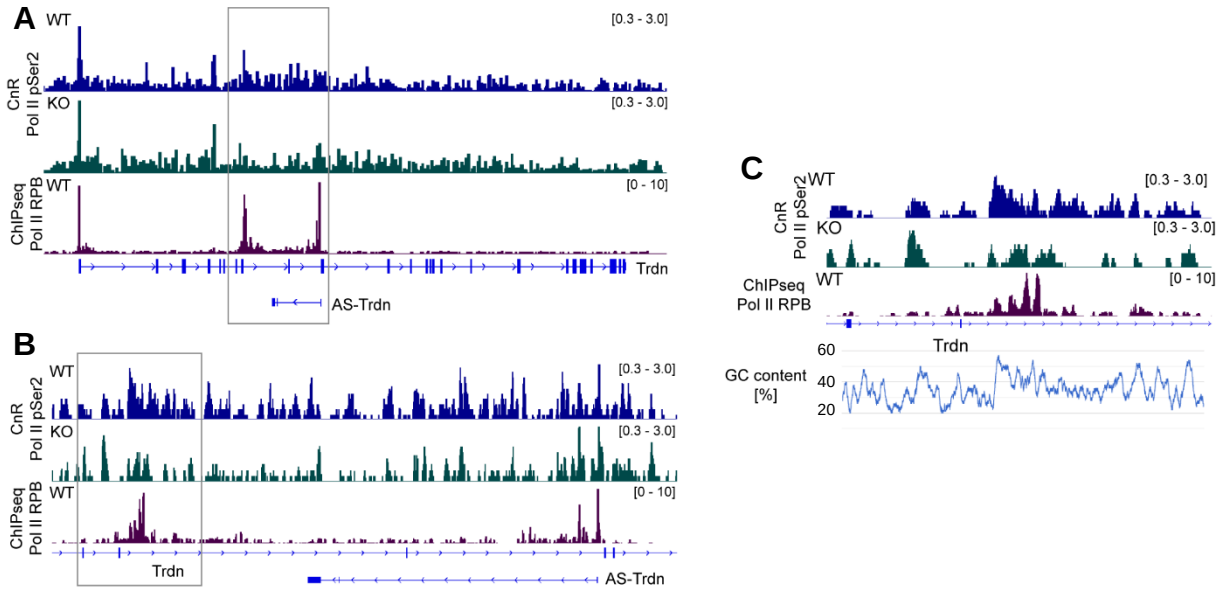

Figure 23 | RNA Polymerase II transcription analysis of AS-Trdn locus revealed stalling before exon 9 of Trdn. A RNA Polymerase II pSer2 CUT&RUN using WT and *AS-Trdn* KO cardiomyocytes nuclei displayed typical promoter proximal polymerase stalling, but also revealed stalling at Exon 9 of triadin, which was lost upon KO of *AS-Trdn*. The same observation was done using public RNA Polymerase II RPB ChIPseq data from mouse left ventricle. **B** Zoomed in region of 3'-UTR and downstream region of *AS-Trdn* including exon 8 and exon 9 of triadin. **C** Close-up on RNA Polymerase II stalling site and schematic representation of GC content [%]. **A-C** grey boxes indicate zoomed-in regions. RNA Pol II RPB ChIPseq ENCODE accession # ENCSR000CBS.Grey box indicates zoomed in regions. CUT&RUN, n = 1. ChIPseq n = 2.

CRISPR/CAS9. Positive clones were subsequently differentiated into cardiac bodies and the isoform abundance examined using TaqMan probes due to limited amounts of RNA. Both deletions led to a reduction in *AS-Trdn* expression and displayed opposing outcomes regarding *triadin* isoform abundance. While the deletion of the exon 8 proximal polyA site (1. polyA) induced an increased cardiac isoform expression, the deletion of the exon 9 proximal polyA sites (2./3. polyA) significantly increased the expression of the long skeletal muscle *Trdn* isoform (Appendix). These results could indicate a mechanistically important role of the newly identified antisense transcripts, as demonstrated using NanoporeSeq, for the formation of the cardiac specific triadin isoform.

Another possible mechanism explaining the RNA polymerase II occupancy and consequently cardiac isoform expression, could be the formation of an RNA:DNA hybrid, inducing the RNA polymerase II termination and which is prone to happen at GC rich genomic loci (Skourti-Stathaki, Proudfoot et al., 2014). In order to test this hypothesis, a new method to identify native R-loops is currently established on WT and

AS-Trdn KO CM nuclei. Even though, I am able to identify known R-loops using MapR, the method still needs further establishment and repetition until clear results can be shown.

Nonetheless, the identified RNA polymerase II stalling as well as the GC content led to the assumption of an R-loop dependent transcriptional stalling. Therefore, another molecular regulator of RNA:DNA hybrid formation and stability was addressed, which is the methyl transferase 3 (*Mettl3*), the main writer of m6A methylation. Studies revealed the occurrence of m6A within R-loops, causing an increased stabilization of the hybrid and thereby inducing RNA polymerase II stalling and consequently termination (Yang et al., 2019). To test, if m6A has a functional role in the stabilization of the *AS-Trdn* associated R-loop and transcription termination, miCLIP2 data sets from mouse hearts were downloaded from a database (Körtel et al., 2021). The dataset includes a miCLIP2 sequencing as well as the m6a boost machine learning track from WT mouse hearts in a stranded manner. Analysing the *AS-Trdn* locus, a high abundance of m6A modifications was found on the antisense strand at exon 3 of *AS-Trdn*, further downstream and at the identified stalling site using the miCLIP2 dataset. These sites were also in accordance to the m6A boost predicted sites (Figure 24 A). To demonstrate the molecular relevance of these m6A sites, RT-qPCR and Western blot analysis of *triadin* isoform abundance was performed on deletion mutants of the m6A writer *Mettl3* in mouse hearts. Therefore, a conditional *Mettl3* KO mouse line was used, which has been established at the MPI in Bad Nauheim by Max Staps. XMLC-Cre positive as well as negative mice were injected with tamoxifen for one week and after 2 additional weeks, the hearts were collected for RNA isolation. RT-qPCR using a TaqMan assay revealed a significant reduction of *Mettl3* transcripts in XMLC-Cre positive hearts, while the remaining expression might be attributed to non-cardiomyocytes in the heart, which are not targeted by the Cre. The expression levels of *AS-Trdn* as well as the cardiac-specific *triadin* isoform remained unchanged, while an increased expression of the skeletal muscle *Trdn* isoform was observed in *Mettl3* KO hearts. By calculating the relative change in cardiac to skeletal muscle *triadin* expression, a significant increase in favour of the skeletal muscle isoform was observed in all KO hearts (Figure 24 B). WB analysis of cardiac and skeletal muscle TRDN was performed on whole heart lysates from WT and *Mettl3* KO hearts using isoform-specific antibodies and compared to the housekeeping gene RalA. A strong shift towards the skeletal muscle isoform compared to the RT-qPCR results were

observed due to a decrease in cardiac TRDN and an increase in skeletal muscle TRDN protein level in *Mettl3* KO compared to WT hearts. Again, calculating the ratio of both isoforms, this observed shift towards the long skeletal muscle isoform upon loss of mettl3 and therefore of m6A formation could be confirmed (Figure 24 C).

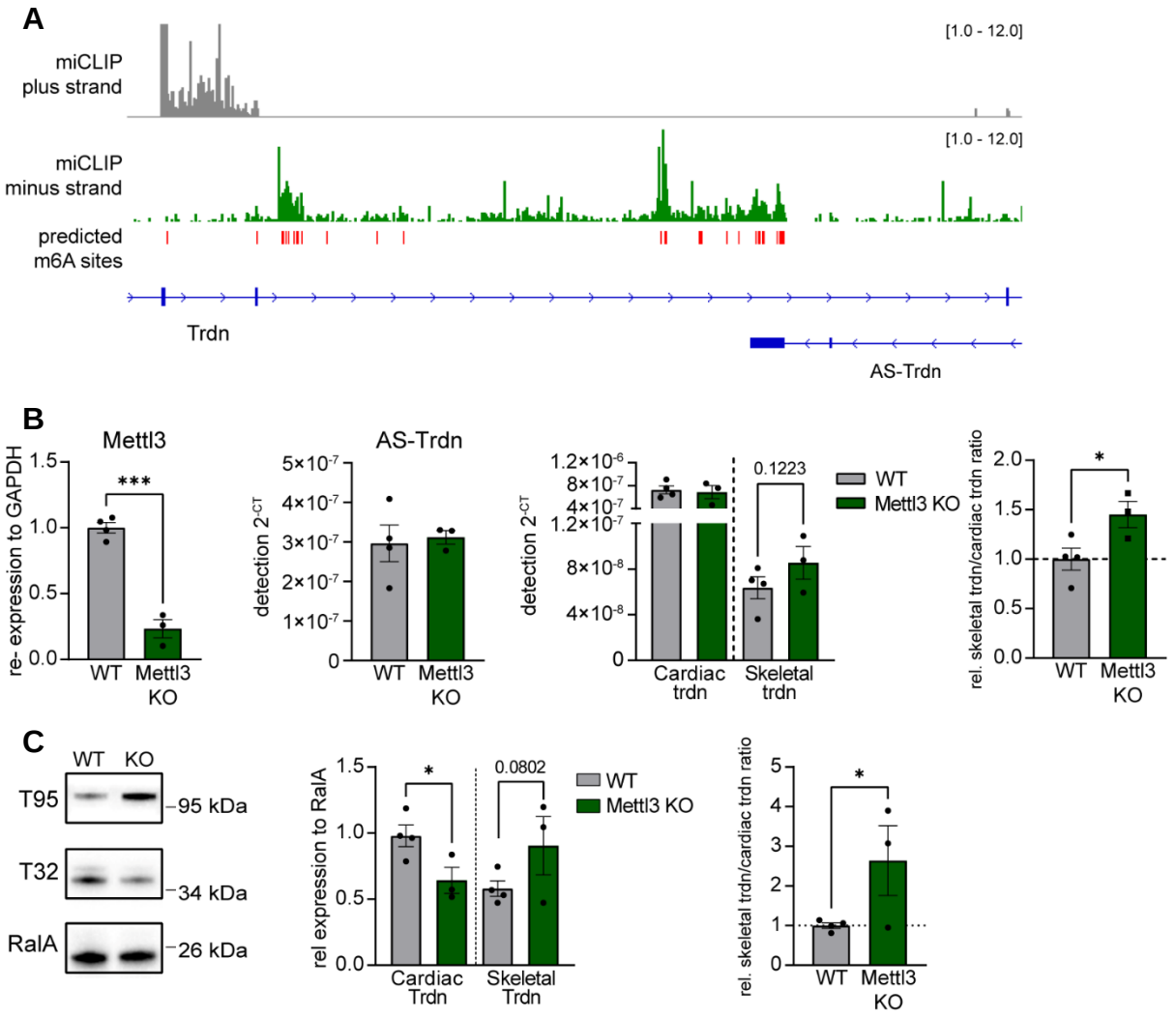

Figure 24 | miCLIP2 analysis of WT hearts reveals accumulation of m6A deposition on the antisense-transcript. A miCLIP2 tracks demonstrating m6A deposition on sense (plus strand) and antisense (minus strand) RNAs in WT mouse hearts. (Körtel et al., 2021; GEO accession GSE163491). The m6A boost machine learning tool was assessed to predict potential m6A sites. **B** TaqMan analysis of *Mettl3* KO mice demonstrating a significant loss in *Mettl3* expression compared to WT hearts. RT-qPCR was performed for *AS-Trdn,* cardiac *Trdn* and skeletal muscle *Trdn* expression. By calculating the relative ratio between skeletal and cardiac *Trdn* RNA levels, a significant shift towards the skeletal muscle isoform was observed in *Mettl3* KO hearts. n = 4 WT/3 KO. Mean ± SEM. **C** WB analysis of skeletal TRDN (trisk95) and cardiac TRDN (trisk32) from WT and *Mettl3* KO heart protein lysates, normalized to RalA. Cardiac TRDN was significantly downregulated in *Mettl3* KO heart lysates (one-tailed unpaired student's t-test). Calculation of the relative skeletal TRDN/cardiac TRDN ratio revealed a significant shift in favour of the skeletal muscle TRDN protein (one-tailed unpaired student's t-test). n = 4 WT/3 KO. Mean ± SEM.

3.2. Phenotypical characterization of the *AS-Trdn* KO mouse model

3.2.1. Loss of *AS-Trdn* and consequent expression of trisk95 leads to elevated calcium cycling, increased heart rate and blunted isoproterenol response

Triadin plays a pivotal role in regulating the activity and localization of the calcium-release complex, mainly by interacting with the ryanodine receptor, junctin and calsequestin as well as by interacting with cytoskeleton proteins, as shown in studies with skeletal muscle. In the heart on the other side, it is known that overexpression of trisk32 leads to aberrant calcium handling and cardiac hypertrophy in mice, while the underlying reasons remain elusive (Kirchhefer et al., 2001/2004). Two different studies on the triadin associated lncRNA *AS-Trdn* demonstrated a deregulation of the lncRNA in human failing hearts resulting in an alteration in triadin isoform abundance and thereby leading to a depressed contractility and consequently to the premature death of the mice (Zhang et al., 2018; Zhao, Riching and Knight et al.. 2022). In the present study, the loss of *AS-Trdn* expression was achieved via a polyA insertion into the first exon leading to an immediate transcriptional termination, resulting in the expression of the skeletal muscle triadin isoform in the heart. This isoform change has never been reported before and therefore the consequences of the long skeletal muscle Trdn isoform in the heart has not been studied yet.

The *AS-Trdn* KO mice displayed overall viability, revealing no significant increase in early lethality until 90 weeks of age. Nevertheless, a tendency towards a decrease in survival after 45 weeks of age could be observed. A total of 112 WT and 151 KO mice were taken into the calculations for the survival curve (Figure 25 A). The first phenotypical analysis was done on 8 weeks old male mice by measuring the heart and body weight as well as the tibia length. To identify possible phenotypical alterations of the heart, the heart weight was normalized to either the body weight or tibia length to exclude differences in size and weight of the animals. A total of nine WT and *AS-Trdn* KO mice were taken into account from each group. The resulting measurements didn't reveal any significant differences, which was also true for the calculated ratios of heart weight to tibia length or heart weight to body weight (Figure 25 B). In order to investigate possible developing phenotypical effects, another group of 16 weeks old male mice were analysed, which again displayed no significant changes in the measured parameters, but indicated a tendency towards a reduced heart weight to body weight ratio (Figure 25 C). Therefore, the focus was set on the already performed RNAseq of WT and KO hearts to investigate possible transcriptomic

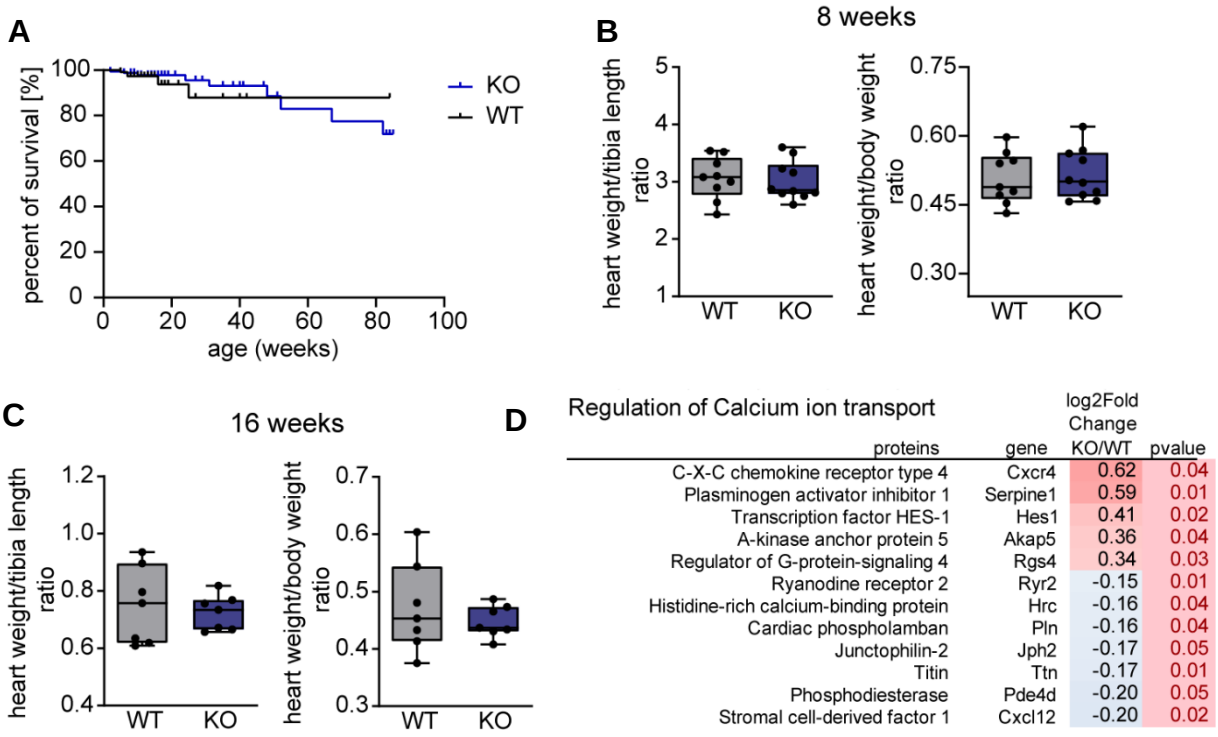

Figure 25 | *AS-Trdn* KO mice exhibit no obvious phenotypical alterations until 16 weeks of age but reveal changes in calcium handling. A Survival curve of 112 WT and 151 male until ~85 weeks of age. **B, C** Ratio calculation of heart weight to tibia length and heart weight to body weight in 8 or 16 weeks old male mice. 8 weeks, n = 9; 16 weeks, n = 7. Mean ± SEM. **D** Gene ontology term 'Regulation of calcium ion transport' from RNAseq of WT and KO hearts demonstrating differentially regulated genes using the log2fold change of expression. The p-value was calculated using a normalized student's t-test. n = 3. Mean ± SEM.

changes in cardiovascular genes. The most significant difference of WT and *AS-Trdn* KO hearts was demonstrated by the loss of *AS-Trdn* and the consequent increase in *triadin* mRNA expression as a result of the increased transcript length (log2Fold change -8.79 and 0.69 respectively). In order to identify sets of genes enriched in specific biological processes in an objective manner, a two-sided Gene Ontology (GO) analysis was performed using the online available tool Gorilla (Gene Ontology enRIchment anaLysis and visuaLizAtion tool; https://cbl-gorilla.cs.technion.ac.il/). Therefore a ranked list of significantly changed RNAs were compared to the non-significantly changed RNAs. The resulting GO terms were listed under three categories including processes, functions and components. The top 20 GO terms of the processes list were used for further analysis. A majority of the identified processes were linked to ion transport, regulation of ion transport and muscle contraction (Table 17). Since triadin is a known regulator of calcium ion transport through RyR2 and Casq2, the genes listed in the GO term "regulation of calcium ion transport" were further investigated. Notably, three direct interaction partners of triadin were significantly

downregulated on RNA level (*RyR2*, *Jph2*, *Hrc* (*histidine-rich calcium binding protein*)). The same was true for the SERCA2 regulator *phospholamban* and the contractility gene *titin*. The most significantly upregulated genes included the chemokine receptor *Cxcr4*, the plasminogen activator inhibitor 1 (*Serpine1)* and *Akap5*, which interacts and directs PKA, PKC as well as calcineurin in the heart (Figure 25 D).

Table 17 | Gorilla Gene Ontology top 20 processes of WT and *AS-Trdn* KO RNAseq

Description	P-value	FDR q-value
regulation of metal ion transport	1.48E-7	2.06E-3
muscle system process	2.12E-7	1.48E-3
regulation of transport	3.56E-7	1.66E-3
regulation of ion transport	3.73E-7	1.3E-3
muscle contraction	3.77E-7	1.05E-3
regulation of localization	4.65E-7	1.08E-3
regulation of multicellular organismal process	1.33E-6	2.66E-3
regulation of calcium ion transport	2.4E-6	4.2E-3
positive regulation of transport	3.49E-6	5.42E-3
response to external stimulus	6.09E-6	8.51E-3
negative regulation of ion transport	6.27E-6	7.96E-3
regulation of calcium ion import	7.68E-6	8.94E-3
positive regulation of ion transport	1.18E-5	1.27E-2
system process	2.11E-5	2.11E-2
multicellular organismal process	2.28E-5	2.12E-2
positive regulation of calcium ion transport	2.91E-5	2.54E-2
positive regulation of glycogen biosynthetic process	3.41E-5	2.8E-2
anatomical structure development	3.42E-5	2.66E-2
regulation of Ryanodine-sensitive calcium-release channel activity	4.71E-5	3.47E-2
positive regulation of glycogen metabolic process	6.35E-5	4.44E-2

Due to these transcriptomic observations as well as previous studies, direct measurements of the calcium release and reuptake was performed in *AS-Trdn* WT and KO cardiomyocytes. Single cardiomyocytes were isolated and cultured overnight, to

ensure attachment to the coverslips and re-establishment of ion homeostasis. Afterwards, the cells were incubated with the calcium-sensitive dye Fura2AM, loaded into the IonOptix measurement system and electrically stimulated with 1 Hz until an equal beating was attained. The IonOptix system measures sarcomere relaxation, cell contraction and calcium cycling depending on either visual changes in cardiomyocyte shape or differential emission of the dye, thereby enabling the evaluation of cell contractility. A total of 36 WT and 27 KO cells were measured from 3 animals of each group. The calcium transients of WT cardiomyocytes showed normal curve progressions, matching with published data of healthy CMs. The *AS-Trdn* KO cells however revealed a major increase in calcium cycling, which was already obvious from the calcium transient curves. WT CMs displayed a normal peak height of 0.15 ΔF, whereas KO CMs showed an increase to 0.21 ΔF (Figure 26 A). To further investigate this observation, time dependent calculations were done on calcium release (elevation) and reuptake as well as on the consequences of sarcomere relaxation. The calculated numbers display the time until a certain percentage to the peak or baseline is reached, thereby directly giving an impression of the calcium cycle pace. As for the WT cardiomyocytes, 10 % of the peak (i.e. calcium release) was reached within 0.004 seconds (s) and 10 % of the baseline (bl.; i.e. calcium reuptake) within ~ 0.09 s. In comparison, *AS-Trdn* KO cardiomyocytes exhibited a two-times faster calcium cycling with a time to 10 % peak below 0.002 s and back to 10 % baseline within approximately 0.05 s. This faster calcium cycling was reflected by the almost two-times faster sarcomere relaxation of ~ 0.08 s to 50 % baseline, while WT cardiomyocytes needed ~ 0.14 s (Figure 26 B). During the course of measuring multiple KO cells, two additional interesting phenomena were observed. One illustrated the appearance of so called ‘spontaneous calcium oscillations’ meaning an uncontrolled calcium efflux and influx, which occurred in 32 % of all KO cells (2 of 3 *AS-Trdn* KO mice) and the second one was the spontaneous extra release of calcium, demonstrated by additional intrinsic peaks in 28 % of all KO cells (3 of 3 *AS-Trdn* KO mice; Figure 26 C).

Comparing these numbers, *AS-Trdn* KO cardiomyocytes indeed exhibited a significant increase in calcium cycling which had a direct effect on sarcomere relaxation and therefore cell contraction. At the same time, uncontrolled extra calcium release and calcium oscillations were observed, indicating a failure in maintaining a steady and normal calcium cycling. If the calcium cycling is drastically increased, one would expect a measurable consequence on the overall heart contractility and therefore on the

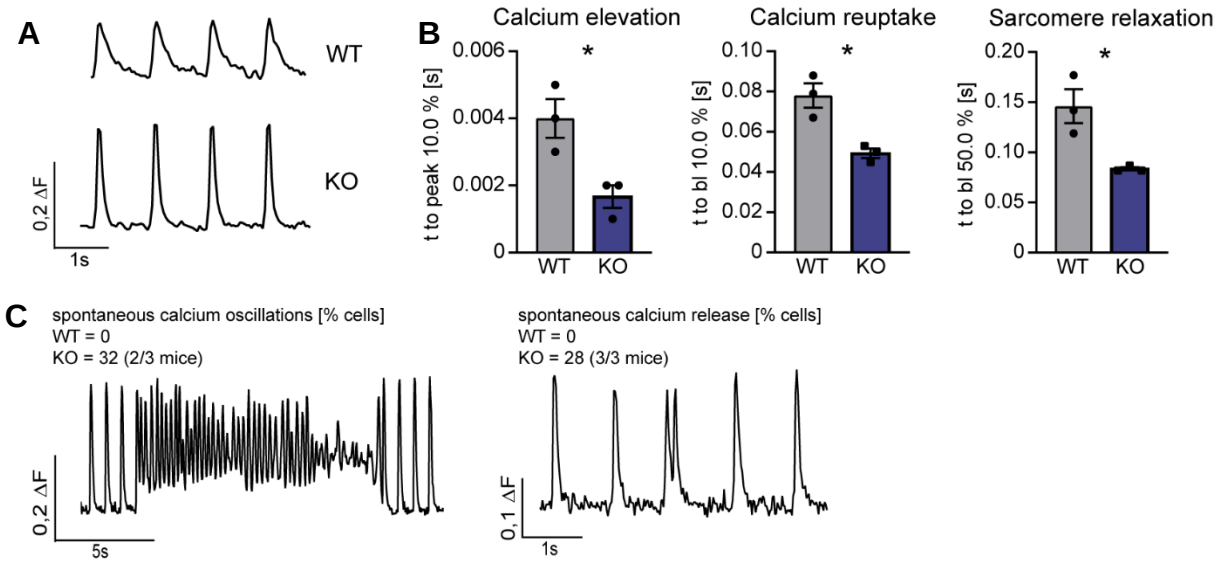

Figure 26 | Elevated calcium cycling and aberrant calcium release after KO of *AS-Trdn* in adult CMs. A Representative calcium transients of WT and *AS-Trdn* KO cardiomyocytes measured using the IonOptix system. n = 3 mice. **B** Time-dependent calculations of calcium transients including time to 10 % peak (calcium elevation), time to 10 % baseline (bl.; calcium reuptake) and time to 50 % bl. of sarcomere relaxation. All measurements revealed a significant increase in calcium cycling in KO CMs. 36 WT cells and 27 KO cells were measured. n = 3 mice. Mean ± SEM. **C** Example traces of calcium oscillations and spontaneous calcium releases in KO cardiomyocytes and the corresponding percentages. 32 % of KO cells exhibited oscillations and 28 % spontaneous calcium releases. n = 3 mice.

beating rate. Another assumption would be the occurrence of premature ventricular contractions (PVCs), which are recognized in ECG measurements by extra heartbeats beginning in the ventricles and potentially induce ventricular tachycardia. Another interesting aspect to investigate demonstrates the competence of the KO hearts to respond to β-adrenergic stimuli. Calcium cycling is mainly controlled via the adrenergic system and therefore alterations in CRC associated proteins could result in a failure to respond and compensate accordingly. In order to answer these questions, the heart rate and rhythm of WT and KO mice was monitored by ECG under normal conditions. Therefore telemetric devices were used to monitor heart rate and rhythm during the course of two weeks in WT and KO mice. The telemetric devices were implanted by Thomas Böttger and afterwards, mice were kept in separated cages and received Novalgin in drinking water for 5 days. After full recovery 7 days post-surgery, the heart rate was measured overnight from 6:00 pm to 6:00 am. Heart rate was measured every 15 minutes and averaged over the course of the night. Next, for β-adrenergic stimulation, mice were treated with 1 µg/BW isoproterenol via intraperitoneal injection (i.p.) and continuously monitored for 1 hour to evaluate changes in heart rate and rhythm. Matching the previous calcium transient increases, the steady-state heart rate

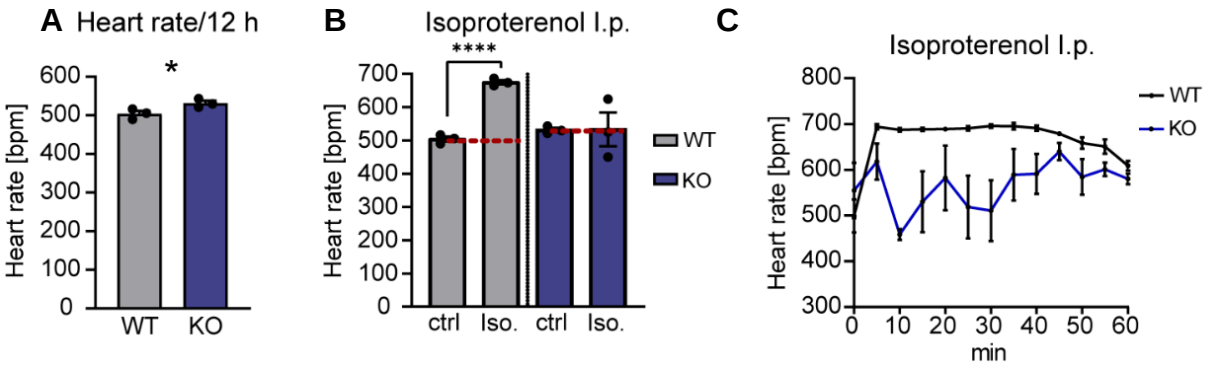

Figure 27 | Telemetric measurements reveal an increased heart rate and blunted β-adrenergic response in *AS-Trdn* KO mice. A Steady-state measurements of WT and KO mice heart rates overnight demonstrating a significant increase in KO hearts. **B** Comparative results of steady-state heart rates and upon isoproterenol treatment in WT and KO mice. WT mice exhibit a significant increase of almost 200 bpm after treatment whereas KO mice revealed no changes in heart rate. **C** Time-course of heart rates after beta-adrenergic stimulation blotted until 60 min post i.p. injection. **A-C** n = 3. Mean ± SEM.

during the night measurements was increased by 30 bpm in *AS-Trdn* KO compared to WT mice (Figure 27 A). Interestingly, the β-adrenergic stimulation with isoproterenol revealed a blunted effect on KO mice heart rates. The overall KO heart rate revealed no significant increase within 30 minutes after injection, while the heart rate of WT mice increased by almost 200 bpm, as expected from published studies (Figure 27 B). In order to examine the β-adrenergic response in more detail, the heart rate was blotted over the time course of 60 minutes after isoproterenol injection. In WT mice the heart rate showed a rapid increase within the first 5 minutes after isoproterenol injection from 500 bpm to 700 bpm and remained at this high level for 40 minutes before slowly decreasing again. In contrast, the *AS-Trdn* KO hearts exhibited a drop in heart rate from 540 bpm to 450 bpm within the first 5 minutes. The subsequent heart rates revealed an unsteady trend, with alternating increases and decreases until 60 minutes post injection, but always remained low compared to heart rates of WT animals after stimulation (Figure 27 C). Overall, *AS-Trdn* KO mice exhibited an increased steady-state heart rate consistent with the previous IonOptix measurements and were additionally not able to react appropriately to β-adrenergic stimulation.

3.2.2. Trisk95 reshapes dyad structure in the heart by binding to the cytoskeleton

In previous studies, the interaction of the transmembrane protein triadin has been intensively studied in skeletal as well as in cardiac muscle. Triadin has been implicated in regulating the calcium-release by binding to Casq2 and RyR2 as well as in anchoring the CRC over direct interactions with junctin and junctophilin and via an indirect interaction with the cytoskeleton proteins, especially in skeletal muscle (Kirchhefer, et al., 2001/2004; Vassilopoulos et al., 2005; Marty et al., 2015). The present study demonstrates that loss of *AS-Trdn* transcription induces the expression of the long skeletal muscle isoform of triadin, namely trisk95, in the heart. As a consequence, a significant disruption of calcium handling, significant changes in heart rate and stress response as well as a decrease in heart rate to body weight ratio were observed. To next elucidate the correlation of these alterations with the change in triadin protein isoform expression, the focus was first put on potential ultra-structural changes in heart morphology. In this regard, WT and *AS-Trdn* KO left ventricles were collected and used for electron microscopy. The cardiac dyad, which can be found at the Z-line of each sarcomere (within the I-band), is characterized by junctional sarcoplasmic reticulum cisternae closely surrounding the invaginated t-tubules, forming a snail like structure. The width of the j-SR cisternae as well as the proximity to the t-tubules is strictly defined to ensure precise induction and cycling of calcium ions (Knollmann et al., 2006). Comparing the ultrastructure of WT and KO hearts, no obvious alterations in sarcomere structure, Z-line localization of dyads or overall dyad abundance was observed. Nonetheless, the analysis of dyadic structure revealed a major deformation in *AS-Trdn* KO cardiomyocytes compared to WT hearts, revealing a massive decrease in dyadic space as well as j-SR cisternae width. The overall dyadic structure displayed therefore a tightened, almost collapsed structure surrounding the t-tubules. Another observation made was the reduction in longitudinal SR running between the Z-lines along the A-band (Figure 28 A). The disturbance of the dyadic structure was more prominent than expected and could be a consequence of the change in triadin protein isoform. To investigate the role of triadin in shaping the dyadic structure, changes on overall protein levels as well as triadin interactions were compared in WT and KO hearts. In this regard, whole heart proteomics, isolated membrane proteomics as well as triadin immunoprecipitations (IPs) were performed using an antibody detecting both isoforms. The changes on whole heart proteomics revealed a significant increase in triadin itself, the ryanodine receptor 2 and an increase in calsequestrin 2, while only

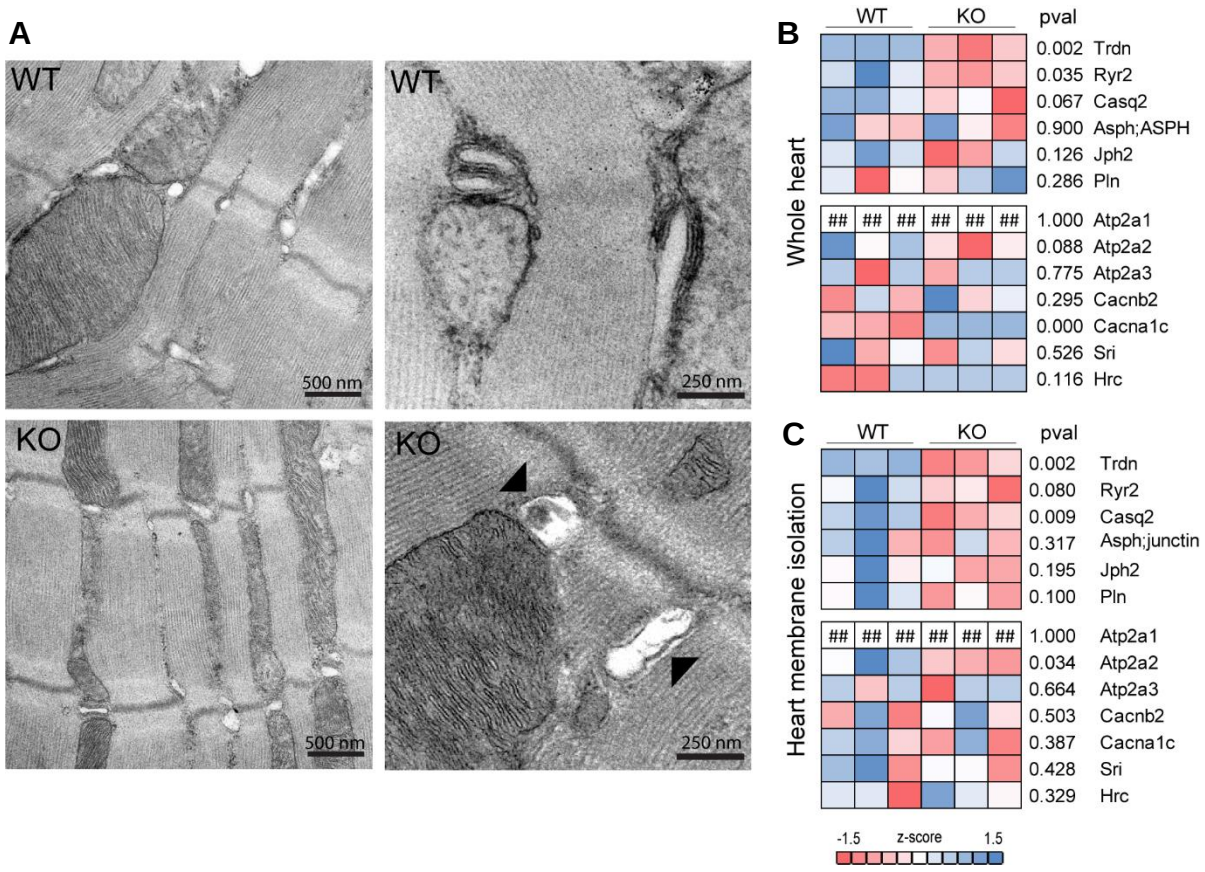

Figure 28 | Expression of trisk95 leads to cardiac dyad deformation and changes in CRC related proteins abundance. A Electron microscopy of WT and *AS-Trdn* KO left ventricle indicating no major changes in sarcomere structure and dyad localization. Close-up analysis of cardiac dyads revealed major loss of dyadic space and SR luminal width as well as overall deformation (black arrow-heads). n = 3. **B** Heat map of ECC related proteins from whole heart proteomics of WT and KO ventricles measured by mass spectrometry revealed a significant increase in TRDN and RyR2 protein levels. Cacna1c protein was significantly downregulated. **C** Heat map of ECC related proteins from membrane isolations measured by mass spectrometry comparing WT and KO ventricles. Protein levels indicated a significant increase in triadin, CASQ2 and ATP2a2. **B-C** Protein levels are displayed as Z-scores with colour code ranging from -1.5 to 1.5. Separation of the top and bottom proteins indicating direct triadin interaction partners and other ECC related proteins respectively. n = 3.

one subunit of the voltage dependent calcium channel CaV1.2 (*Cacna1c*) revealed a significant decrease (Figure 28 B). Since triadin is a transmembrane protein, the next aim was to investigate potential changes in the protein composition within or at the SR-membrane. If only the localization of certain proteins was changed, but not the overall protein levels, the whole heart proteomics would not have revealed it. Therefore isolations of membrane fractions were performed on heart ventricles using differential ultracentrifugation and send again for mass spectrometry analysis. The analysis comparing WT and *AS-Trdn* KO membrane fractions revealed an overall increase in proteins bound to the SR membrane, of which triadin, CASQ2 and the ATPase ATP2a2

were significantly enriched. The ryanodine receptor 2 showed an increased abundance at the SR membrane, but without significance (Figure 28 C). Both methods revealed an increase in TRDN protein levels, which might be explained due to the increase in protein size as a consequence of the skeletal muscle isoform expression rather than an actual increase in TRDN abundance.

In order to fully understand these observations, triadin IPs were performed on WT and *AS-Trdn* KO heart lysates to discover alterations in triadin interactions upon isoform changes. The IP using an antibody targeting the first amino acids of triadin, thus interacting with the cardiac as well as the skeletal muscle isoform of TRDN worked efficiently and revealed a uniform PCA distribution of WT, KO and IgG control samples (Figure 29 A). Mass spectrometry analysis of proteins pulled-down with TRDN exhibited a huge amount of differentially bound proteins and to get a first hint of changed protein families, a gene ontology analysis using the PANTHER software was performed (https://pantherdb.org). Therefore the significantly changed proteins of WT and KO samples were compared and the top hits analysed. Out of the top 20 results regarding the GO term ‘cellular component’, 15 were related to sarcomere structure and anchoring, with a majority pointing towards a connection to the actin and microtubule cytoskeleton within the j-SR (ER exit site) at the Z-disc (Figure 29 B).

A first analysis of the differentially bound proteins confirmed the rather minor changes in CRC related proteins, with only CASQ2 showing a significant loss in binding to triadin in KO hearts. At the same time, an increased binding to the CASQ2 competitor HRC was detected, while the binding of the RyR2 inhibitor sorcin (*Sri*) was significantly reduced, representing a potential elevated calcium-cycling situation in *AS-Trdn* KO hearts. Another observation in this regard, was the reduced binding of Triadin to Atp2a1 and Atp2a2 as well as the loss of its co-activator sarcalumenin (*Srl*; Figure 29 C). As the PANTHER analysis already indicated, many proteins related to the actin or microtubule cytoskeleton were found differentially binding to triadin in WT vs KO hearts. Many of these cytoskeleton genes were found to be enriched in binding to the long skeletal muscle isoform of triadin in KO hearts, as revealed by volcano blot analysis of all differentially bound genes (Figure 29 D). One protein, which has already been shown to directly interact with trisk95 in skeletal muscle is the cytoskeleton-associated protein 4 (*Ckap4*; CLIMP-63) and its homolog CKAP5. Both homologues were found to be significantly binding to triadin in *AS-Trdn* KO samples as well as its

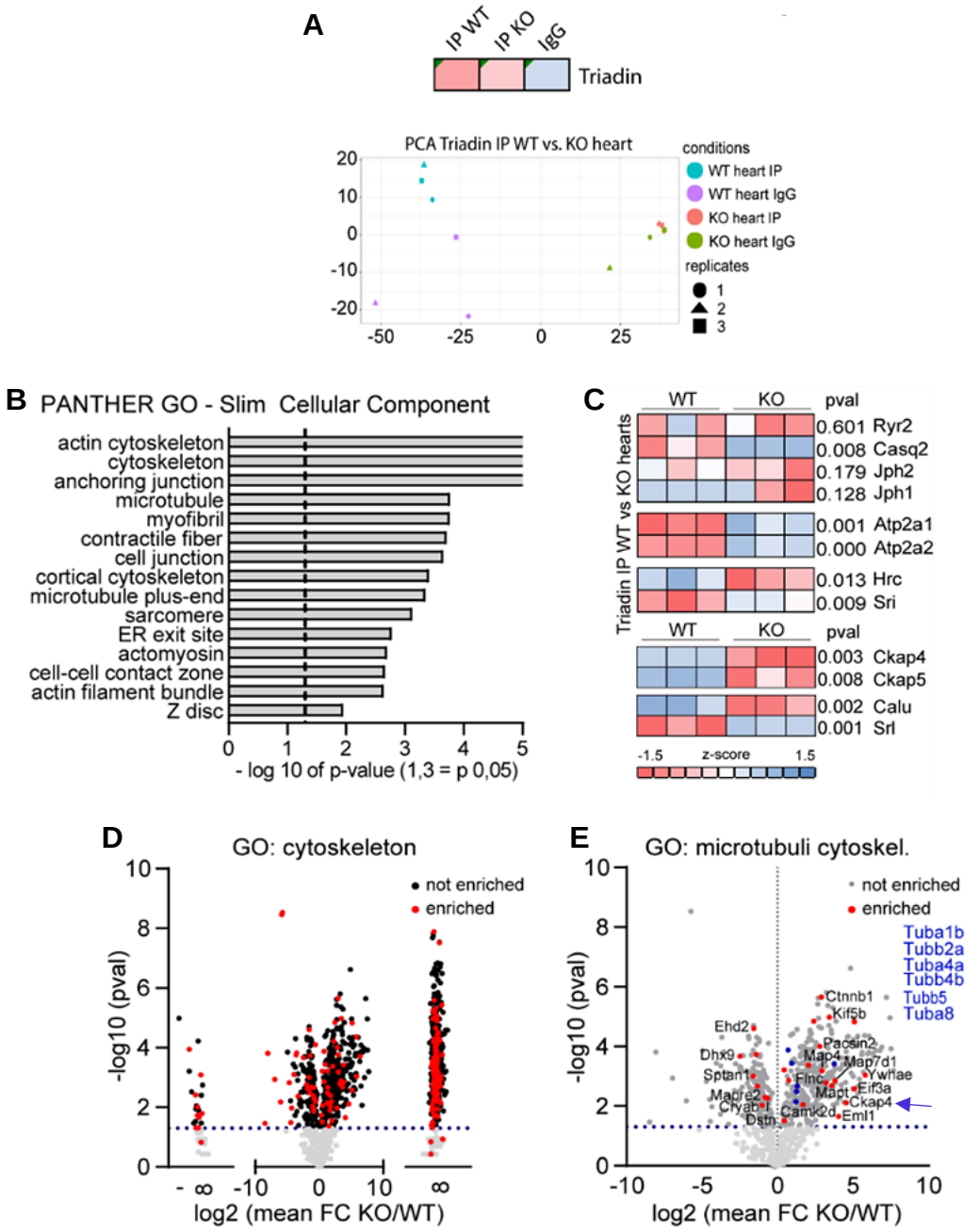

Figure 29 | Triadin immunoprecipitation in WT and KO hearts reveals strong binding of trisk95 to the microtubule cytoskeleton over CKAP4/5. A Validation of the triadin IP confirmed successful pull-down of trisk32 and trisk95 in equal amounts and no detection in IgG controls. PCA blot validation of single replicates confirms close correlation. n = 3 for WT/KO IP and IgG. **B** GO term analysis of significantly bound proteins using PANTHER. Displayed are 15 of the most significantly changed GO terms of 'Cellular Component'. **C** Heat map of WT and KO IPs representing ECC related proteins. Upper panel demonstrating CRC related interaction partners of TRDN. Lower panel depicts CKAP4/5 and its regulators. **D** Volcano blot representing all differentially bound proteins of WT and KO IPs. All proteins enriched in the GO term 'cytoskeleton' were marked red to demonstrate distribution. Proteins assigned to -∞were exclusively pulled-down in WT hearts while proteins assigned to ∞ were exclusively found to interact with trisk95 in KO hearts. **E** Volcano blot close-up of all differentially bound proteins in black and GO term 'microtubule cytoskeleton' enriched proteins demonstrated in red. CKAP4 is indicated by a blue arrow as well as the significantly bound tubulins in KO hearts indicated in blue. **D, E** The mean ratio of the detection of all proteins (mean FC (log2)) from WT and KO IPs was blotted against the respective p-values (-log10 (pval)). n = 3.

interaction partner calumenin-1 (*Calu1*; Calu) and the related tubulin isoforms (TUBA1b/4a/8; TUBB2a/4b/5; Figure 29 C & E, Figure 30 A). Additionally to the stronger interaction to the microtubule cytoskeleton, an increased interaction of Triadin with actin-related proteins was identified in the GO analysis as well as in the volcano blot analysis in *AS-Trdn* KO hearts. Analysing the differentially bound proteins, a significant increase in binding to actinin (ACTN1/2/4) as well as to actin-related proteins ACTR2, MACF1 or ARPC1a was found. Simultaneously, the binding to cardiac α-actin 1 (ACTC1), to β-Actin (ACTB) and the actin binding lim protein 1 (ABLIM1) was significantly decreased (Figure 30 A & B).

In sum, the *AS-Trdn* KO IPs revealed no major changes in the binding of CRC related proteins in the heart, but changes in calcium-cycling related proteins (SRC, HRC, SRL, ATP2a1/2) and a major increase in binding to the microtubule (CKAP4/5, Tubulins and tubulin-related proteins) as well as the actinin (ACTN1/2/4; actin-related proteins) cytoskeleton.

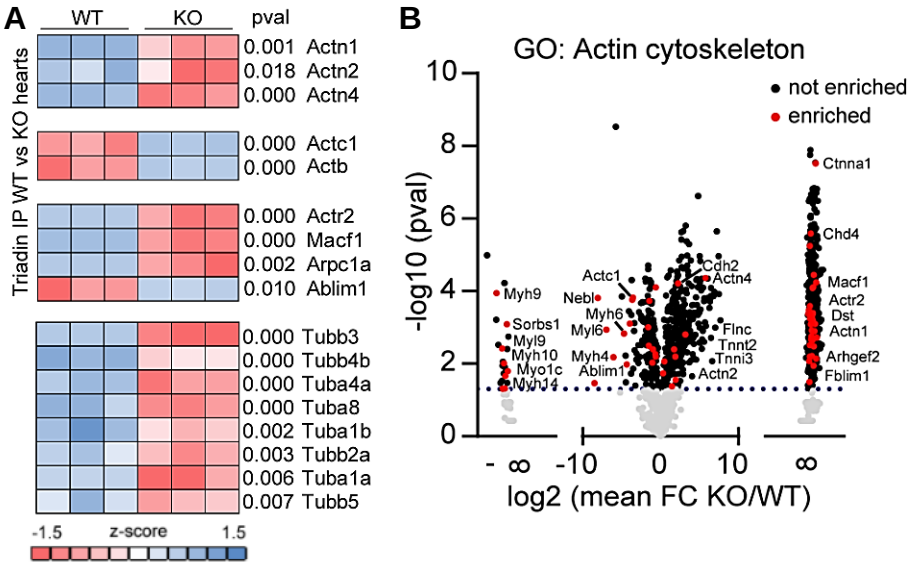

Figure 30 | The induced expression of trisk95 in KO hearts leads to an increased actinin and tubulin binding accompanied by interactions with related proteins. A Heat map of triadin WT and KO IPs with all significantly regulated actin, actinin and tubulin proteins as well as some relevant actinin- and actin-related proteins. **B** Volcano blot demonstrating all differentially bound proteins of WT and KO TRDN IPs. All proteins enriched in the GO term 'Actin cytoskeleton' were marked red to demonstrate distribution. The mean ratio of the detection of all proteins (mean FC (log2)) from WT and KO IPs was blotted against the respective p-values (-log10 (pval)). Proteins assigned to -∞were exclusively pulled-down in WT hearts while proteins assigned to ∞ were exclusively found to interact with trisk95 in *AS-Trdn* KO hearts. -log10 pval (1.3 = p 0.05). n = 3.

3.2.3. Loss of *AS-Trdn* and consequent expression of trisk95 induces dilated cardiomyopathy in ageing mice

Since young mice revealed no obvious physiological alterations regarding body size or heart morphology, but displayed dramatic changes in calcium handling as well as changes in heart rate and stress-response, the question was risen if these changes could have physiological consequence in ageing mice. In order to answer this question, mice were left undisturbed until approximately 40 weeks of age and afterwards send for cardiac magnetic resonance imaging (MRI). Already in the MRI pictures, the difference in blood volume in the end systolic state was obvious and could be confirmed by measurement of all 4 WT and *AS-Trdn* KO animals using the MRI evaluation software Medis Suite V4.0 (Figure 31 A). The end systolic volume (ESV) was increased by approx. 12 µl in *AS-Trdn* KO hearts while the end diastolic volume (EDV; data not shown) stayed unchanged, indicating a failure to fully contract and sufficiently pump the blood out of the heart. This observation was further confirmed by a significant decrease in the stroke volume (WT 43.44 ± 3.50 µl, KO 34.37 ± 3.37 µl; data not shown), a decrease in ejection fraction by ~15 % as well as a significant decrease in the fractional shortening of ~ 19 % in KO hearts (Figure 31 B). The ejection fraction describes the percentage of blood which is ejected from the left ventricle during one cardiac contraction and is therefore an indication for cardiac output as well as the fractional shortening, which is an indication for the cardiac contraction ability. Both parameters indicate a failure to fully contract and therefore a decreased cardiac output in *AS-Trdn* KO hearts. Interestingly, the left ventricular mass was also decreased, even though missing significance (p-value = 0.0797 (Figure 31 B)).

In order to closer investigate the changes in heart morphology, 40 weeks old mice were used for histological analysis using H&E (haematoxylin and eosin) staining as well as for weight parameter analysis as preformed on 16 week old mice. H&E staining was performed on 4-chamber paraffin sections to compare overall heart morphology of WT and KO hearts. Using these two approaches it was possible to further confirm the commencing dilative cardiomyopathy (DCM) of the ageing *AS-Trdn* KO hearts as was already indicated by MRI (Figure 32 A). KO hearts displayed an increase in heart size but a relative decrease in ventricular mass, resulting in an overall decrease in heart weight to body weight ratio (Figure 32 A & B) Since another sign of DCM is the reduction in CM diameter, ageing hearts underwent cryotome sectioning and were subsequently stained using WGA (wheat germ agglutinin). WGA binds glycoproteins

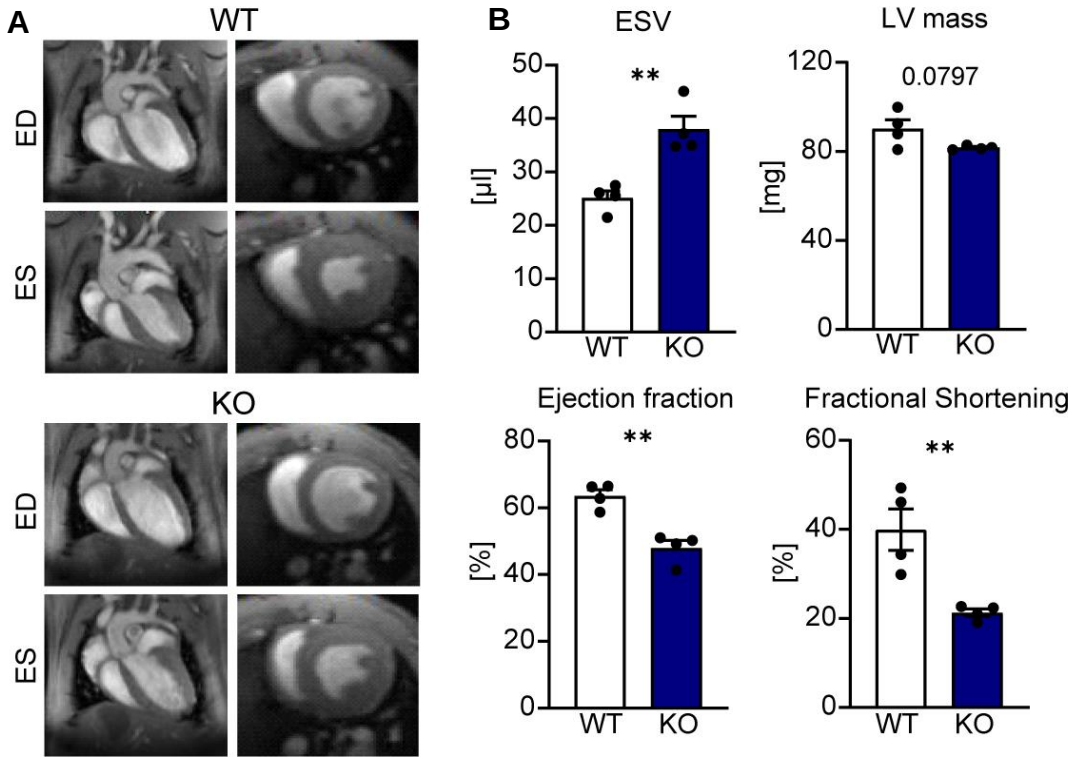

Figure 31 | MRI measurements reveal depressed cardiac contraction in *AS-Trdn* KO mice and commencing DCM. A Representative MRI pictures of 40 weeks old WT and *AS-Trdn* KO hearts in end-diastole (ED) and end-systole (ES). Pictures on the left presenting long-axis four-chamber views and pictures on the right presenting mid-level short axis views. **B** Using the software Medis Suite 4.0 the end-systolic volume (ESV), left ventricular (LV) mass, ejection fraction and fractional shortening was quantified in 4 WT and 4 KO mice. The analysis revealed a significant increase in ESV and a significant decrease in ejection fraction and fractional shortening. Additionally the left ventricular mass was reduced. Mean ± SEM. n = 4.

in plasma membranes and can therefore be used to stain skeletal and cardiac sarcolemma to determine cross sectional areas of fibres. Already by visual examination of the WT and KO myofibers sections, the difference in cross sectional area was quite obvious, but to confirm this observation, the area was measured and quantified using the ImageJ platform. Thereby the first impression could be confirmed, that KO cardiomyocytes indeed displayed a reduced cross-sectional area with most cells ranging between 150 – 250 µm and almost none above 400 µm, while WT cardiomyocytes mostly ranged from 200 – 500 µm (Figure 32 C & D).

Taken together, these observations indicate a progressive dilative cardiomyopathy as a result of the failing heart contraction upon loss of *AS-Trdn* and the consequent expression of the skeletal muscle isoform of Triadin in the heart.

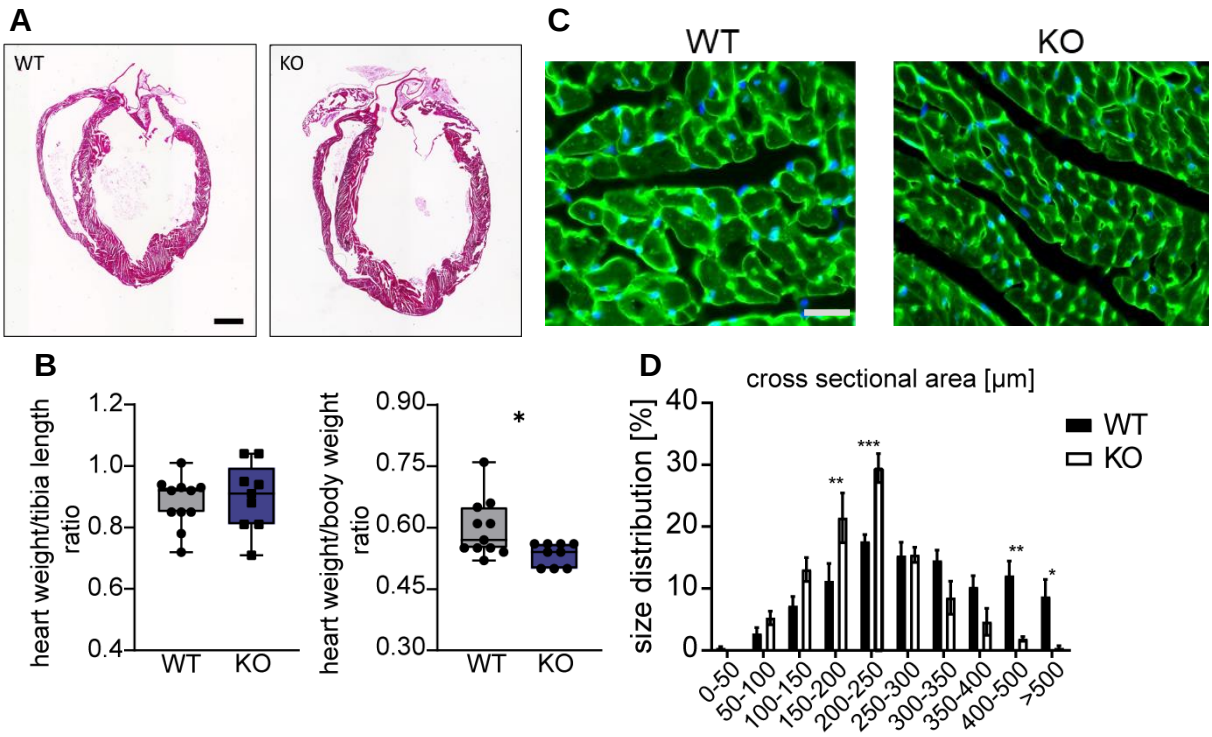

Figure 32 | *AS-Trdn* KO mice exhibit a progressive dilative cardiomyopathy after 40 weeks of age. A Representative images of H&E stainings on 4-chamber paraffin sections of 40 weeks old WT and KO hearts. Scale bar = 1 mm. n = 4. **B** Measurements of heart weight to tibia length ratio and heart weight to body weight ratio revealed a significant decrease in heart weight in ageing *AS-Trdn* KO mice. n = 11 WT/9 KO. Mean ± SEM. **C** WGA staining of left ventricular cross sections from 40 weeks old WT and *AS-Trdn* KO hearts. Scale bar = 25 µm. n = 4. Blue = Dapi (353 nm); Green = WGA (488 nm). **D** Graphical demonstration of cross sectional area percentage distribution comparing WT and *AS-Trdn* KO hearts ranging from 0 to > 500 µm. The *AS-Trdn* KO distribution exhibited a significant shift towards smaller cross sectional areas compared to WT hearts. n = 4. Mean ± SEM.

4. Discussion

4.1. *AS-Trdn* is a conserved nuclear lncRNA, expressed upon CM transition

Long non-coding RNAs have been implicated in a variety of biological functions, as chromatin and transcription regulation (*HOTAIR*, *lncMyh*), interchromosomal interactions (*FIRRE*) and splicing (*ZEB2-AS1*, *Brd1as*; Liu & Lim, 2018). One of these lncRNAs is called *AS-Trdn*, named due to its antisense localisation to the protein coding gene triadin. Two different studies demonstrated the importance of *AS-Trdn* in regulating triadin isoform balance, a pivotal gene of the sarcoplasmic reticulum membrane, in skeletal and cardiac muscle (Zhang et al., 2017; Zhao, Riching and Knight et al., 2022). Even though the correlation between *AS-Trdn* expression and triadin isoform abundance was demonstrated using bioinformatics as well as experimental approaches, the molecular mechanism behind this regulation remains elusive. Therefore, in this study the molecular function of the long non-coding RNA *AS-Trdn* was experimentally assigned and in a first approach the sequence identity and conservation was investigated.

AS-Trdn is localized on chromosome 10 in *mus musculus* while in humans it is localized on chromosome 6, both compromising 3 exons with a similar spliced-transcript length. Compared to other lncRNAs, *AS-Trdn* exhibits a high conservation concerning sequence consistency (approx. 45 %), genomic organisation and expression. In fact, the human orthologue of *AS-Trdn*, named *TRDN-AS* or *HRAT13*, was the first one to be discovered in a bioinformatics screening approach comparing RNAseq data sets of 15 different human organs and failing hearts. *AS-Trdn* raised interest due to its genomic proximity to an important cardiac contraction gene and its differential expression in failing human heart biopsies. In the same study, the mouse homolog was discovered and with a 21 % coding probability confirmed to be non-coding by using a coding-potential assessment tool (Zhang et al., 2017). In this study, *AS-Trdn* was reconfirmed as non-coding using the Coding Potential Calculator 2 (CPC2; Kang et al., 2017), revealing a coding probability of 0.45 and a putative ORF of 148 AA. Interestingly, a new field of research has gained attention in recent years, which describes the occurrence of micro proteins expressed from lncRNAs and one of them was *AS-Trdn*. Van Heesch demonstrated, that the *AS-Trdn* transcript gives rise to a translated microprotein, which could explain the quite big putative ORF (Van

Heesch et al., 2019). The biological function or even relevance of this microprotein remains to be elucidated, but since we found no major transcriptomic or proteomic changes upon *AS-Trdn* deletion, besides the triadin related ones, its relevance seems rather minor or even non-existent.

Nevertheless, the relevance of *AS-Trdn* itself in regulating triadin isoform expression is evident due to previous studies and therefore the investigation was focused on the non-coding transcript. Analysing publicly available RNA sequencings of developmental stages, it was demonstrated, that *AS-Trdn* starts to be highly expressed shortly after birth (P0). This observation was interesting, since it resembles the maturation of cardiomyocytes from a neonatal to postnatal stage. After birth, neonatal cardiomyocytes undergo a drastic change in structure, metabolism and function, transitioning from a hyperplastic neonatal cell growth to a hypertrophic adult cell growth. Fetal cardiomyocytes are characterized by their incomplete sarcomere, mitochondria and nuclei structure, while adult cardiomyocytes are tightly structured and organized (Piquereau & Ventura-Clapier, 2018; Maroli & Braun, 2021). During the transition, many structural proteins need to be de-novo expressed or relocated and one of these structural proteins in sarcomere and especially sarcoplasmic reticulum structure is triadin, which has been shown in several studies before (Fourest-Lieuvin et al., 2012; Marty, 2015). Therefore it is plausible, that the cardiac isoform of triadin is needed whilst this transition is happening and in this regard *AS-Trdn* expression needs to be established. Even though there is no published data about triadin isoform abundance in neonatal hearts, one can assume that the skeletal muscle specific triadin isoform is the dominant one due to the non-existing *AS-Trdn* expression, as shown using RNAseq data of different neonatal stages. Nevertheless, it would be interesting to check for the triadin isoform expression and localisation in developing hearts as well as to check for the differences in calcium cycling.

Another striking point about *AS-Trdn* is its exclusive expression in cardiomyocytes, which could be confirmed using microarray data-sets of multiple mouse tissues as well as comparing the expression of cardiomyocytes to non-cardiomyocytes. Within cardiomyocytes, the expression is restricted to the nucleus as shown with RT-qPCR and FiSH experiments, confirming the results of previous studies on *AS-Trdn* (Zhang et al., 2017; Zhao, Riching and Knight et al.. 2022).

4.2. *AS-Trdn* regulates triadin isoform balance in the heart on a transcriptional level

To investigate the molecular function of the long non-coding RNA *AS-Trdn*, a KO mouse line was established by inserting a 2 x polyA sequence into the first exon of *AS-Trdn*, thereby leading to an immediate transcription termination. This approach has been used in different studies before and is suitable to study the transcription dependent function of non-coding genes, whilst genomic deletions only cover the transcript dependent functions. The loss of *AS-Trdn* was confirmed by RT-qPCR as well as RNAseq, demonstrating no remaining transcription or transcript. Remarkably, the prevention of *AS-Trdn* transcription resulted in the expression of the long skeletal muscle isoform of triadin while cardiac triadin expression was nearly abolished. The same change in triadin isoform abundance was achieved using the *AS-Trdn* KO model in hIPS cells, again demonstrating the conserved function of the antisense lncRNA. This observation was especially interesting, since previous studies displayed no effect on the expression of skeletal muscle triadin upon genomic deletion of *AS-Trdn* exon 2 and 3. In this study, the deletion induced a decrease in cardiac triadin expression but no increase in other isoforms, therefore mimicking a partial loss of triadin phenotype (Zhao, Riching and Knight et al.. 2022). These results were in accordance to the postulated mechanism by Zhang et al., the first ones to describe *AS-Trdn*, which is a transcriptional interference by the two convergent RNA polymerases independent of the spliced transcript (Zhang et al., 2017). The *AS-Trdn* polyA KO used in this study and the resulting expression of the long skeletal muscle triadin isoform, demonstrates a further confirmation for this hypothesis, which is why the focus was set on the transcription of the lncRNA rather than the interactions of the spliced transcript.

In this regard, the first approach was to closer analyse the RNAseq data of WT and KO hearts, whereby two major observations were made. The first one presents the ongoing antisense transcription beyond the annotated 3'-UTR of *AS-Trdn* reaching until exon 9 of triadin, which could be confirmed using stranded sequencing. Exon 8 exhibits the last exon of cardiac *triadin* and is only 2.5 kB upstream of exon 9, another hint for a potential transcriptional interference of the two transcribing polymerases. The second observation was, that the expression level of the long *Trdn* isoform associated exons, meaning exon 11 onwards, remained comparatively high despite *AS-Trdn* expression. This finding was quite surprising since no splicing over the *AS-Trdn* locus was observed and the western blot analysis clearly demonstrated the exclusive

expression of the short cardiac triadin isoform in WT hearts. Using a JunctionSeq analysis, this observation was confirmed, revealing an only 50 %reduction in long isoform exon reads, whilst exon 9 and 10 expression was nearly abolished. In sum, this observation could indicate a second protein or peptide, which arises from the C-terminal domain of triadin, which is not detected using TRDN specific antibodies, and potentially from a different promoter. Both observations have not been described yet and initiated further investigations.

4.3. GATA4 is the main driver of *AS-Trdn*, inducing bi-directional expression of the lncRNA

Comparing publicly available human stranded heart RNAseq data sets with the mouse WT hearts, the extended transcription could again be observed and using RT-qPCR, the heart specific occurrence of these transcripts could be confirmed. To elucidate the actual *AS-Trdn* transcript, a long-range sequencing (NanoporeSeq) of WT mouse hearts was analysed. Thereby the definite antisense transcript was demonstrated, revealing an increased transcript length reaching beyond exon 9 of triadin consistent with the RNAseq results. Since recent studies only used the annotated *AS-Trdn* transcript, it is questionable if the demonstrated phenotype is indeed a result of *AS-Trdn* or a side-effect of the larger genomic deletion. In defence of former studies, one has to question the current annotation state of the genome, which obviously lacks the inclusion of various new NGS approaches (e.g. long-range sequencings) for a better description of coding and non-coding transcripts. In case of *AS-Trdn* a new annotation would definitely be appropriate. Nonetheless, a second observation was made whilst analysing the NanoporeSeq, explaining the comparatively high expression levels of the 3' exons of the long triadin isoform. Upstream of the *AS-Trdn* promoter, a new spliced exon was identified, which was only evident upon *AS-Trdn* expression. Therefore, the hypothesis was put forward, that *AS-Trdn* exhibits bi-directional transcription and consequently induces the expression of a putative C-terminal transcript. To delve deeper into this observation and to elucidate the cardiac exclusive expression of *AS-Trdn,* an *in-vitro* model was designed using the dual luciferase system. Using this experimental approach, *AS-Trdn* was confirmed to be bi-directionally active, even if transfected into non-cardiac cells, but only to a very low extend. Under WT conditions, the antisense lncRNA is exclusively expressed in cardiomyocytes, so another mechanism or factor needs to be involved. To get another

insight, different publicly available sequencing data sets were analysed and thereby the promoter as well as two dominant enhancer regions were identified. Interestingly, in an ATACseq developmental series the promoter region only displayed open chromatin structure upon P0, explaining the age-related expression profile of *AS-Trdn*, but not the high cardiac expression. The whole locus exhibited a widespread acetylation, making it highly active, with two dominant enhancer raising interest. Analysing potential transcription factors binding to these enhancers, several candidates were identified, but only GATA4 induced a significant increase in transcription. To conclude, the expression of *AS-Trdn* is regulated through two distinct mechanisms: on one side the accessibility of the promoter and enhancer regions, regulated through epigenetic modifications and on the other side on the cardiac specific transcription factor GATA4 (potentially accompanied by other transcription factors like SRF and EP300) which further increased the expression upon enhancer accessibility. In multiple cases, lncRNAs display tissue and time specific expression profiles and the dependency on enhancer and transcription factors has been shown before (*Fendrr*; *Xist*; Szafranski et al., 2021; Lustig et al., 2023 respectively). Additionally to common lncRNAs, many antisense non-coding transcripts, which have been linked to the regulation of neighbouring protein-coding genes, arise from enhancer regions, without counting eRNAs (Onodera et al., 2012).

What remains to be validated, is the newly transcribed putative C-terminal peptide or protein. My former master student Sara Hettrich was able to attach a V5 tag to the C-terminal domain of triadin in mESC derived cardiac bodies and was further able to detect a potential protein of the expected size on western blot. Nevertheless, the biological relevance of this lowly expressed C-terminal domain remains elusive. Since the C-terminal domain of triadin has no transmembrane domain, this putative protein would be an interesting candidate for further studies, since its localization and function could be independent of triadin. The known binding sites within this C-terminal domain mainly relate to cytoskeleton and microtubule binding, making it a potential structural protein, maybe a linker protein of different parts of the cytoskeleton which is needed upon cardiomyocyte transition from a neonatal to an adult stage (Marty et al., 2015; Osseni et al., 2016). In order to investigate its role, an *in-vivo* V5 tag of the C-terminal domain compared to an N-terminal V5 tag could be a starting point as well as the insertion of a polyA sequence upstream of the *AS-Trdn* promoter to terminate sense transcription.

4.4. *AS-Trdn* regulates triadin isoform balance by transcriptional interference

Knowing that *AS-Trdn* expression proceeds the annotated 3'-UTR and leads indeed to the exclusive expression of the cardiac triadin isoform, the hypothesis was set off, that the transcription itself is crucial for the molecular mechanism independent of the spliced transcript. This hypothesis was already strengthened by the study of Zhao, Riching and Knight et al., demonstrating that the spliced *AS-Trdn* transcript is only needed for the correct splicing of the short cardiac specific isoform, namely trisk32, by recruitment of SR splicing factors (SRSF). The genomic deletion of exon 2 and 3 had no effect on the occurrence of the long skeletal muscle isoform of triadin (Zhao, Riching and Knight et al.. 2022). The *AS-Trdn* KO mouse model used in this study harbours an early transcriptional stop signal, resulting indeed in the formation of the skeletal muscle triadin isoform, namely trisk95, again strengthening the initial hypothesis. To be fully convinced by the transcriptional dependency, we aimed for a proof-of-concept experiment, where *AS-Trdn* was either exogenously or endogenously expressed in isolated satellite cells. Thereby the induced expression of *AS-Trdn* from the promoter region was able to induce the expression of cardiac *triadin*, whilst the exogenous expressed lncRNA transcript had no effect. The same was true for the newly found downstream transcript, where transgenic overexpression in TA muscle had no effect on *triadin* isoform abundance. This experiments again demonstrated, that the expression of cardiac triadin depends merely on the *AS-Trdn* transcription itself and the architecture of the genomic loci.

The question remained, which exact molecular mechanism is behind the transcriptional interference leading to the switch in triadin isoforms and how to scientifically pin-point it. An important factor, which lays at the basis of transcriptional interference, depicts the expression level of the antisense non-coding transcript, which needs to remain constantly high. The expression level must at least match the expression level of the corresponding protein-coding gene, as in the example of the lncRNA *Airn* (Latos et al., 2012; Santoro et al., 2013). One generally found feature of lncRNAs displays the relatively low expression level, which is especially true for antisense intergenic lncRNAs, which is why they have long been underestimated, as already mentioned in the introduction (section 1.3; Uchida & Dimmeler 2015). Therefore, it also comes with no surprise, that these antisense lncRNAs don't affect the expression or transcription of the protein-coding gene. In the case of *AS-Trdn*, the expression level is comparable to the protein-coding gene triadin as is *Airn* to Igf2r, making it a highly transcribed

lncRNA. The cause of this enhanced expression, as already elucidated in this study, mainly depends on the binding of additional transcription factors (GATA4, EP300, and SRF). Therefore, the chances of the two convergent RNA polymerases bypassing each other, seemed rather improbable. This point could also be proven by performing the RNA Pol II CUT&RUN and ChIPseq experiments. Using these approaches, the stalling of the antisense polymerase shortly before exon 9 of triadin was visualized and was shown to be lost upon *AS-Trdn* KO. Therefore, the proposed collision of the convergent polymerases was further strengthened. This interference will consequently lead to the transcription termination of both polymerases due to the supercoiling of the DNA strand in between (Pannunzio et al., 2016).

Still, a simple clash of the two convergent RNA polymerases, as proposed by Zhang et al., seemed quite unlikely because of different reasons. First of all, the uncoordinated collision of two polymerases can lead to genomic instability, e.g. DNA damage in the case of transcribing-replicating colliding polymerases (Gómez-González & Aguilera, 2019). Lastly, there are multiple examples of antisense non-coding transcripts, which have no influence on the sense transcribing polymerase and can easily bypass each other as long as no additional factors contribute. These factors could be additional DNA binding factors, like chromatin remodellers, histone modifiers or different transcription factors, e.g. the well-studied CCCTC-binding factor (CTCF; Ali et al., 2016; Rao et al., 2017; Li et al., 2020). In the case of CTCF no alterations upon loss of either CTCF or Rad21, the basic component of Cohesin, were found regarding triadin isoform expression (see Appendix). Additional investigations of topologically associated domains (TADs) using HiC datasets again revealed no changes within the *AS-Trdn* locus (Appendix). No other changes in chromatin accessibility or histone modifications were found at the site of RNA polymerase II stalling. Now the question on how this interference is established and resolved in a coordinated regulatory manner, without causing DNA damage, still remained to be elucidated.

In this regard, an interesting feature about lncRNAs raised attention, which is the co-transcriptional formation of R-loops, commonly stirring at sites of stalling and termination. Most studies regarding R-loops were done in relation to transcription-replication collisions, where RNA:DNA hybrids occurred at DNA damage sites and are said to increase genomic instability and need to be resolved quickly. Different endo- and exonucleases as well as helicases were shown to resolve these R-loops in order

to release the stalled polymerases as well as for DNA damage repair to take place (Zardoni et al., 2021; Brambati et al., 2020). Controversially, more recent studies implicate, that R-loops are not cause but consequence of DNA double-strand breaks and can act as a coordinating mechanism for either the NHEJ (non-homologous end-joining) or HR (homologous recombination) repair system (Gómez-González & Aguilera, 2023).In this case, the RNA:DNA hybrid is formed at the site of DNA strand break after the DNA damage has already happened, whereas regulatory R-loops form co-transcriptionally, leading to a displaced single-strand DNA. Therefore, we now distinguish between break-induced RNA:DNA hybrids (BIRDHs) and co-transcriptionally forming as well as regulatory R-loops (R-loops; Gómez-González & Aguilera, 2023). Nevertheless, unscheduled formations of R-loops promoted by mutations or elevated gene expression conditions can also lead to DNA damage and potentially interfere with DNA and RNA pathways (transcription, replication or RNA processing; Aguilera & Gomez-Gonzalez, 2008). Focusing on the involvement of regulatory R-loops in transcription termination, it has been shown, that overstretched RNA:DNA hybrids have a negative effect on the processing RNA polymerase II. This can result in enhanced transcription termination and prompt backtracking of the polymerase into the R-loop pocket, thereby keeping the polymerase tracked at one spot and increasing termination time (Ginno et al., 2013; Niehrs and Luke, 2020). In the case of *AS-Trdn*, an extensive RNA polymerase II stalling was demonstrated specifically at one genomic region with a comparatively high GC content, another factor prone to induce the formation of R-loops as well as transcription termination (Ginno et al., 2013).

Even though *AS-Trdn* already exhibits high expression levels, its genomic locus is significantly smaller compared to the triadin locus. Still, the transcriptional interference takes place at a specific genomic region, whereas a simple polymerase interference could happen anywhere along the *AS-Trdn* locus. Therefore, a new mechanism was postulated, which could explain the tightly coordinated transcription dependent cardiac triadin isoform formation. If the GC-rich sequence leads to a slowing down of the antisense polymerase, while no factors are bound to the nascent antisense RNA transcript, this could promote an R-loop formation. This R-loop could in return induce a transcriptional stalling followed by a complete transcription termination of the antisense polymerase. The establishment as well as the resolution of stalled polymerases as well as R-loops takes time, meaning that the polymerase stays at the

site of termination for a while, building up a “Roadblock” for the incoming sense transcribing polymerase. To test the postulated mechanism, the first aim in the future will be to show the formation of R-loops at the *AS-Trdn* locus, predominantly at the site of transcriptional stalling. Due to the limited technical possibilities when it comes to working with cardiomyocytes (big cells with a high cytoplasmic proportion, low cell numbers), a new technique needs to be established. In this regard, MapR is a method used to map native R-loops by exposing cell nuclei to an inactive form of RNase H coupled to a MNase. Upon R-loop recognition, the MNase cleaves the associated DNA region, which then diffuses out of the nucleus and can be used for downstream analysis (Jauregui-Lozano et al., 2022). Hopefully the postulated mechanism can be further elucidated in the future using this new technique.

4.5. The *AS-Trdn* regulatory stalling site is stabilized by widespread m^{6}A deposition

Regardless of the missing R-loop detection, the prior performed ChIPseq and CUT&RUN analysis indicated a regulatory stalling of the antisense polymerase and the accompanied GC-rich sequence indicate a possible R-loop involvement. To not only focus on the mere occurrence of a DNA:RNA hybrid, other possible accompanying proteins or enzymes were considered. Different studies have already delved into the formation, stabilization as well as in the resolution of co-transcriptionally forming regulatory R-loops and the responsible proteins. The resolution of R-loops is by far the most intensively studied field, whereas the formation as well as the stabilization is still under debate. A study by the Proudfoot lab, for example, indicated a link between R-loops and heterochromatinization which promotes transcription termination in fission yeast. In their work, G-rich sequences were shown to promote R-loop formation and the de-novo synthesis of an antisense RNA, which induces double-stranded RNA arraignment over the termination region. This double-stranded RNA attracts the RNA interference RNase Dicer and the histone lysine methyltransferase G9a (EHMT2) via an unknown mechanism, resulting in the local deposition of H3K9me2. This methylation in turn enhances RNA Pol II pausing and termination (Skourti-Stathaki et al., 2011/2014). Unfortunately, no publicly available data sets of H3K9me2 for cardiomyocytes or human hearts were available, but there was also no indication for another de-novo synthesized antisense or sense RNA, making this mechanism rather unlikely.

A more recently proposed regulator of R-loop stability is the N^6-methyladenosine (m^6A) modification, which is the most abundant reversible RNA modification playing crucial roles in various processes post-transcriptionally (Yang et al., 2018). Installed by the N6-adenosine-methyltransferase complex MT-A, where mettl3 displays the key enzyme, this modification was suggested to increase R-loop stability and thereby promotes transcription termination. The loss of *mettl3* was demonstrated to majorly reduce the abundance of R-loops, resulting in transcription termination side read-through at different genomic loci (Yang et al., 2019). Another group was able to demonstrate that m^6A is abundant at R-loops in human cells and is recognized by the reader YTHDF2, which is pivotal for the removal of m^6A and therefore R-loop resolution (Abakir et al., 2020). The role of mettl3 and m^6A has been intensively studied throughout the last years and different groups put major efforts in establishing robust m^6A detection as well as prediction tools. The dataset used in this study composed predicted m^6A sites in mouse hearts using an m^6A boost machine learning program, which were afterwards verified using a miCLIP2 experiment (Körtel et al., 2021). Using these datasets to analyse the *AS-Trdn* locus, a high abundance of m^6A modifications was found within the intronic region flanked by triadin exon 9 and *AS-Trdn* exon 3. Interestingly, a major pile up of m^6A sites were located at the RNA polymerase II stalling/termination site and the putative R-loop location as well as in a broader area downstream of *AS-Trdn* exon 3. Due to the stranded analysis, all those modifications cold be mapped to the antisense strand, meaning they belong to the extended *AS-Trdn* transcript. This finding was quite remarkable, since the abundance of m^6A modifications is normally located within the last coding exons of protein-coding genes and much less abundant, especially in intronic regions. Such a widespread m^6A deposition could indicate either a stabilization effect on these downstream transcripts or a fast degradation.

To investigate whether m^6A is involved in the transcriptional interference mechanism carried out by *AS-Trdn*, *mettl3* KO hearts were provided by the Schneider group at the MPI in Bad Nauheim. Interestingly and consistent with the proposed mechanism by Yang et al., an increased expression of the skeletal muscle triadin isoform was detected on RNA as well as on protein level. A complete switch in isoform as demonstrated by the *AS-Trdn* KO mouse model was not expected, since m^6A will unquestionably not be the only regulator of this mechanism. As already mentioned, the high expression level of *AS-Trdn* and the GC-rich sequence are already likely to

increase the transcriptional interference, other yet unknown involved proteins or enzymes not to mention. The whole process of transcription depends on a variety of proteins, which have to be tightly organized as well as the still under-investigated functions of regulatory R-loops and the various possibilities of proteins to recognize and interact with these structures.

4.6. Conclusion and outlook of the molecular mechanism of *AS-Trdn*

In this study, various next-generation sequencing approaches, cell-culture systems and CRIPSR/CAS9 based genomic modifications were used to elucidate the molecular function of the long non-coding RNA *AS-Trdn*. The KO mouse model as well as the demonstrated transcriptional interference mechanism have not been described yet and display a new regulatory mechanism of non-coding RNAs in regulating alternative splicing of a protein coding gene. It was demonstrated, that antisense lncRNAs can directly induce the transcriptional termination of a sense transcribing RNA polymerase II by establishment of a sequence dependent Roadblock formation. The sequence is further recognized by the m6A writer mettl3, leading to an increased pausing time at a specific genomic locus. Stimulatingly, a very recent study in *Escherichia coli* demonstrated the global occurrence of these head-on collisions in a gene-regulatory manner (Wang et al., 2023). The scientists were able to demonstrate, that these programmed genomic conflicts prevent genomic read-through as well as apposite transcription termination of multiple genes. Another interesting aspect demonstrates that co-directional collision of a trailing RNA polymerase II into the collided complex drastically enhances the termination efficiency. These programmed-collisions only occur at well-defined regions, as in the case of *AS-Trdn*, and only happen when the nascent RNA forms a stem-loop like structure (Wang et al., 2023). The authors propose that this mechanism is not only restricted to prokaryotes but resembles a conserved mechanism across species which needs to be further investigated. *AS-Trdn* demonstrates a good example, where evolution might even took one step further and made use of non-coding antisense transcripts in combination with programmed head-on collisions, or Roadblock formations as phrased in this study. To further elucidate this mechanism, the first step will be to clearly validate the appearance of an R-loop by repeating the newly established method. In a next step, the deletion of the GC-rich genomic sequence as well as the insertion of additional polyA sites, prior to the site of

Roadblock formation, could unveil further insights into the mechanism and strengthen the postulated mechanism. Since the polyA insertions had no effect on the transcribing polymerases, we assume that these intrinsic polyA sites are shielded by U1 snRNA and are therefore not recognized (Berg et al., 2012). In the future, an additional KD of U1 snRNA using morpholinos will be performed to stop transcription at the desired genomic loci (Kaida et al., 2010).

Since the group around Wang showed the occurrence of a stem-loop structure of the nascent RNA, a prediction of the secondary structure of the newly found downstream transcript would be interesting as well.

Without doubt, the transcriptional regulation of coding and non-coding RNAs demonstrates a field of vast regulatory possibilities which is still rather poorly understood and the study of *AS-Trdn* sheds another light into this scientific field.

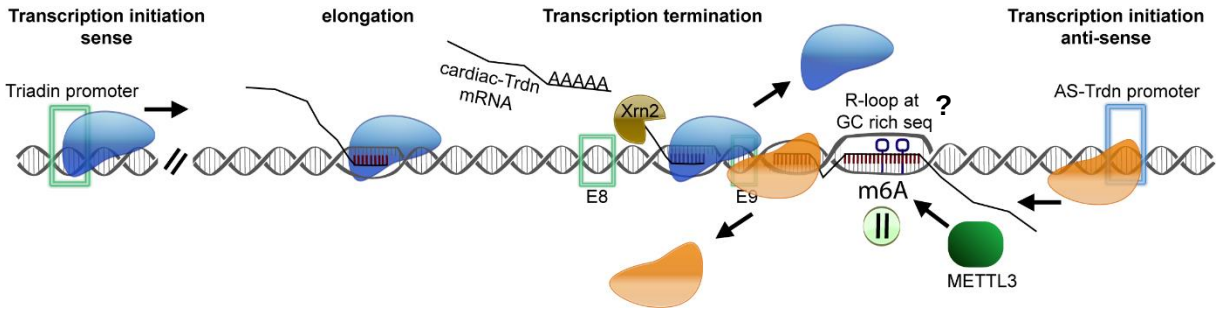

Figure 33 | *AS-Trdn* regulates triadin isoform balance via an R-loop dependent transcriptional interference. Schematic representation of the triadin and *AS-Trdn* locus whilst active transcription in cardiac cells. Upon travelling along the GC-rich sequence, the antisense RNA Polymerase II stalls and subsequently terminates. At the same time, mettl3 methylates the RNA within the R-loop and thereby enhances the stability and the transcription termination. As soon as the sense transcribing RNA Pol II trails into the roadblock forming antisense RNA Pol II, transcription termination is provoked. Thereby the pre-mRNA of the short cardiac triadin isoform is generated, which is further processed by SR splicing factors recruited by the splices *AS-Trdn* transcript.

4.7. The skeletal muscle isoform of triadin is able to increase CRC activity resulting in a “fight or flight” response failure

The regulation of the calcium-release complex and its relevance in cardiac contraction as well as in cardiac diseases has been intensively studied for over 40 years in science. The relevance of the transmembrane protein triadin has been pointed out by different *in vitro* and *in vivo* studies, where multiple dysregulations upon mutation or loss of triadin have been linked to mishandling of cardiac contraction and heart failure. The well-studied Triadin Knock-out syndrome (TKOS) is a human genetic disorder, where mutations lead to early cardiac arrhythmias and even cardiac arrest. What makes triadin even more interesting for scientists, is the fact that it comes in multiple isoforms, even within the same tissue. The most abundant triadin isoforms are trisk32 (cardiac exclusive, little expression in skeletal muscle), trisk52 and trisk95 (both skeletal muscle exclusive). Even though most triadin related human diseases are linked to the cardiovascular system, the majority of studies have been carried out on the skeletal muscle isoform of triadin and its function in SR structure and muscle contraction (Kobayashi YM, Jones LR, 1999; Kirchhefer, et al., 2001/2004; Vassilopoulos et al., 2005; Marty et al., 2015). In this study, the loss of *AS-Trdn* and the consequent expression of the long skeletal muscle triadin isoform trisk95 enables completely new possibilities to study the function of triadin isoforms in the heart.

The first observations of the *AS-Trdn* KO mice revealed no implications on the overall viability or physiology of the mice until 16 weeks of age. This result was on one side surprising, but also not completely far-fetched. Prior studies on trisk32 in the heart have shown obvious impacts on the mice, where deletion as well as overexpression of trisk32 induced either dilative or hypertrophic cardiomyopathies, but no changes in overall viability consistent with the current results (Kirchhefer et al., 2001/2004; Chopra et al., 2009). In contrast, the recent study from Zhao, Riching and Knight et al. demonstrated a decreased survival rate of their *AS-Trdn* KO mice, even though no changes in triadin isoform abundance, major changes in calcium cycling or heart physiology was implicated. The most significant change displayed a reduction in cardiac triadin expression at 8 months of age and the occurrence of premature ventricular contractions (Zhao, Riching and Knight et al., 2022).

A common observation made in all triadin studies, displays a misregulation of the calcium release complex, reflected by alterations in calcium cycling and calcium storage. Measurements of single cardiomyocytes in this study indicate an overall

increased calcium release as well as reuptake upon expression of trisk95, resulting in enhanced sarcomere contraction, which was also reflected by an increased heart rate. Remarkably, the increased calcium handling was able to trigger spontaneous extra calcium sparks as well as uncontrolled calcium oscillations, a sign for an overloaded system unable to cope with the faster cycling. At the same time, these extra-sparks are a hallmark of triadin misregulation, since both loss of triadin as well as overexpression of triadin can induce extra-releases of calcium. Controversy, the expression of trisk95 in the heart was the only one to induce an increased calcium cycling, while all other studies reported a blunted calcium cycling with increased times to decay as well as an SR calcium overload (Kirchhefer et al., 2001/2004; Chopra et al., 2009). A similarity again exhibits the blunted response to beta adrenergic stimulation using isoproterenol treatment. Whenever triadin expression is altered, the heart is not able to react accordingly by increasing the heart rate to induce the “fight or flight” response. This phenomenon is particularly interesting, since stressors additionally to the incapability to respond appropriate are one trigger for cardiac arrhythmias and sudden cardiac arrest. Unfortunately, the underlying reason of why alterations in triadin lead to a blunted response remains elusive. One aspect which was investigated in this regard, are changes in the phosphorylation status of all involved CICR proteins as well as of triadin itself. Different studies have shown, that a change in e.g. RyR2 phosphorylation can massively change calcium handling and result in various cardiac diseases (Wehrens et al., 2003; Yuan et al., 2014). At the same time, loss of PKA phosphorylation could explain the blunted Isoproterenol response, as shown in recent studies (Zhang et al., 2019) Even though whole heart phoshpho-protemonics were performed on *AS-Trdn* KO hearts, the resulting data was inconclusive due to intense outliers as well as low detectability of the phosphorylation sites and therefore needs further establishment (data not shown).

4.8. Triadin is an important regulator of CRC structure and integrity – and beyond?

In trisk32 loss and gain of function studies, the resulting changes in overall CRC related proteins as well as the loss in dyadic structure might be one aspect explaining the dysregulated calcium-handling and the failure to respond to beta adrenergic stimulation (Chopra et al., 2009/2013). In the present study, a loss in dyadic structure was consistently observed, with a major decrease in SR luminal width and dyadic

space, resembling a tightened overall terminal cisternae structure. This finding is another ratification for the structural probabilities of Triadin in reshaping SR structure and therefore resembling an important SR and CRC protein.

However, a major difference comparing published triadin studies and the present work exhibits the changes in CRC related protein abundances. While prior studies demonstrated the reduction in CRC related proteins (e.g. RYR2, CASQ2, JPH2, and JUN) upon changes in trisk32 expression, a minor increase in RYR2 and CASQ2 abundance was measured in membrane fractions of *AS-Trdn* KO hearts. This loss in CRC related proteins could already explain the underlying decrease in calcium cycling as well as the blunted beta adrenergic response in prior studies. In the present study, a different mechanism has to be responsible for the huge increase in calcium release and reuptake. Due to the huge differences in binding possibilities comparing trisk32 and trisk95, the focus was set on changes in triadin interactions. With this approach major changes in CRC and CICR related proteins was observed. Remarkably, the trisk95 results in *AS-Trdn* KO hearts already indicated a higher calcium cycling. For example, the histidine rich calcium binding protein (HRC), which has been shown to be a competitor of CASQ2 in states of moderate and high SR calcium load, was strongly bound to trisk95 while CASQ2 binding was significantly reduced (Rani et al., 2016; Lee et al., 2001). Another important indicator, displays the loss of the RYR2 inhibitor sorcin (SRI), which could again be a result of the higher [Ca^{2+}], leading to the modulation of the receptor. SRI has been shown to inhibit RYR2 opening following Ca^{2+} release, thereby inhibiting further release and preventing positive feedback loops (Farrel et al., 2003). Another interesting aspect displays the loss in binding to ATP2a1/a2 and the Ca^{2+} binding protein Sarcalumenin (SRL), which are known interaction partners of trisk32 within the longitudinal SR (Yoshida et al., 2005; Oddoux 2009; Marty et al., 2015). Having now the sole expression of trisk95, this interaction, if direct or indirect, is absent. This observance again strengthens the differences in triadin isoform localization and functions, as already demonstrated by the Marty lab (Oddoux 2009; Marty et al., 2015).

As already mentioned, the changes directly linked to CRC or CICR were rather minor, even though volcano blot analysis revealed huge changes in overall triadin binding upon loss of *AS-Trdn*. Interestingly, most changes upon trisk95 expression were linked to newly established bindings to the cytoskeleton. Thereby two major pathways raised

attention, where one resembled the strong binding to the microtubule cytoskeleton and the second one the changes in actin and actinin binding. Marty and colleagues demonstrated in previous studies, that trisk95 overexpression in non-muscle cells leads to a massive remodelling of ER structure and assumed an association of triadin with cytoskeleton proteins (Fourest-Lieuvin et al., 2012). Using truncated TRDN proteins, the group was able to proof an interaction with the cytoskeleton-linking membrane protein 63 kDa (CLIMP63; *Ckap4*) specifically within the C-terminal domain of trisk95 (Osseni et al., 2016). CKAP4 is a known type II transmembrane protein, which forms membrane-spanning dimers and thereby functions as a luminal spacer in SR as well as ER sheets, with microtubule binding sites within its cytosolic domain (Sandoz et al., 2015). Due to the exclusive expression of trisk32 in WT hearts, lacking the C-terminal interaction domain, this relation has not been reported in cardiac cells before. Interestingly, in *AS-Trdn* KO hearts, this interaction was newly established, followed by a massive binding of diverse tubulin associated proteins (TUBA1b/4a/8; TUBB2a/4b/5) as well as the binding to the CKAP4 related protein calumenin-1, another protein regulating ER structure (Shen et al., 2019).

At the same time, a change in actin associated interactions was detected. While the binding to actin-related proteins was lost (ACTC1, ACTB, ABLIM1), a significantly increased binding to the actinin cytoskeleton (ACTN1/2/4) as well as to actin-related proteins ACTR2, MACF1 and ARPC1a was demonstrated. A possible explanation for this observation could be a blocked interaction of TRDN and ABLIM1, a modulator of F-actin binding localized at the Z-disk which is rather poorly understood (Roof et al., 1997; Stachowski-Doll et al., 2022). The new established interactions by trisk95 to the actinin and microtubule cytoskeleton could shield the binding site for ABLIM1 and therefore actin interactions are lost. Still, this hypothesis needs further proofing, which could be done by performing proximity-ligation assays, immunoprecipitations using TRDN truncations and rescue experiments using single and double KOs of *AS-Trdn* with putative interaction partners.

Nonetheless, the changes in triadin interactions in *AS-Trdn* KO hearts concerning cytoskeleton proteins could already link the observed SR structural changes to the observed changes in Ca^{2+} handling. All observed changes point towards and increased calcium cycling, with the loss in RYR2 inhibitor, binding of high [Ca^{2+}] sensing proteins and a tightening in SR structure, making the whole system extremely instable at the same time.

4.9. Trisk95 expression in the heart induces DCM in ageing mice

In the context of the present work, the loss of *AS-Trdn* and the consequent expression of the skeletal muscle triadin isoform trisk95 was able to unveil new interactions and functions of triadin isoforms in the heart, thereby contributing to the understanding of triadin dependent calcium regulation. Triadin plays a pivotal role in anchoring and regulating the calcium-release complex, but is also able to reshape SR structure by interacting with the cytoskeleton in great extent (Fourest-Lieuvin et al., 2012; Osseni et al., 2016; current study). Overall expressional changes of triadin and a misbalance of the triadin isoforms can equally induce calcium-induced cardiac contraction disorders, as demonstrated by IonOptix and ECG measurements. In humans, the ablation of triadin is known to induce cardiac arrhythmias followed by cardiac arrest and even sudden cardiac death (Altmann et al., 2015). The *AS-Trdn* KO mice in this study displayed a significant increase in heart rate and a blunted response to β-adrenergic signalling, but no increase in early lethality. Here to mention, the mice are kept in a highly monitored animal facility without facing huge environmental changes, meaning a stress-free environment. The onset of triadin related physiological effects is mostly stress-dependent, which might be the reason behind the mild phenotype observed in this and other mouse related studies.

To study potential time-dependent consequences of trisk95 expression in the heart, mice were kept until 40 weeks of age. Using MRI measurements a decreased heart function and left ventricular mass was evaluated in these ageing mice. The decrease in fractional shortening in combination with the increased heart rate again strengthened that *AS-Trdn* hearts suffer a compensatory failure to cope with the increase in calcium cycling. Even though the time between single contractions in KO hearts is faster, the heart is not able to adapt accordingly, which is displayed by an incomplete contraction cycling. Together with the fact, that *AS-Trdn* KO mice exhibit an increased heart size and the decrease in cardiomyocyte cross sectional area, a commencing dilative cardiomyopathy (DCM) was assumed. Additionally, the overall heart weight was significantly decreased, despite the overall increase in heart size. The pathophysiology of left ventricular DCM includes the decrease in stroke volume, cardiac output; an impaired left ventricular filling and relaxation as well as a decrease in end-diastolic pressure (Schönberger & Seidman, 2001; Schultheiss et al., 2019). Except the end-diastolic pressure, which was slightly but not significantly decreased, all characteristics applied. The origin of LV dilatation is most often correlated with cardiac remodelling

and fibrosis development. Using trichrome staining, no obvious fibrotic tissue was observed, which might be due to the early stage of dilation, whilst the heart itself clearly displayed an increased, more roundish shape. The causes of DCM can be of diverse origins, including drugs and toxins, infections, autoimmune diseases as well as genetic mutations and disorders. A major group of genes correlated with the occurrence of dilative cardiomyopathy, encode for sarcomere and cytoskeleton proteins (Schönberger & Seidman, 2001; Weintraub et al., 2017). Since the *AS-Trdn* KO displays major changes in SR structure and triadin interactions with the cytoskeleton were found to be newly established, it seemed probable that an accumulation of changes related to these genes led to the observed DCM. Possible gene candidates, which are known to induce dilatation, include *Actc1*, *Actn2*, *Tnnt2*, *Tnni3*, *Flnc*, *Myh6* and *Nebl* (sarcomere) as well as desmin, which was the most significantly decreased gene comparing WT and KO IPs (Olson et al., 1998; Li et al., 1999; Weintraub et al., 2017; Frank et al., 2019; Hinson, 2022). Therefore the observed phenotype in *AS-Trdn* KO mice depends merely on the change in triadin isoform interactions resulting in a reshaping of the dyadic and cytoskeleton structure within the dyad and at the Z-line.

4.10. Conclusion and outlook on the physiological mechanism and function of triadin in the heart

Taken together, multiple different experimental techniques were used to analyse the consequences of trisk95 expression in the mouse heart upon loss of *AS-Trdn*. Using molecular as well as physiological measurements, the structural capacity of Triadin isoforms was further elucidated, revealing huge differences regarding skeletal muscle and cardiac function. A change in this isoform abundance can induce cardiac malfunctioning, leading to a loss in dyadic structure, an abnormal calcium cycling and heart rate together resulting in a commencing dilated cardiomyopathy. Nevertheless, there are multiple questions which still need to be further elucidated. The increase in calcium cycling is demonstrated by an increase in release and reuptake, but the question remains if there is an accumulation of calcium within the SR and the reuptake is just a consequence of the fast release or if the whole calcium cycling is enhanced. Therefore more IonOptix experiments using caffeine to empty the SR calcium content could be performed.

Using telemetric devices, the consequences of this enhanced calcium cycling on overall heart rate and upon β-adrenergic signalling has been demonstrated, but the electrocardiographic records remain to be analysed. Different studies reported the occurrence of delayed afterdepolarizations (DADs) and atrial fibrillations as a consequence of increased calcium cycling and calcium sparks as well as SR calcium leakage, which could also apply for the *AS-Trdn* KO mice (Hove-Madsen et al., 2004; Neef et al., 2010; Wakili et al., 2011; Voigt et al., 2012) Since Isoproterenol was not able to increase the heart rate and led to a discontinuous heart rate, the application of a sporting activity under Ivabradine could be a great possibility to monitor heart rate, echocardiography traces and potential abnormalities (Du, Xiao-Jun, et al, 2004). Additionally, the heart rate variability under normal conditions could be of interest to evaluate overall cardiac performance.

The blunted response upon β-adrenergic stimulation is in accordance to multiple triadin studies, even though the underlying mechanism has not been uncovered (Kirchhefer et al., 2001/2004/2007; Chopra et al., 2009). To unveil this mechanism, another study using telemetric devices could be to apply different beta-blockers and channel inhibitors to unveil the involved pathways leading to the observed failure in response.

Another aspect regards the structural changes in dyadic integrity, which has been outlined but not pin-pointed. As already suggested, multiple interaction studies of triadin and cytoskeleton proteins could shed light on the direct interaction partners, linking the SR membrane compartment to the actin and microtubule cytoskeleton.

The regulation of cardiac contraction through the transmembrane protein triadin displays a complex and multi-facetted molecular mechanism, making it a highly interesting protein. The regulation of triadin isoform abundance by the long-non coding RNA *AS-Trdn* just adds another layer of complexity on-top, which will also in the future keep us scientifically challenged and motivated.

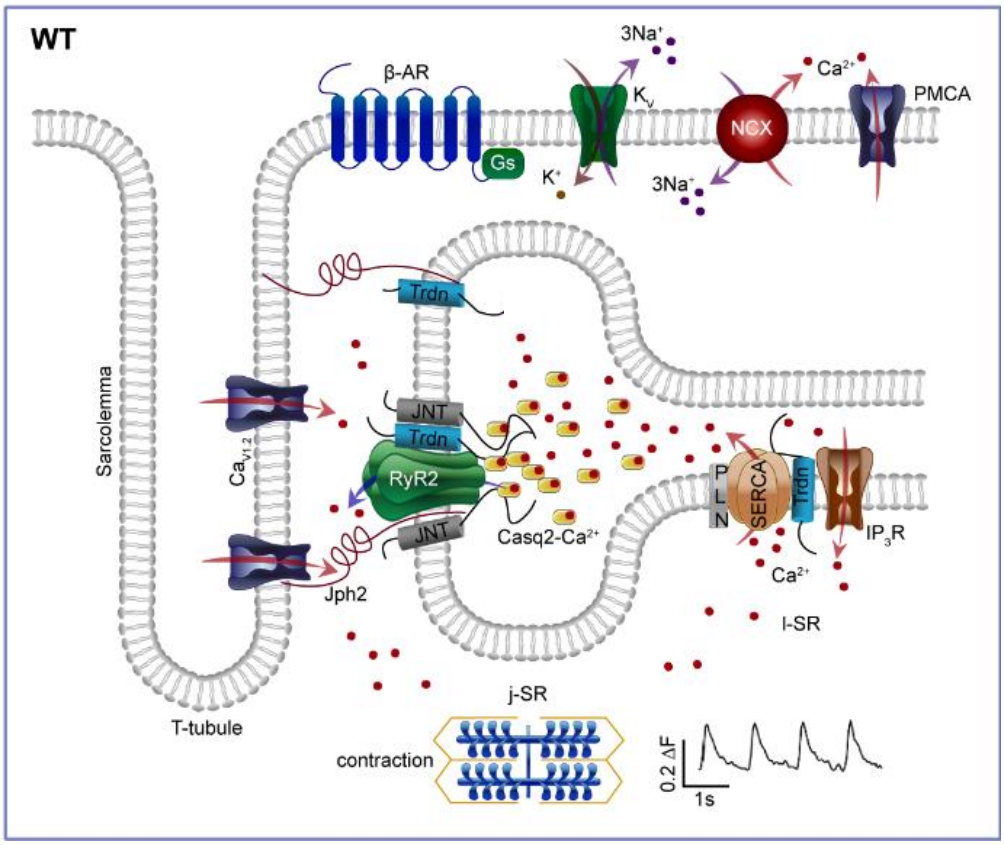
WT
β-AR
Gs
3Na+
K+
Kv
NCX
Ca2+
PMCA
3Na+
Trdn
Sarcolemma
JNT
Trdn
RyR2
JNT
CaV1.2
Jph2
Casq2-Ca2+
PLN
SERCA
Trdn
IP3R
Ca2+
l-SR
j-SR
T-tubule
contraction
0.2 ΔF
1s

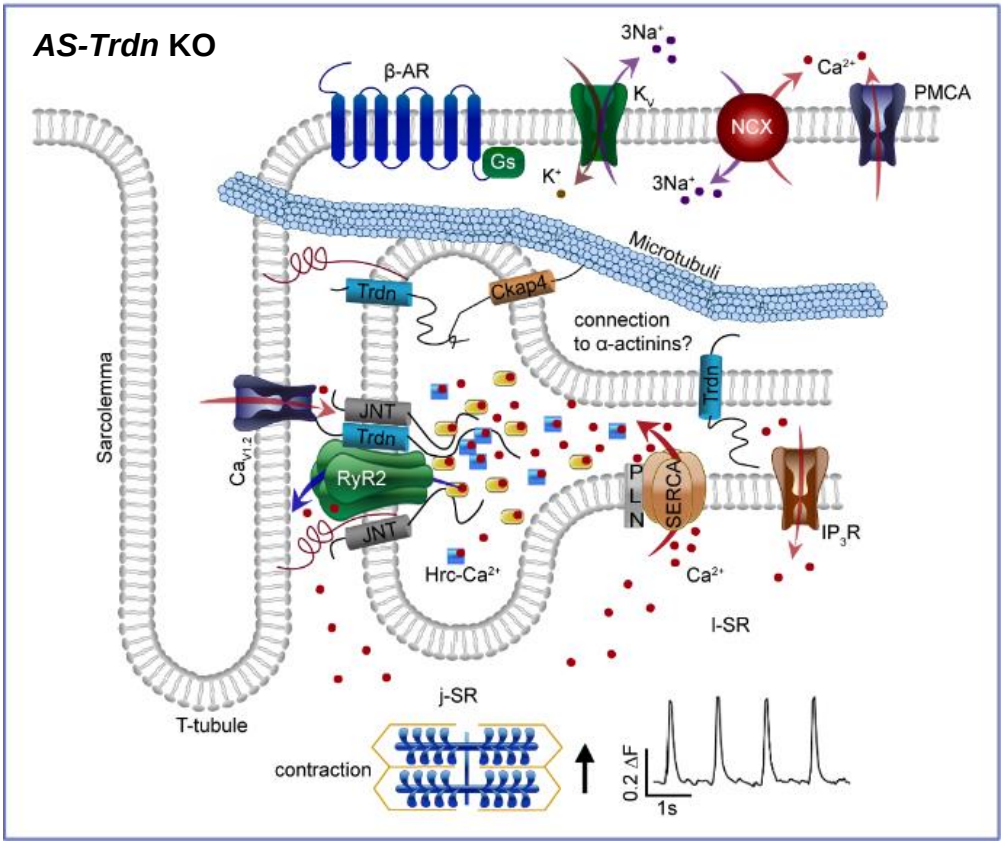
AS-Trdn KO
β-AR
Gs
3Na+
K+
Kv
NCX
Ca2+
PMCA
3Na+
Microtubuli
Trdn
Ckap4
connection
to α-actinins?
Trdn
Sarcolemma
JNT
Trdn
RyR2
JNT
CaV1.2
PLN
SERCA
IP3R
Hrc-Ca2+
Ca2+
l-SR
j-SR
T-tubule
contraction
0.2 ΔF
1s

Figure 34 | *AS-Trdn* KO leads to a change in triadin isoform abundance resulting in a change in cardiac dyad structure and excitation contraction coupling. Schematic representation summarizing the excitation-contraction coupling in WT and *AS-Trdn* KO cardiomyocytes including all CICR involved proteins. **A** Under normal conditions, trisk32 is localized within the junctional and longitudinal SR and is a major component of the cardiac dyad and the CRC (RYR2, JNT, CASQ2, JPH2). Trisk32 binds the Ryanodine receptor as well as the calcium-binding protein Casq2 to facilitate calcium release as well as accurate localization. Within the lSR, trisk32 is closely associated with the calcium ATPase SERCA2 (ATP2a2) and the IP_3R. The dyadic space is mainly dependent on the luminal spacer JPH2 with no direct contact between RyR2 and the voltage-dependent calcium release channel $Ca_V1.2$. The calcium cycling (indicated by blue and red arrows) displays normal traces leading to a steady contraction. **B** In *AS-Trdn* KO hearts, trisk32 is replaced by trisk95, displayed by a major increase in C-terminal domain length. The association in the lSR with SERCA2 is absent, while new interactions within the j-SR are established. These interactions are displayed by the biding of trisk95 to the CACQ2 competitor HRC and the newly established interaction between trisk95 and the cytoskeleton-binding protein Ckap4, accompanied by binding to the microtubule network. The connection of trisk95 to the actinin cytoskeleton has been demonstrated, even though the linking factor remains elusive (question mark). The decrease in dyadic space is displayed by the closer proximity between the sarcolemma and the SR membrane, with RyR2 and $Ca_V1.2$ in closer juxtaposition. The change in triadin interactions, followed by a tightening in SR structure results in an increased calcium cycling (thick blue and red arrows; IonOptix trace) and therefore to an enhanced contraction force. A, B β-AR, beta-adrenergic receptor; Casq2, calsequestrin 2; $Ca_V1.2$, calcium channel, voltage-dependent, L type, alpha 1C; CKAP4, cytoskeleton-associated protein 4; Gs, G-proteins; Hrc, histidine-rich calcium-binding protein; IP_3R, inositol 1,4,5-trisphosphate receptors; JNT, junctin; Jph2, junctophilin 2; K_V, voltage-gated potassium channel; NCX, Na^+/Ca^{2+} exchanger; PLN, phospholamban; PMCA, plasma membrane Ca^{2+} ATPase; RyR2, ryanodine receptor 2; SERCA, sarcoplasmic/endoplasmic reticulum Ca^{2+} ATPase 2a; Trdn, triadin.

Literature

1. Abakir, Abdulkadir, et al. "N 6-methyladenosine regulates the stability of RNA: DNA hybrids in human cells." Nature genetics 52.1 (2020): 48-55.
2. Aguilera, Andrés, and Belén Gómez-González. "Genome instability: a mechanistic view of its causes and consequences." Nature Reviews Genetics 9.3 (2008): 204-217.
3. Ali, Tamer, Rainer Renkawitz, and Marek Bartkuhn. "Insulators and domains of gene expression." Current opinion in genetics & development 37 (2016): 17-26.
4. Altmann, Helene M., et al. "Homozygous/compound heterozygous Triadin mutations associated with autosomal-recessive long-QT syndrome and pediatric sudden cardiac arrest: elucidation of the Triadin knockout syndrome." Circulation 131.23 (2015): 2051-2060.
5. Amaral, Paulo P., et al. "The eukaryotic genome as an RNA machine." science 319.5871 (2008): 1787-1789.
6. Andergassen, Daniel, and John L. Rinn. "From genotype to phenotype: genetics of mammalian long non-coding RNAs in vivo." Nature Reviews Genetics 23.4 (2022): 229-243.
7. Andergassen, Daniel, et al. "The Airn lncRNA does not require any DNA elements within its locus to silence distant imprinted genes." PLoS Genetics 15.7 (2019): e1008268.
8. Anderson, Kelly M., and Douglas M. Anderson. "LncRNAs at the heart of development and disease." Mammalian Genome 33.2 (2022): 354-365.
9. Anderson, Mark E., Joan Heller Brown, and Donald M. Bers. "CaMKII in myocardial hypertrophy and heart failure." Journal of molecular and cellular cardiology 51.4 (2011): 468-473.
10. Arab, Khelifa, et al. "GADD45A binds R-loops and recruits TET1 to CpG island promoters." Nature genetics 51.2 (2019): 217-223.
11. Ariel, Federico, et al. "R-loop mediated trans action of the APOLO long noncoding RNA." Molecular Cell 77.5 (2020): 1055-1065.
12. Beckedorff, Felipe C., et al. "The intronic long noncoding RNA ANRASSF1 recruits PRC2 to the RASSF1A promoter, reducing the expression of RASSF1A and increasing cell proliferation." PLoS genetics 9.8 (2013): e1003705.
13. Beltran, Manuel, et al. "A natural antisense transcript regulates Zeb2/Sip1 gene expression during Snail1-induced epithelial–mesenchymal transition." Genes & development 22.6 (2008): 756-769.
14. Berg, Michael G., et al. "U1 snRNP determines mRNA length and regulates isoform expression." *Cell* 150.1 (2012): 53-64.
15. Bers, Donald M. "Cardiac excitation–contraction coupling." Nature 415.6868 (2002): 198-205.
16. Bochenek, Gregor, et al. "The large non-coding RNA ANRIL, which is associated with atherosclerosis, periodontitis and several forms of cancer, regulates ADIPOR1, VAMP3 and C11ORF10." Human molecular genetics 22.22 (2013): 4516-4527.
17. Brambati, Alessandra, et al. "The dark side of RNA: DNA hybrids." Mutation Research/Reviews in Mutation Research 784 (2020): 108300.
18. Brandt, N.R., Caswell, A.H., Wen, S.-R., Talvenheimo, J.A. 1990. Molecular interactions of the junctional foot protein and dihydropyridine receptor in skeletal muscle triads.J. Membrane Biol. 113:237–251
19. Brandt, Neil R., et al. "Detection and localization of Triadin in rat ventricular muscle." The Journal of membrane biology 131 (1993): 219-228.
20. Bravo-Sagua, Roberto, et al. "Sarcoplasmic reticulum and calcium signaling in muscle cells: Homeostasis and disease." International review of cell and molecular biology 350 (2020): 197-264.
21. Brockdorff, Neil, et al. "Conservation of position and exclusive expression of mouse Xist from the inactive X chromosome." Nature 351.6324 (1991): 329-331.

22. Cabili, Moran N., et al. "Integrative annotation of human large intergenic noncoding RNAs reveals global properties and specific subclasses." Genes & development 25.18 (2011): 1915-1927.
23. Chaudhry, Raheel, Julia H. Miao, and Afzal Rehman. "Physiology, cardiovascular." StatPearls [Internet]. StatPearls Publishing, 2022.
24. Chen, Ling-Ling, et al. "A guide to naming eukaryotic circular RNAs." Nature Cell Biology 25.1 (2023): 1-5.
25. Cheng, Heping, W. Jonathan Lederer, and Mark B. Cannell. "Calcium sparks: elementary events underlying excitation-contraction coupling in heart muscle." Science 262.5134 (1993): 740-744.
26. Chopra, Nagesh, et al. "Ablation of Triadin causes loss of cardiac Ca2+ release units, impaired excitation–contraction coupling, and cardiac arrhythmias." Proceedings of the National Academy of Sciences 106.18 (2009): 7636-7641.
27. Colognori, David, et al. "Xist deletional analysis reveals an interdependency between Xist RNA and polycomb complexes for spreading along the inactive X." Molecular cell 74.1 (2019): 101-117.
28. Crick, Francis, et al. "General nature of the genetic code for proteins." (1961): 1227-1232.
29. Deetjen, P., E.-J. Speckmann und J. Hescheler (2005). Physiologie. München, Elsevier GmbH.
30. Derrien, Thomas, et al. "The GENCODE v7 catalog of human long noncoding RNAs: analysis of their gene structure, evolution, and expression." Genome research 22.9 (2012): 1775-1789.
31. Devaux, Yvan. "Transcriptome of blood cells as a reservoir of cardiovascular biomarkers." Biochimica et Biophysica Acta (BBA)-Molecular Cell Research 1864.1 (2017): 209-216.
32. Djebali, Sarah, et al. "Landscape of transcription in human cells." Nature 489.7414 (2012): 101-108.
33. Du, Xiao-Jun, et al. "If channel inhibitor ivabradine lowers heart rate in mice with enhanced sympathoadrenergic activities." British journal of pharmacology 142.1 (2004): 107-112.
34. Eisner, David A., et al. "Calcium and excitation-contraction coupling in the heart." Circulation research 121.2 (2017): 181-195.
35. El-Armouche, Ali, and Thomas Eschenhagen. "β-Adrenergic stimulation and myocardial function in the failing heart." Heart failure reviews 14 (2009): 225-241.
36. Fabiato, Alexandre. "Calcium-induced release of calcium from the cardiac sarcoplasmic reticulum." American Journal of Physiology-Cell Physiology 245.1 (1983): C1-C14.
37. Fan, Jiahui, et al. "LncRNA ZNF593-AS alleviates contractile dysfunction in dilated cardiomyopathy." Circulation Research 128.11 (2021): 1708-1723.
38. Farrell, Emily F., et al. "Sorcin inhibits calcium release and modulates excitation-contraction coupling in the heart." Journal of Biological Chemistry 278.36 (2003): 34660-34666.
39. Florea, Viorel G., and Jay N. Cohn. "The autonomic nervous system and heart failure." Circulation research 114.11 (2014): 1815-1826.
40. Fourest-Lieuvin, Anne, et al. "Role of triadin in the organization of reticulum membrane at the muscle triad." Biophysical Journal 102.3 (2012): 363a.
41. Frank, Derk, et al. "Cardiac α-actin (ACTC1) gene mutation causes atrial-septal defects associated with late-onset dilated cardiomyopathy." Circulation: Genomic and Precision Medicine 12.8 (2019): e002491.
42. Gelfand, Brian, et al. "Regulated antisense transcription controls expression of cell-type-specific genes in yeast." Molecular and cellular biology 31.8 (2011): 1701-1709.
43. Ghildiyal, Megha, and Phillip D. Zamore. "Small silencing RNAs: an expanding universe." Nature reviews genetics 10.2 (2009): 94-108.
44. Ginno, Paul A., et al. "GC skew at the 5′ and 3′ ends of human genes links R-loop formation to epigenetic regulation and transcription termination." Genome research 23.10 (2013): 1590-1600.

45. Giudicessi, John R., and Michael J. Ackerman. "Calcium revisited: new insights into the molecular basis of long-QT syndrome." Circulation: Arrhythmia and Electrophysiology 9.7 (2016): e002480.
46. Gómez-González, Belén, and Andrés Aguilera. "Break-induced RNA–DNA hybrids (BIRDHs) in homologous recombination: friend or foe?." EMBO reports (2023): e57801.
47. Gómez-González, Belén, and Andrés Aguilera. "Transcription-mediated replication hindrance: a major driver of genome instability." Genes & development 33.15-16 (2019): 1008-1026.
48. Gregersen, Lea H., and Jesper Q. Svejstrup. "The cellular response to transcription-blocking DNA damage." Trends in Biochemical Sciences 43.5 (2018): 327-341.
49. Grote, Phillip, et al. "The tissue-specific lncRNA Fendrr is an essential regulator of heart and body wall development in the mouse." Developmental cell 24.2 (2013): 206-214.
50. Gründer, Stefan, and Klaus-Dieter Schlüter, eds. Physiologie hoch2. Elsevier Health Sciences, 2023
51. Guo, Wei, et al. "Biochemical Characterization and Molecular Cloning of Cardiac Triadin (∗)." Journal of Biological Chemistry 271.1 (1996): 458-465.
52. Guttman, Mitchell, et al. "Chromatin signature reveals over a thousand highly conserved large non-coding RNAs in mammals." Nature 458.7235 (2009): 223-227.
53. Hinson, John Travis. "Molecular genetic mechanisms of dilated cardiomyopathy." Current opinion in genetics & development 76 (2022): 101959.
54. Hove-Madsen, Leif, et al. "Atrial fibrillation is associated with increased spontaneous calcium release from the sarcoplasmic reticulum in human atrial myocytes." Circulation 110.11 (2004): 1358-1363.
55. Jauregui-Lozano, Juan, Kendall Cottingham, and Hana Hall. "Tissue-Specific, Genome-wide Mapping of R-loops in Drosophila Using MapR." Bio-protocol 12.18 (2022): e4516-e4516.
56. Kaida, Daisuke, et al. "U1 snRNP protects pre-mRNAs from premature cleavage and polyadenylation." *nature* 468.7324 (2010): 664-668.
57. Kang Y. J., Yang D. C., Kong L., Hou M., Meng Y. Q., Wei L., Gao G. 2017. CPC2: a fast and accurate coding potential calculator based on sequence intrinsic features. Nucleic Acids Research 45(Web Server issue): W12–W16.
58. Kirchhefer, Uwe, et al. "Cardiac hypertrophy and impaired relaxation in transgenic mice overexpressing Triadin 1." Journal of Biological Chemistry 276.6 (2001): 4142-4149.
59. Kirchhefer, Uwe, et al. "Transgenic Triadin 1 overexpression alters SR Ca2+ handling and leads to a blunted contractile response to β-adrenergic agonists." Cardiovascular research 62.1 (2004): 122-134.
60. Kirchhefer, Uwe, et al. "Triadin is a critical determinant of cellular Ca cycling and contractility in the heart." American Journal of Physiology-Heart and Circulatory Physiology 293.5 (2007): H3165-H3174.
61. Klattenhoff, Carla A., et al. "Braveheart, a long noncoding RNA required for cardiovascular lineage commitment." Cell 152.3 (2013): 570-583.
62. Knollmann, Björn C., et al. "Casq2 deletion causes sarcoplasmic reticulum volume increase, premature Ca 2+ release, and catecholaminergic polymorphic ventricular tachycardia." The Journal of clinical investigation 116.9 (2006): 2510-2520.
63. Kobayashi, Yvonne M., and Larry R. Jones. "Identification of Triadin 1 as the predominant Triadin isoform expressed in mammalian myocardium." Journal of Biological Chemistry 274.40 (1999): 28660-28668.
64. Kohlmaier, Alexander, Lesca M. Holdt, and Daniel Teupser. "Long noncoding RNAs in cardiovascular disease." Current Opinion in Cardiology 38.3 (2023): 179.
65. Kornienko, Aleksandra E., et al. "Gene regulation by the act of long non-coding RNA transcription." BMC biology 11 (2013): 1-14.
66. Korostowski, Lisa, Natalie Sedlak, and Nora Engel. "The Kcnq1ot1 long non-coding RNA affects chromatin conformation and expression of Kcnq1, but does not regulate its imprinting in the developing heart." (2012): e1002956.

67. Körtel N, Rücklé C, Zhou Y, Busch A et al. Deep and accurate detection of m6A RNA modifications using miCLIP2 and m6Aboost machine learning. Nucleic Acids Res 2021 Sep 20;49(16):e92. PMID: 34157120
68. Lanner, Johanna T., et al. "Ryanodine receptors: structure, expression, molecular details, and function in calcium release." Cold Spring Harbor perspectives in biology 2.11 (2010): a003996.
69. Lapidot, Michal, and Yitzhak Pilpel. "Genome-wide natural antisense transcription: coupling its regulation to its different regulatory mechanisms." EMBO reports 7.12 (2006): 1216-1222.
70. Larson, Andrew C., et al. "Self-gated cardiac cine MRI." Magnetic Resonance in Medicine: An Official Journal of the International Society for Magnetic Resonance in Medicine 51.1 (2004): 93-102.
71. Latos, Paulina A., et al. "Airn transcriptional overlap, but not its lncRNA products, induces imprinted Igf2r silencing." Science 338.6113 (2012): 1469-1472.
72. Lee, Han Gil, Hara Kang, and Woo Jin Park. "Interaction of HRC (histidine-rich Ca2+-binding protein) and Triadin in the lumen of sarcoplasmic reticulum." Journal of Biological Chemistry 276.43 (2001): 39533-39538.
73. Li, Duanxiang, et al. "Desmin mutation responsible for idiopathic dilated cardiomyopathy." Circulation 100.5 (1999): 461-464.
74. Li, Yan, et al. "The structural basis for cohesin–CTCF-anchored loops." Nature 578.7795 (2020): 472-476.
75. Liu, S. John, and Daniel A. Lim. "Modulating the expression of long non-coding RNA s for functional studies." EMBO reports 19.12 (2018): e46955.
76. Lyu, Yankun, et al. "Protocol to record and quantify the intracellular pH in contracting cardiomyocytes." STAR protocols 3.2 (2022): 101301.
77. Marks, Andrew R. "Calcium cycling proteins and heart failure: mechanisms and therapeutics." The Journal of clinical investigation 123.1 (2013): 46-52.
78. Marnef, Aline, and Gaëlle Legube. "m6A RNA modification as a new player in R-loop regulation." Nature Genetics 52.1 (2020): 27-28.
79. Maroli, Giovanni, and Thomas Braun. "The long and winding road of cardiomyocyte maturation." Cardiovascular Research 117.3 (2021): 712-726.
80. Martens, Joseph A., Lisa Laprade, and Fred Winston. "Intergenic transcription is required to repress the Saccharomyces cerevisiae SER3 gene." Nature 429.6991 (2004): 571-574.
81. Marty, Isabelle. "Triadin regulation of the Ryanodine receptor complex." The Journal of Physiology 593.15 (2015): 3261-3266.
82. Mattick, John S., and John L. Rinn. "Discovery and annotation of long noncoding RNAs." Nature structural & molecular biology 22.1 (2015): 5-7.
83. Mattick, John S., et al. "Long non-coding RNAs: definitions, functions, challenges and recommendations." Nature Reviews Molecular Cell Biology 24.6 (2023): 430-447.
84. Mattioli, Kaia, et al. "High-throughput functional analysis of lncRNA core promoters elucidates rules governing tissue specificity." Genome research 29.3 (2019): 344-355.
85. Mendell, Joshua T., and Eric N. Olson. "MicroRNAs in stress signaling and human disease." Cell 148.6 (2012): 1172-1187.
86. Mohammad, Faizaan, et al. "Kcnq1ot1 noncoding RNA mediates transcriptional gene silencing by interacting with Dnmt1." Development 137.15 (2010): 2493-2499.
87. Morrissy, A. Sorana, Malachi Griffith, and Marco A. Marra. "Extensive relationship between antisense transcription and alternative splicing in the human genome." Genome research 21.8 (2011): 1203-1212.
88. Neef, Stefan, et al. "CaMKII-dependent diastolic SR Ca2+ leak and elevated diastolic Ca2+ levels in right atrial myocardium of patients with atrial fibrillation." Circulation research 106.6 (2010): 1134-1144.
89. Niehrs, Christof, and Brian Luke. "Regulatory R-loops as facilitators of gene expression and genome stability." Nature reviews Molecular cell biology 21.3 (2020): 167-178.
90. Oddoux, Sarah, et al. "Triadin deletion induces impaired skeletal muscle function." *Journal of Biological Chemistry* 284.50 (2009): 34918-34929.

91. Olson, Timothy M., et al. "Actin mutations in dilated cardiomyopathy, a heritable form of heart failure." Science 280.5364 (1998): 750-752.
92. Onodera, Courtney S., et al. "Gene isoform specificity through enhancer-associated antisense transcription." (2012): e43511.
93. Osseni, Alexis, et al. "Triadin and CLIMP-63 form a link between triads and microtubules in muscle cells." Journal of Cell Science 129.20 (2016): 3744-3755.
94. Pannunzio, Nicholas R., and Michael R. Lieber. "RNA polymerase collision versus DNA structural distortion: twists and turns can cause break failure." Molecular cell 62.3 (2016): 327-334.
95. Pelechano, Vicent, and Lars M. Steinmetz. "Gene regulation by antisense transcription." Nature Reviews Genetics 14.12 (2013): 880-893.
96. Peng, Mei. Molecular identification and characterization of rabbit skeletal muscle Triadin: A novel protein with a potential to link the excitation-contraction coupling in skeletal muscle. University of Cincinnati, 1994.
97. Peterson, Blaise Z., Carla D. DeMaria, and David T. Yue. "Calmodulin is the Ca2+ sensor for Ca2+-dependent inactivation of L-type calcium channels." Neuron 22.3 (1999): 549-558.
98. Piquereau, Jérôme, and Renée Ventura-Clapier. "Maturation of cardiac energy metabolism during perinatal development." Frontiers in Physiology 9 (2018): 959.
99. Pogwizd, Steven M., et al. "Arrhythmogenesis and contractile dysfunction in heart failure: roles of sodium-calcium exchange, inward rectifier potassium current, and residual β-adrenergic responsiveness." Circulation research 88.11 (2001): 1159-1167.
100. Rani, Shilpa, Chang Sik Park, and Pradeep Kumar Sreenivasaiah. "Characterization of Ca2+-dependent protein-protein interactions within the Ca2+ release units of cardiac sarcoplasmic reticulum." Molecules and Cells 39.2 (2016): 149.
101. Rao, Suhas SP, et al. "Cohesin loss eliminates all loop domains." Cell 171.2 (2017): 305-320.
102. Ravid Lustig, L., Sampath Kumar, A., Schwämmle, T. et al. GATA transcription factors drive initial Xist upregulation after fertilization through direct activation of long-range enhancers. Nat Cell Biol 25, 1704–1715 (2023). https://doi.org/10.1038/s41556-023-01266-x
103. Rinn, John L., and Howard Y. Chang. "Genome regulation by long noncoding RNAs." Annual review of biochemistry 81 (2012): 145-166.
104. Roof, Dorothy J., et al. "Molecular characterization of abLIM, a novel actin-binding and double zinc finger protein." The Journal of cell biology 138.3 (1997): 575-588.
105. Rosenthal, Nadia, and Richard P. Harvey, eds. Heart development and regeneration. Vol. 1. Academic Press, 2010.
106. Roux-Buisson, Nathalie, et al. "Absence of Triadin, a protein of the calcium release complex, is responsible for cardiac arrhythmia with sudden death in human." Human molecular genetics 21.12 (2012): 2759-2767.
107. Sandow, Alexander. "Excitation-contraction coupling in muscular response." The Yale journal of biology and medicine 25.3 (1952): 176.
108. Sandoz, Patrick A., and F. Gisou Van der Goot. "How many lives does CLIMP-63 have?." Biochemical Society Transactions 43.2 (2015): 222-228.
109. Santoro, Federica, et al. "Imprinted Igf2r silencing depends on continuous Airn lncRNA expression and is not restricted to a developmental window." Development 140.6 (2013): 1184-1195.
110. Sarah Oddoux. Fonctions des Triadines dans le muscle squelettique. Caractérisation de l'isoforme Trisk 32.. Biologie cellulaire. Université Joseph-Fourier - Grenoble I, 2009. Français.
111. Schönberger, Jost, and Christine E. Seidman. "Many roads lead to a broken heart: the genetics of dilated cardiomyopathy." The American Journal of Human Genetics 69.2 (2001): 249-260.
112. Schonrock, Nicole, Richard P. Harvey, and John S. Mattick. "Long noncoding RNAs in cardiac development and pathophysiology." Circulation research 111.10 (2012): 1349-1362.

113. Schultheiss, Heinz-Peter, et al. "Dilated cardiomyopathy." Nature reviews Disease primers 5.1 (2019): 32.
114. Schutt, Christian, et al. "Linc-MYH configures INO 80 to regulate muscle stem cell numbers and skeletal muscle hypertrophy." The EMBO journal 39.22 (2020): e105098.
115. SEER Training Modules, Anatomy & Physiology. U. S. National Institutes of Health, National Cancer Institute. 08.08.2023 <https://training.seer.cancer.gov/>.
116. Shearwin, Keith E., Benjamin P. Callen, and J. Barry Egan. "Transcriptional interference–a crash course." TRENDS in Genetics 21.6 (2005): 339-345.
117. Shen, Birong, et al. "Calumenin-1 interacts with Climp63 to cooperatively determine the luminal width and distribution of endoplasmic reticulum sheets." Iscience 22 (2019): 70-80.
118. Skourti-Stathaki, K., Kamieniarz-Gdula, K. & Proudfoot, N. J. R-loops induce repressive chromatin marks over mammalian gene terminators. Nature 516, 436–439 (2014).
119. Skourti-Stathaki, K., Proudfoot, N. J. & Gromak, N. Human senataxin resolves RNA/DNA hybrids formed at transcriptional pause sites to promote Xrn2-dependent termination. Mol. Cell 42, 794–805 (2011).
120. Skourti-Stathaki, Konstantina, and Nicholas J. Proudfoot. "A double-edged sword: R loops as threats to genome integrity and powerful regulators of gene expression." Genes & development 28.13 (2014): 1384-1396.
121. Song, Lei, et al. "Calsequestrin 2 (CASQ2) mutations increase expression of calreticulin and Ryanodine receptors, causing catecholaminergic polymorphic ventricular tachycardia." The Journal of clinical investigation 117.7 (2007): 1814-1823.
122. Speckmann, Erwin-Josef . Physiologie. Available from: ClinicalKey Student, (7th Edition). Elsevier GmbH, Urban & Fischer Verlag, 2019.
123. Srijyothi, Loudu, et al. "Roles of non-coding RNAs in transcriptional regulation." Transcriptional and Post-transcriptional regulation 55 (2018).
124. Stachowski-Doll, Marisa J., et al. "GSK-3β localizes to the cardiac Z-disc to maintain length dependent activation." Circulation Research 130.6 (2022): 871-886.
125. Statello, Luisa, et al. "Gene regulation by long non-coding RNAs and its biological functions." Nature reviews Molecular cell biology 22.2 (2021): 96-118.
126. Szafranski, P., et al. "Unraveling regulation of the FOXF1 adjacent long non-coding RNA FENDRR in lungs." (2021).
127. Taft, Ryan J., et al. "Non-coding RNAs: regulators of disease." The Journal of Pathology: A Journal of the Pathological Society of Great Britain and Ireland 220.2 (2010): 126-139.
128. Tan-Wong, Sue Mei, Somdutta Dhir, and Nick J. Proudfoot. "R-loops promote antisense transcription across the mammalian genome." Molecular cell 76.4 (2019): 600-616.
129. Terentyev, Dmitry, et al. "Modulation of SR Ca release by luminal Ca and Calsequestrin in cardiac myocytes: effects of CASQ2 mutations linked to sudden cardiac death." Biophysical journal 95.4 (2008): 2037-2048.
130. Tiso, Natascia, et al. "Identification of mutations in the cardiac Ryanodine receptor gene in families affected with arrhythmogenic right ventricular cardiomyopathy type 2 (ARVD2)." Human molecular genetics 10.3 (2001): 189-194.
131. Uchida, Shizuka, and Stefanie Dimmeler. "Long noncoding RNAs in cardiovascular diseases." Circulation research 116.4 (2015): 737-750.
132. Van Heesch, Sebastiaan, et al. "The translational landscape of the human heart." Cell 178.1 (2019): 242-260.
133. Van Petegem, Filip. "Ryanodine receptors: structure and function." Journal of Biological Chemistry 287.38 (2012): 31624-31632.
134. Vassilopoulos, Stéphane, et al. "Triadins are not triad-specific proteins: two new skeletal muscle Triadins possibly involved in the architecture of sarcoplasmic reticulum." Journal of Biological Chemistry 280.31 (2005): 28601-28609.
135. Vausort, Mélanie, Daniel R. Wagner, and Yvan Devaux. "Long noncoding RNAs in patients with acute myocardial infarction." Circulation research 115.7 (2014): 668-677.
136. Vest, John A., et al. "Defective cardiac Ryanodine receptor regulation during atrial fibrillation." Circulation 111.16 (2005): 2025-2032.

137. Voigt, Niels, et al. "Enhanced sarcoplasmic reticulum Ca2+ leak and increased Na+-Ca2+ exchanger function underlie delayed afterdepolarizations in patients with chronic atrial fibrillation." Circulation 125.17 (2012): 2059-2070.
138. Vučićević, Dubravka, et al. "Long ncRNA expression associates with tissue-specific enhancers." Cell cycle 14.2 (2015): 253-260.
139. Waisman, Ariel, et al. "Cell cycle dynamics of mouse embryonic stem cells in the ground state and during transition to formative pluripotency." Scientific Reports 9.1 (2019): 8051.
140. Wakili, Reza, et al. "Recent advances in the molecular pathophysiology of atrial fibrillation." The Journal of clinical investigation 121.8 (2011): 2955-2968.
141. Wamstad, Joseph A., et al. "Dynamic and coordinated epigenetic regulation of developmental transitions in the cardiac lineage." Cell 151.1 (2012): 206-220.
142. Wang, Kevin C., and Howard Y. Chang. "Molecular mechanisms of long noncoding RNAs." Molecular cell 43.6 (2011): 904-914.
143. Wang, Qian, and Marek Michalak. "Calsequestrin. Structure, function, and evolution." Cell Calcium 90 (2020): 102242.
144. Wang, Wenlun, et al. "Biological function of long non-coding RNA (LncRNA) Xist." Frontiers in cell and developmental biology 9 (2021): 645647.
145. Wehrens, Xander HT, et al. "FKBP12. 6 deficiency and defective calcium release channel (Ryanodine receptor) function linked to exercise-induced sudden cardiac death." Cell 113.7 (2003): 829-840.
146. Wehrens, Xander HT, et al. "Ryanodine receptor/calcium release channel PKA phosphorylation: a critical mediator of heart failure progression." Proceedings of the National Academy of Sciences 103.3 (2006): 511-518.
147. Weintraub, Robert G., Christopher Semsarian, and Peter Macdonald. "Dilated cardiomyopathy." The Lancet 390.10092 (2017): 400-414.
148. Wu, Huang, Li Yang, and Ling-Ling Chen. "The diversity of long noncoding RNAs and their generation." Trends in genetics 33.8 (2017): 540-552.
149. Xie, Chaoyong, et al. "NONCODEv4: exploring the world of long non-coding RNA genes." Nucleic acids research 42.D1 (2014): D98-D103.
150. Yan, Qingqing, et al. "Mapping native R-loops genome-wide using a targeted nuclease approach." Cell reports 29.5 (2019): 1369-1380.
151. Yang, Xin, et al. "m6A promotes R-loop formation to facilitate transcription termination." Cell research 29.12 (2019): 1035-1038.
152. Yang, Ying, et al. "Dynamic transcriptomic m6A decoration: writers, erasers, readers and functions in RNA metabolism." Cell research 28.6 (2018): 616-624.
153. Yanofsky, Charles. "Establishing the triplet nature of the genetic code." Cell 128.5 (2007): 815-818.
154. Yoshida, Morikatsu, et al. "Impaired Ca2+ store functions in skeletal and cardiac muscle cells from sarcalumenin-deficient mice." Journal of Biological Chemistry 280.5 (2005): 3500-3506.
155. Yuan, Qi, et al. "Functional role of Calstabin2 in age-related cardiac alterations." Scientific reports 4.1 (2014): 7425.
156. Zardoni, Luca, et al. "Elongating RNA polymerase II and RNA: DNA hybrids hinder fork progression and gene expression at sites of head-on replication-transcription collisions." Nucleic Acids Research 49.22 (2021): 12769-12784.
157. Zhang, Lu, et al. "A heart-enriched antisense long non-coding RNA regulates the balance between cardiac and skeletal muscle Triadin." Biochimica et Biophysica Acta (BBA)-Molecular Cell Research 1865.2 (2018): 247-258.
158. Zhang, Ying, et al. "Cardiomyocyte PKA ablation enhances basal contractility while eliminates cardiac β-adrenergic response without adverse effects on the heart." Circulation Research 124.12 (2019): 1760-1777.
159. Zhao, Yuanbiao, et al. "Cardiomyocyte-specific long noncoding RNA regulates alternative splicing of the Triadin gene in the heart." Circulation 146.9 (2022): 699-714.
160. Zhihao, Liu, et al. "SERCA2a: a key protein in the Ca 2+ cycle of the heart failure." Heart failure reviews 25 (2020): 523-535.

161. Zhou, Haibo, et al. "In vivo simultaneous transcriptional activation of multiple genes in the brain using CRISPR–dCas9-activator transgenic mice." Nature neuroscience 21.3 (2018): 440-446.
162. Pisignano, Giuseppina, and Michael Ladomery. "Epigenetic regulation of alternative splicing: how lncRNAs tailor the message." Non-coding RNA 7.1 (2021): 21.
163. Cong, Le, et al. "Multiplex genome engineering using CRISPR/Cas systems." Science 339.6121 (2013): 819-823.
164. Ran, F. Ann, et al. "Genome engineering using the CRISPR-Cas9 system." Nature protocols 8.11 (2013): 2281-2308.

Appendix

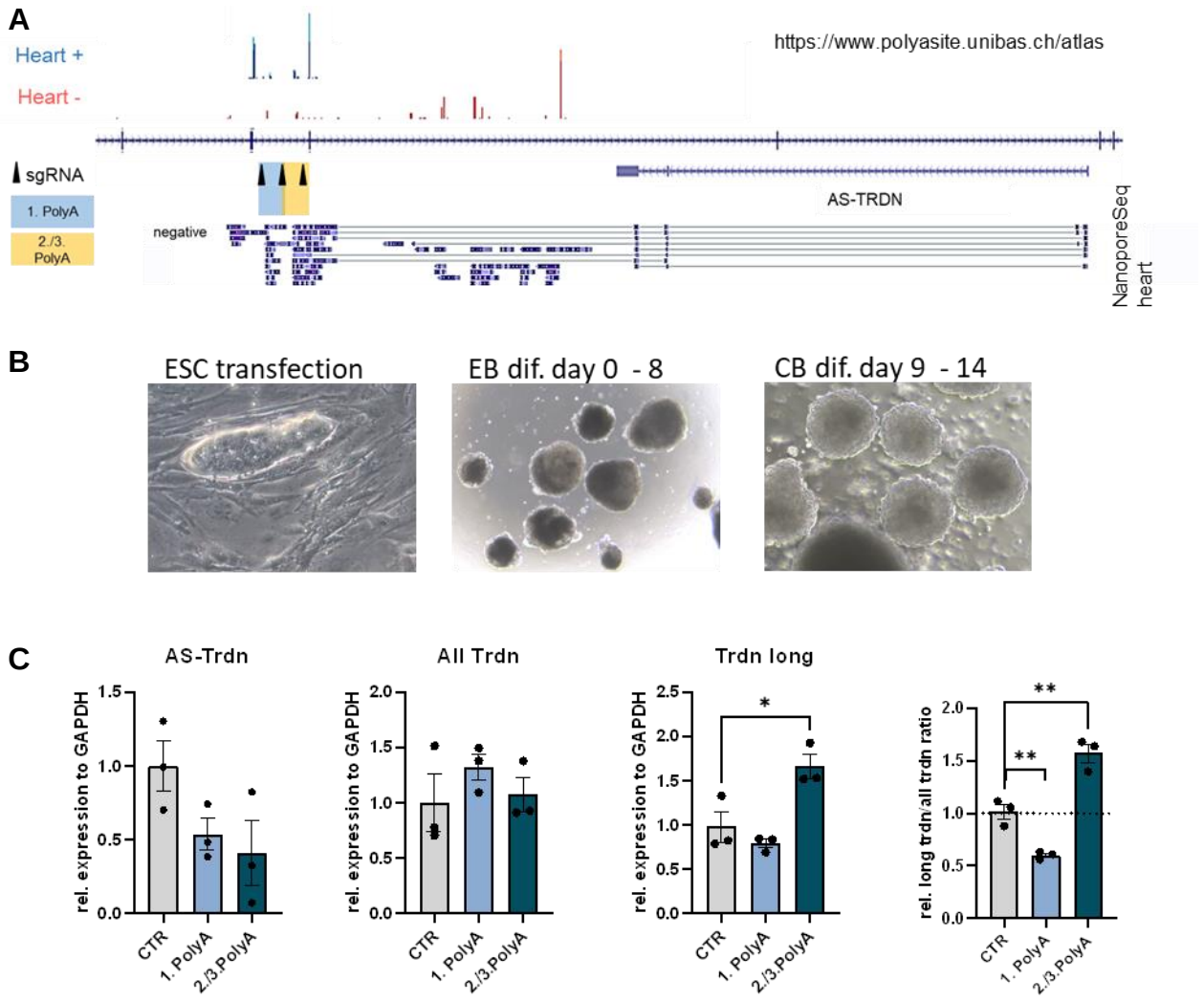

Figure 35 | Deletion of intronic polyA sites between exon 8 & 9 of triadin has contradictory effects on triadin isoform abundance. A Publicly available polyA atlas displays multiple polyA sites on the antisense strand, matching the NanoporeSeq TES (transcriptional end site). Either the blue or yellow marked area was deleted in mESC using CRISPR/CAS9. **B** Microscopic pictures demonstrating the mESC differentiation stages. Single colonies of ESC were transfected and positive clones picked for further differentiation. A view hours after differentiation start, embryoid bodies are formed and increase in size until day 8. On day 9, the differentiation into cardiac bodies (CBs) is initiated by G418 selection. The bodies become light and more see-through and start beating at day 10. **C** Taqman analysis of the *AS-Trdn* and *triadin* isoform expression in Ctr. and *AS-Trdn* DS 1 (1. polyA) and *AS-Trdn* DS 2 (2./3. polyA) cardiac bodies. Both deletions exhibit a reduction in *AS-Trdn* expression, with no difference in overall *triadin* expression. While the Ctr. and 1. PolyA CBs revealed no difference in the long triadin isoform (skeletal muscle triadin), deletion of the 2. and 3. polyA induced an increase in the long *Trdn* isoform, which was further confirmed by calculating the rel. difference between all triadin and long triaidn (>1 = > skeletal *Trdn*; <1 = > cardiac *Trdn*).n = 3. Mean ± SEM.

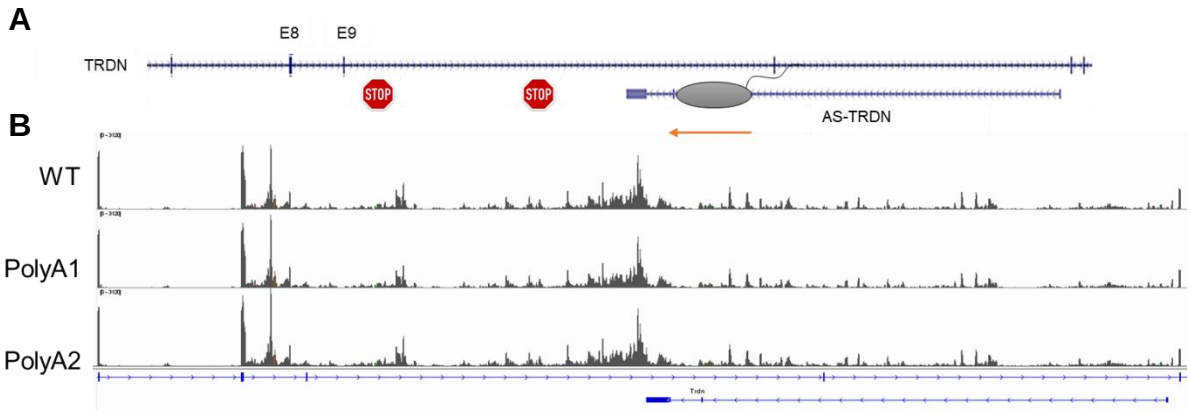

Figure 36 | Insertion of additional polyA sites downstream of *AS-Trdn* exhibit no effect on antisense transcription. **A** Schematic representation of additional antisense polyA insertions into the intronic region downstream of *AS-Trdn* and of exon 9 of triadin to induce additional transcription termination sites. **B** RNAseq of WT and polyA insertions displays no difference in transcript abundance, demonstrating the unsuccessful transcription termination.

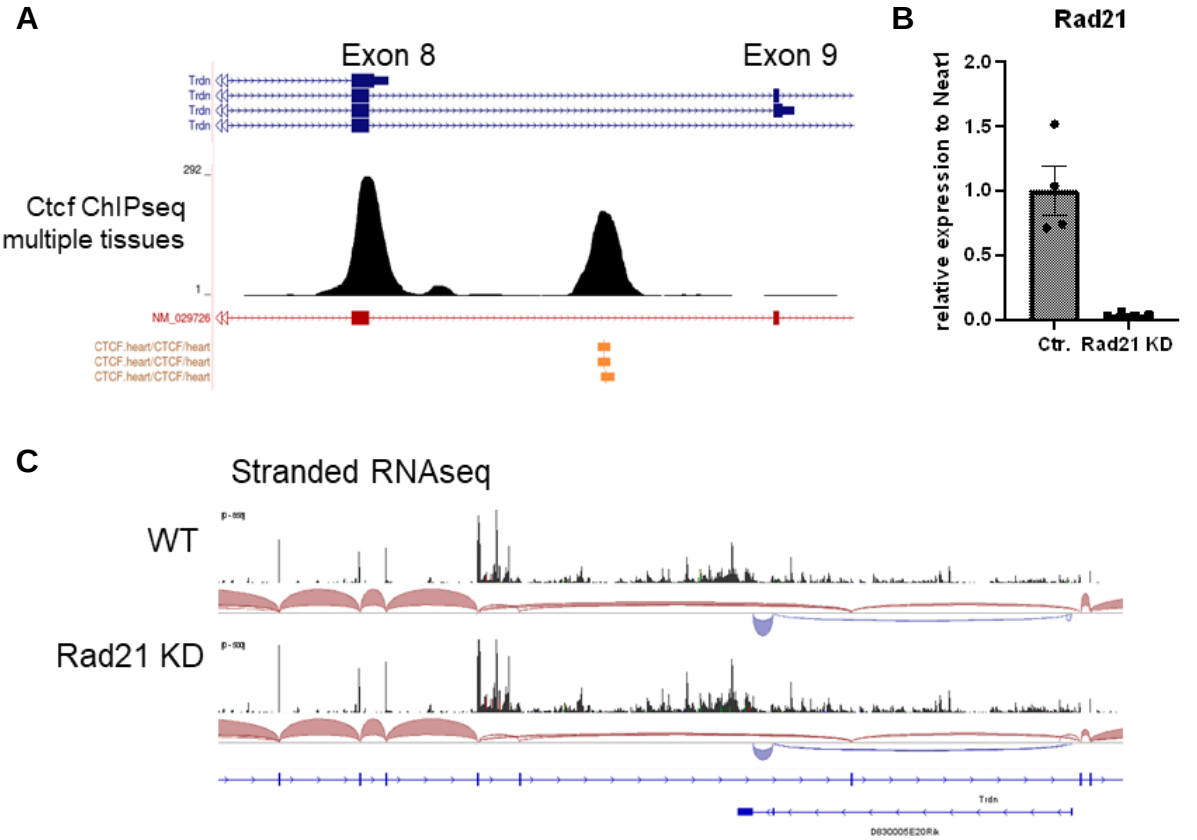

Figure 37 | Putative CTCF binding site has no functional role in triadin termination. A UCSC genome browser view of CTCF ChIPseq peak in the heart between exon 8 and 9 of triadin (cardiac *Trdn* last exon = 8). GRCm39/mm39. **B** KD of *Rad21* in neoCMs using siRNA displays significant loss of expression compared to *Neat1*. n = 4. **C** RNAseq analysis of *AS-Trdn* and *Trdn* in WT and *Rad21* KD neoCMs demonstrates no difference in expression and isoform abundance. Loss of Cohesin therefore has no effect on the triadin locus.

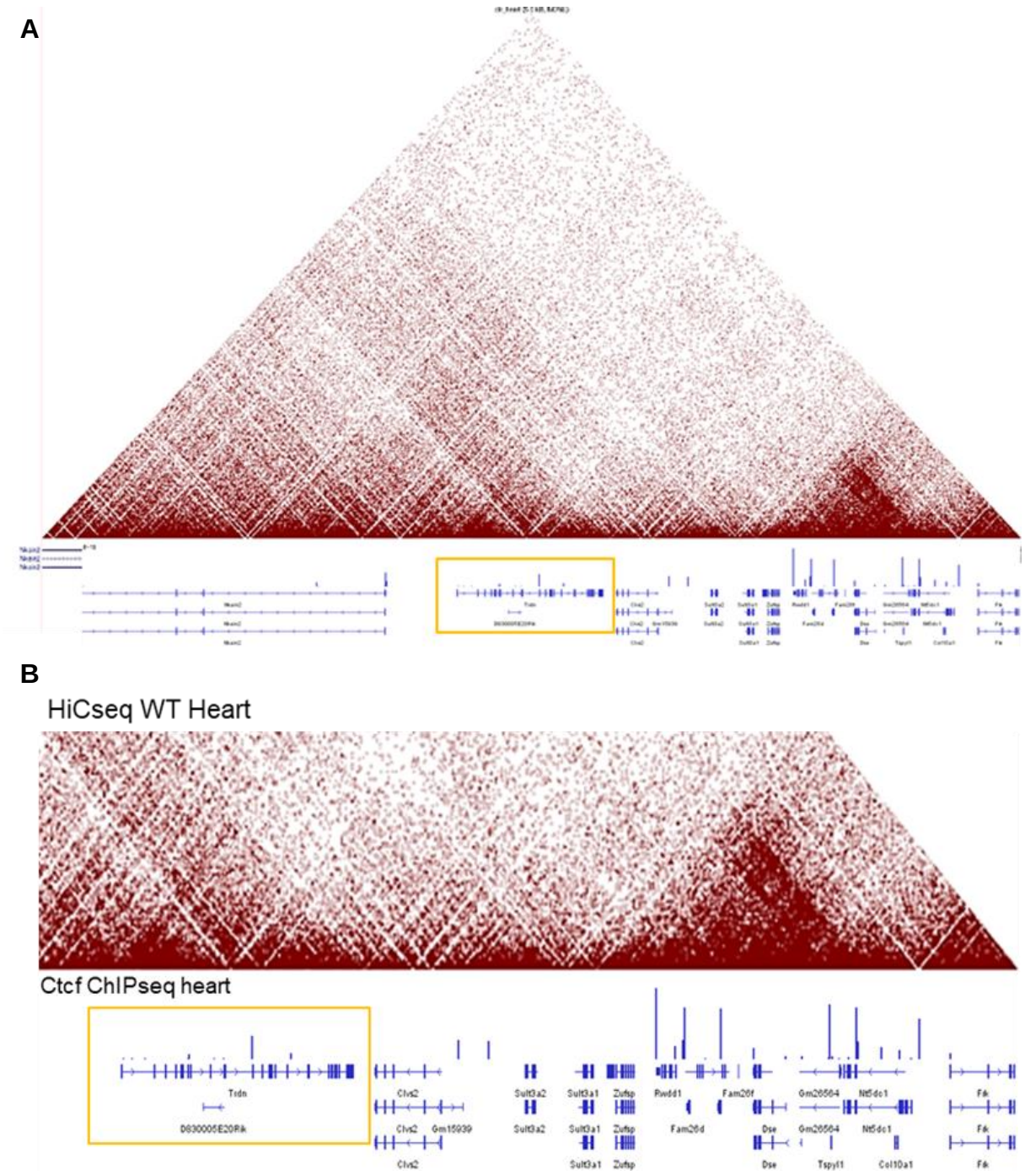

Figure 38 | HiCseq analysis of publicly available heart data reveals no TAD boundaries at the triadin locus. A UCSC genome browser representation of WT heart HiCseq data and CTCF binding sites (CTCF ChIPseq, ENCODE accession #ENCSR000CBI; HiCseq, GEO accession # GSE96692) Representing the triadin (yellow box) as well as neighbouring genomic loci. No TAD boundaries are obvious at the site of CTCF binding, which gets more obvious in the zoomed in picture (**B**). Using this view, the adjacent TAD boundary and its corresponding CTCF binding sites become obvious, while the CTCF binding within the triadin locus appears comparatively minor.

Acknowledgment

I would like to express my gratitude to the following persons, who have supported me throughout the course of this research:

First, to my supervisor Prof. Dr. Thomas Böttger for providing me with the opportunity to pursue my own research within the framework of this project. His continual support, encouragement and especially the engaging discussions have been instrumental in pushing me to achieve my full potential and fostering personal growth throughout this endeavour.

Prof Dr. Dr. Thomas Braun for giving me the opportunity to carry out my PhD in the department of cardiac development and remodelling at the MPI in Bad Nauheim. I am sincerely grateful for his continual support and advice throughout my PhD.

Prof. Dr. Albrecht Bindereif for the support throughout the RTG and as my second supervisor.

The Deutsche Forschungsgemeischaft (DFG) for funding my projects within the framework of the Collaborative Research Centre (CRC)/Transregio TRR 267: Non-coding RNA in the cardiovascular system. A special thanks goes out to the amazing PhD committee of the TRR 267 which I'm thankful to have been a part of.

My work group for their unwavering support over the past years, their team spirit and the open discussions. First and foremost Salma, Christian and Maria for their steadfast companionship through every challenge and triumph. Their strength and support have been a constant source of inspiration and encouragement. To Dafina and Jonas for the diligent support with genotyping and the great conversations.

Everyone at the MPI who supported me personally or this work.

Last but not least, I want to express my deepest gratitude to my husband, Peter, for his everlasting support, constant encouragement and persistent strong spirit. Thank you for always being by my side.